Mechanistic Analysis and Antibiotic Target Validation of Aminodeoxychorismate Synthase and Anthranilate Synthase

DISSERTATION

ZUR ERLANGUNG DES DOKTORGRADES
DER NATURWISSENSCHAFTEN (DR. RER. NAT.) DER FAKULTÄT FÜR
BIOLOGIE UND VORKLINISCHE MEDIZIN DER UNIVERSITÄT REGENSBURG

vorgelegt von

Franziska Jasmin Funke

aus Illertissen

Mai 2024

Das Promotionsgesuch wurde eingereicht am: 08.05.2024

Die Arbeit wurde angeleitet von: Prof. Dr. Reinhard Sterner

Unterschrift:

…….
Franziska Jasmin Funke

Abstract

Glutamine amidotransferases are responsible for the incorporation of ammonia into a variety of metabolites of primary and secondary metabolism. They minimally consist of a glutaminase subunit, which abstracts ammonia from glutamine, and a synthase subunit, which incorporates the generated ammonia into a specific substrate. To avoid the unproductive hydrolysis of glutamine, the activity of the glutaminase is controlled by the synthase and, in some cases, by additional allosteric substrates or ligands.

In the first part of this thesis, the molecular mechanism of the glutamine amidotransferase aminodeoxychorismate synthase (ADCS), which catalyses the first step of folate biosynthesis, is examined. To elucidate the mechanism of the glutaminase PabA in conjunction with the synthase PabB, an X-ray crystal structure of the isolated PabA subunit and four structures of the PabA-PabB complex in various catalytic states were determined. Furthermore, a thorough mutational analysis was conducted by determining the catalytic activity and complex affinity of selected protein variants. These experiments indicated that a catalytically competent orientation of residues in the active site of PabA is adopted only in the presence of PabB. Within the PabA-PabB complex, the formation of the covalent glutamyl-thioester reaction intermediate at the active site of PabA induces a relative rotational movement of PabB by 23°, which results in an expansion of the PabA-PabB interface and an apparent closure of the complex. As demonstrated by analytical gel filtration and isothermal titration calorimetry experiments, the closure of the complex is accompanied by a stabilization of the PabA-PabB complex. Moreover, steady-state kinetics revealed that the closed complex state facilitates the direct participation of PabB residues in a shared and secluded glutamine binding pocket. The ADCS complex thus can adopt at least two states: An open state allowing the binding of glutamine and a closed state promoting the solvent-excluded hydrolysis of glutamine as well as the transport of reactive ammonia to the active site of the synthase.

The second part of this thesis deals with the validation of ADCS and anthranilate synthase (AS) as novel targets for antibacterial compounds that promise high robustness against resistance-mediating mutations. The two evolutionary related glutamine amidotransferase complexes are required for the biosynthesis of folate and tryptophan in most prokaryotic organisms. The catalytic activities of both enzymes rely on the interplay of a glutaminase and a synthase subunit that is conferred by a highly conserved subunit interface. Consequently, inhibiting subunit

association in both enzymes by one competing bispecific inhibitor has the potential to suppress bacterial proliferation. Two conserved interface hotspot residues were verified *in silico* and *in vitro* as potential inhibitor binding sites by demonstrating their crucial role in subunit association and enzymatic activity via computational alanine scanning, analytical gel filtration and steady-state activity titrations. For *in vivo* target validation, genomically modified *Escherichia coli* strains were generated, in which subunit association was disrupted by modifying these central interface residues. The growth of such strains was drastically impeded on liquid and solid minimal medium due to the lack of folate and tryptophan. Remarkably, the bacteriostatic effect was observed even in the presence of heat-inactivated human plasma, demonstrating that accessible host metabolite concentrations do not compensate for the lack of folate and tryptophan within the tested bacterial cells. In conclusion, a potential inhibitor targeting both enzyme complexes will be effective against a broad spectrum of pathogens and offer increased resilience against antibiotic resistance.

In summary, this thesis expands the knowledge on glutamine amidotransferases by a detailed mechanistic characterization of the ADCS enzyme complex and offers a clinical application of these insights through the validation of ADCS and AS as antibiotic targets.

Zusammenfassung

Glutamin-Amidotransferasen sind für den Einbau von Ammoniak in eine Vielzahl von Metaboliten des Primär- und Sekundärstoffwechsels verantwortlich. Sie bestehen mindestens aus einer Glutaminase-Untereinheit, die Ammoniak von Glutamin abstrahiert, und einer Synthase-Untereinheit, die den entstandenen Ammoniak in ein spezifisches Substrat einbaut. Um dabei die unproduktive Hydrolyse von Glutamin zu vermeiden, wird die Glutaminase-Aktivität durch die Synthase und in einigen Fällen durch zusätzliche allosterisch wirkende Substrate oder Liganden gesteuert.

Im ersten Teil der vorliegenden Arbeit wird der molekulare Mechanismus der Glutamin-Amidotransferase Aminodeoxychorismat-Synthase (ADCS), die den ersten Schritt in der Biosynthese von Folat katalysiert, beleuchtet. Um den Mechanismus der Glutaminase PabA im Zusammenspiel mit der Synthase PabB aufzuklären, wurde eine Röntgenkristallstruktur der isolierten PabA-Untereinheit und vier Strukturen des PabA-PabB-Komplexes in verschiedenen katalytischen Stadien aufgenommen. Außerdem wurden in einer umfangreichen Mutationsanalyse die katalytische Aktivität und Komplexaffinität von ausgewählten Proteinvarianten untersucht. Diese Experimente wiesen darauf hin, dass eine katalytisch kompetente Ausrichtung der Residuen im aktiven Zentrum von PabA erst in Anwesenheit von PabB erfolgt. Im PabA-PabB-Komplex induziert die Bildung des kovalenten Glutamyl-Thioester-Reaktionsintermediates am aktiven Zentrum von PabA eine relative Rotationsbewegung von PabB um 23°, die eine Vergrößerung der Kontaktfläche zwischen PabA und PabB und eine apparente Schließbewegung des Komplexes zur Folge hat. Experimentelle Untersuchungen mittels analytischer Gelfiltration und isothermer Titrationskalorimetrie zeigten, dass die Schließung des Komplexes mit einer Stabilisierung des PabA-PabB-Komplexes einhergeht. Zudem erwiesen *Steady-State*-Kinetiken, dass im geschlossenen Komplex die direkte Beteiligung von PabB-Residuen an einer gemeinsamen, nach außen abgeschlossenen Glutamin-Bindetasche ermöglicht wird. Der ADCS-Komplex kann also mindestens zwei Zustände einnehmen: Eine offene Form, die die Bindung von Glutamin erlaubt, und eine geschlossene Form, in der unter Lösungsmittel-Ausschluss Glutamin hydrolysiert und der reaktive Ammoniak zum aktiven Zentrum der Synthase transportiert wird.

Der zweite Teil dieser Arbeit befasst sich mit der Validierung der ADCS und der Anthranilat-Synthase (AS) als neue Targets für antibakterielle Wirkstoffe, die eine hohe Beständigkeit

gegenüber resistenzvermittelnden Mutationen versprechen. Die beiden evolutionär verwandten Glutamin-Amidotransferase-Komplexe sind in den meisten Bakterien essenziell für die Biosynthese von Folat und Tryptophan und die katalytischen Aktivitäten beider Enzyme beruhen auf dem Zusammenspiel einer Glutaminase- und einer Synthase-Untereinheit, das durch eine hoch-konservierte Kontaktfläche vermittelt wird. Eine Hemmung der Assoziation der Untereinheiten in beiden Enzymen durch einen konkurrierenden bi-spezifischen Inhibitor hat daher das Potenzial, bakterielles Wachstum zu unterdrücken. Zwei konservierte Hotspot-Residuen der Kontaktfläche wurden *in silico* und *in vitro* als potenzielle Inhibitor-Bindestellen verifiziert, indem ihre maßgebliche Rolle bei der Komplexbildung und der enzymatischen Aktivität über computerbasierte Alanin-Scans, analytische Gelfiltration und *Steady-State*-Aktivitätstitrationen nachgewiesen wurde. Für eine *in vivo* Target-Validierung wurden genomisch veränderte *Escherichia coli*-Stämme erzeugt, bei denen die Assoziation der Untereinheiten durch eine Modifikation dieser zentralen Reste gestört wurde. Das Wachstum solcher Stämme auf flüssigem und festem Minimalmedium war aufgrund eines Mangels an Folat und Tryptophan drastisch verzögert. Die bemerkenswerte Beständigkeit dieses Effekts sogar in der Anwesenheit von hitzeinaktiviertem humanem Plasma demonstriert, dass die verfügbaren Metabolit-Konzentrationen im Wirt den Mangel an Folat und Tryptophan in den getesteten bakteriellen Zellen nicht kompensieren können. Ein potenzieller Inhibitor, der auf beide Enzymkomplexe abzielt, wird also gegen ein breites Spektrum von Krankheitserregern wirksam sein und eine erhöhte Resilienz gegen Antibiotika-Resistenzen aufweisen.

Zusammenfassend erweitert die vorliegende Arbeit das Verständnis über Glutamin-Amidotransferasen durch eine detaillierte mechanistische Charakterisierung des ADCS-Enzymkomplexes und bietet eine klinische Anwendung dieses Wissens durch die Validierung von ADCS und AS als Antibiotika-Targets.

List of Publications

This thesis consists of two research projects, which are described in chapters 2 and 3. While the results of the first study described in chapter 2 are still being prepared for publication, the second project has already been accepted for publication. Chapter 3 of this thesis contains the following corresponding manuscript.

A **Funke, FJ.**, Schlee, S., & Sterner, R. (2024). Validation of aminodeoxychorismate synthase and anthranilate synthase as novel targets for bispecific antibiotics inhibiting conserved protein-protein interactions. *Journal of Applied and Environmental Microbiology*, DOI: https://doi.org/10.1128/aem.00572-24.

Personal contributions to Publication A:

The research was designed by myself, Sandra Schlee and Reinhard Sterner. Sandra Schlee optimized the recombinant expression of the proteins, all experiments were performed and analyzed by myself. The manuscript was drafted by myself and revised by Reinhard Sterner and Sandra Schlee.

During my work, I contributed to further publications that are not part of this thesis.

B Hertle, R., Nazet, J., Semmelmann, F., Schlee, S., **Funke, F.**, Merkl, R., & Sterner, R. (2021). Reprogramming the specificity of a protein interface by computational and data-driven design. *Structure*, *29*(3), 292-304.

C Klein, T., **Funke, F.**, Rossbach, O., Lehmann, G., Vockenhuber, M., Medenbach, J., Suess, B., Meister, G., & Babinger, P. (2023). Investigating the Prevalence of RNA-Binding Metabolic Enzymes in *E. coli*. *International Journal of Molecular Sciences*, *24*(14), 11536.

Table of Contents

Abstract v

List of Publications ix

List of Figures xii

List of Tables xiii

Abbreviations xiv

1 General introduction 1

1.1 Protein-protein interactions amplify biological complexity 1

1.2 Protein-protein interactions as drug targets 4

1.3 Glutamine amidotransferases – a versatile group of enzyme complexes 6

1.4 Aims of this thesis 11

2 Molecular mechanism of glutaminase activation in aminodeoxychorismate synthase 12

2.1 Introduction 12

2.2 Results 14

2.2.1 The glutaminase activity of ADCS depends on complexation with its synthase 14

2.2.2 Structural characterization of the PabA-PabB complex 16

2.2.3 Glutamyl-thioester formation induces PabA-PabB subunit rearrangements 21

2.2.4 Model for glutamine binding and turnover 23

2.2.5 A zinc ion binding to the active site of PabA 28

2.2.6 PabB induces a catalytically competent active site conformation in PabA 31

2.3 Discussion 35

2.4 Material and Methods 40

2.4.1 Cloning and mutagenesis 40

2.4.2 Gene expression and protein purification 40

2.4.3 Purification of chorismate 40

2.4.4 Analysis of PabA-PabB complex formation by analytical gel filtration 41

2.4.5 Analysis of PabA-PabB complex formation by ITC 41

2.4.6 Steady-state enzyme kinetics 42

2.4.7 Crystallization 42

2.5 Supplemental data 44
3 Validation of aminodeoxychorismate synthase and anthranilate synthase as novel targets for bispecific antibiotics inhibiting conserved protein-protein interactions 49
3.1 Abstract 49
3.2 Importance 49
3.3 Introduction 50
3.4 Results 52
3.4.1 *In silico* and *in vitro* validation of interface hotspot residues in the ADCS and AS complexes 52
3.4.2 *In vivo* validation of ADCS and AS as targets for a PPI inhibitor 57
3.5 Discussion 61
3.6 Material and Methods 64
3.6.1 Computational alanine scanning 64
3.6.2 Cloning and protein purification 65
3.6.3 Activity titrations 65
3.6.4 Analysis of glutaminase-synthase complex formation 66
3.6.5 Genomic modification of *E. coli* 66
3.6.6 Growth assays on liquid and solid medium 68
3.7 Acknowledgement 68
3.8 Supplemental data 69
4 Comprehensive discussion and outlook 73
5 References 76
6 Acknowledgement 89

List of Figures

Figure 1.1: Principle of reduced resistance formation propensities in PPI inhibitors compared to competitive inhibitors. 5
Figure 1.2: Quaternary structure of selected GATases. 7
Figure 1.3: Reaction mechanism of class I glutaminases with a catalytic triad Cys-His-Glu. .. 8
Figure 1.4: MST enzymes acting on the central metabolite chorismate. 10
Figure 2.1: Crystals of the PabA-PabB complex and SDS-PAGE crystal analysis. 16
Figure 2.2: Crystal structures of *E. coli* PabA and PabA-PabB. 19
Figure 2.3: Binding sites of Cho and Trp and ammonia tunnel. 20
Figure 2.4: PabA-PabB subunit rearrangements upon Gln-TE formation. 22
Figure 2.5: The impact of Gln-TE formation on selected residues. 24
Figure 2.6: Conformational variability of PabA in its apo form and in complex with PabB. . 32
Figure 3.1. Reaction scheme and hotspot interface residues in ADCS and AS. 53
Figure 3.2: Growth in liquid M9 minimal medium of *E. coli* strains with genomic manipulations of ec*pabA* or/and ec*trpG*. 59
Figure 3.3: Growth on solid M9 minimal medium of *E. coli* strains with genomic manipulations of ec*pabA* or/and ec*trpG*. 60
Figure 3.4 Growth of *E. coli* strains with genomic manipulations of ec*pabA* or/and ec*trpG* on solid M9 minimal medium supplemented with heat-inactivated human plasma. 61
Figure 4.1: Strategies for inhibitors disrupting functional PPIs in ADCS and AS. 74

Supplementary Figures

Figure S2.1: Elution profiles from analytical GF of PabA and PabB variants. 48
Figure S3.1: Activity titrations monitoring glutaminase-dependent synthase activities. 70
Figure S3.2: Assessment of glutaminase-synthase association by analytical size exclusion chromatography. 71
Figure S3.3: Growth of *E. coli* strains with genomic manipulations of ec*pabA* or/and ec*trpG* on solid M9 minimal medium supplemented with untreated or “heat inactivated” pABA and Trp. 72

List of Tables

Table 2.1: Stimulation of glutaminase activities by the respective synthases and chorismate in ADCS and AS. 15
Table 2.2: Summary of crystal structures solved in collaboration with Dr. Sihyun Sung. 18
Table 2.3: Effects of mutations in PabA or PabB on PabA-PabB assembly and the catalytic activity of PabA. 25
Table 2.4: Quantification of zinc in PabA-PabB by ICP-OES with different methods of sample preparation. 29
Table 2.5: Effects of chorismate, EDTA and $MgCl_2$ on the catalytic activity of PabA. 30
Table 3.1: Turnover number and complex formation of synthases with wild-type and double mutant glutaminases at 25°C. 56

Supplementary Table

Table S3.1: Computational alanine scanning using a homology model of the ecPabA-ecPabB complex and the TrpG-TrpE complex structure from *Serratia marcescens*. 69

Abbreviations

ADCS	Aminodeoxychorismate synthase
ADICS	Aminodeoxyisochorismate synthase
AS	Anthranilate synthase
B. subtilis	*Bacillus subtilis*
bs	*B. subtilis* enzyme or gene
Cam	Chloramphenicol
Cho	Chorismate
DTT	Dithiothreitol
E. coli	*Escherichia coli*
ec	*E. coli* enzyme or gene
EDTA	Ethylenediaminetetraacetic acid
GATase	Glutamine amidotransferase
GDH	Glutamate dehydrogenase
GDP	Guanosine diphosphate
GF	Gel filtration
Gln-TE	Glutamyl-thioester
GTP	Guanosine triphosphate
HisF	Synthase subunit of imidazole glycerol phosphate synthase
HisH	Glutaminase subunit of imidazole glycerol phosphate synthase
ICP-OES	Inductively coupled plasma-optical emission spectrometry
IS	Isochorismate synthase
ITC	Isothermal titration calorimetry
k_{cat}	Turnover number
k_{cat}/K_M	Catalytic efficiency
K_D	Dissociation constant

K_M	Michaelis constant
MES	2-(*N*-morpholino)ethanesulfonic acid
MST enzymes	Menaquinone, siderophore, tryptophan biosynthetic enzymes
NAD^+	Nicotinamide adenine dinucleotide (oxidized)
NADH	Nicotinamide adenine dinucleotide (reduced)
OD	Optical density
P. aeruginosa	*Pseudomonas aeruginosa*
pa	*P. aeruginosa* enzyme or gene
pABA	*para*-aminobenzoic acid
PabA	Glutaminase subunit of aminodeoxychorismate synthase
PabB	Synthase subunit of aminodeoxychorismate synthase
PabC	Aminodeoxychorismate lyase
PapAB	Fused aminodeoxychorismate synthase from secondary metabolism
PPI	Protein-protein interaction
r.m.s.d.	Root mean square deviation
rpm	Revolutions per minute
S. marcescens	*Serratia marcescens*
S. venezuelae	*Streptomyces venezuelae*
SD	Standard deviation
SDS-PAGE	Sodium dodecyl sulfate polyacrylamide gel electrophoresis
SEC	Size exclusion chromatography
SS	Salicylate synthase
T. maritima	*Thermotoga maritima*
TEV	Tobacco etch virus
TrpE	Synthase subunit of anthranilate synthase
TrpG	Glutaminase subunit of anthranilate synthase
wt	Wild-type

1 General introduction

1.1 Protein-protein interactions amplify biological complexity

All forms of life, however simple and primordial they may appear at first glance, actually reveal an extremely high degree of complexity as soon as we try to understand the underlying biochemical and cellular processes. In general, all information of an organism is stored in long chains of nucleic acids, the genome, that is used as template for the production of small RNA snippets and, based on these, the linear assembly of a set of 20 amino acids to highly specialized proteins. While the sheer number of different proteins is limited by the size of the respective genome, the interactions of these individual proteins lead to a burst of complexity within the system. For example, the gram-negative bacterium *Escherichia coli* holds genes for about 4000-5500 different proteins.[1] One can easily imagine that the simple coexistence of these proteins, blindly interacting via diffusing metabolites, would not yield a robust and adaptive organism. To gain real complexity, the functions of the individual polypeptide chains need to be linked to each other, resulting in a large network of protein-protein interactions (PPI), also called the interactome.[2] The unequivocal quantification of PPIs within a given organism has been proven challenging due to their dependence on local environmental conditions,[3] the formation of unstable or transient complexes and constraints of the applied method:[4] While high-throughput experiments identified 9000-13000 PPIs in *E. coli*,[5-7] a more recent computational analysis estimates a number of about 35000 different PPIs.[8] Other estimates state that over 80% of all proteins act in a complex rather than by themselves.[9, 10] Irrespective of the exact numbers, it is undisputed that PPIs are crucial for the function and regulation of most, if not all, inter- and intra-cellular processes, including transcription, translation, signal transmission, membrane transport and enzymatic catalysis. The central importance of PPIs is reflected by a range of diseases associated with dysfunctional PPIs including neurodegenerative disorders or cancer.[11-13]

The properties of PPIs are adapted to the specific demands imposed on the complex.[14, 15] In 2003, Nooren and Thornton[16] proposed a system to classify the different kinds of PPIs found in nature: First, they differentiate obligate and non-obligate interactions, the latter in turn are further subdivided into permanent and transient complexes. Furthermore, protein complexes

can be either homooligomers or heterooligomers, depending on whether they consist of identical or different individual polypeptide chains. Complexes with *obligate* PPIs consist of protomers that are not stable and usually also non-functional without their interaction partner *in vivo* and are thus often co-expressed or assembled with the aid of chaperones.[17] Obligate PPIs are found for example in different G protein complexes[17], the Arc repressor[18] or Ku proteins.[19] Protomers that form *permanent* protein-protein complexes are stable on their own, but interact with nanomolar affinity such that they virtually stay associated as soon as they encounter.[15] Similar to obligate complexes, their functionality tends to depend on complexation, but the protomers may be spatially or temporally separated until they are united by a specific trigger or event. A classic example are antibody-antigen interactions upon intrusion of a pathogen, which trigger the effector function of the respective antibody.[20] Inversely, the controlled disruption of permanent complexes provides yet another level of regulation, as observed in type II toxin-antitoxin complexes in which the activity of the toxin is inhibited within the complex. Under stress conditions however, the antitoxin is proteolytically cleaved, leading to a release of the active toxin.[21] *Transient* PPIs in turn can be formed either by low affinity binders that are in a dynamic equilibrium between monomer and oligomer or proteins whose interaction is controlled by an external factor, such as an allosteric or competitive ligand.[15] They are an essential part of adaptive processes such as signal cascades and regulatory pathways.

In practice, the nature of PPIs is often highly dependent on the physiological state of a given cell and must be seen as a spectrum rather than a strict categorization. In this manner, different types of interactions may be involved in one multi-subunit complex, as observed for the G protein which forms a stable $G_{\alpha\beta\gamma}$ trimer when GDP is bound, but readily dissociates to the G_{α} subunit and the permanent $G_{\beta\gamma}$ complex in the presence of GTP.[16] Moreover, one protein can participate in multiple PPIs assigned to different 'classes' depending on its interaction partner, such as the small protein calmodulin. Calmodulin undergoes conformational changes at increased cytosolic Ca^{2+} levels to interact with a range of different proteins with dissociation constants between 10^{-7} and 10^{-11} M to either activate or inhibit their function.[22] In contrast, another set of proteins binds calmodulin in an irreversible and Ca^{2+}-independent manner.[23]

The actual interactions between proteins within a cell and, importantly, the resulting biological functions are however not only dictated by dissociation constants between two molecules, but also by local protein concentrations and the specificity of interactions. Functional interactions of one protein with multiple other proteins are generally found at central metabolic, signaling

or regulatory nodes.[16] The underlying molecular mechanisms of promiscuity are as versatile as the involved proteins and include conserved interfaces or domains with only small variations or an intrinsic structural plasticity that allows the promiscuous protein to change its conformation to accommodate binding of the respective partner.[24, 25] Promiscuous PPIs usually involve an intricate balance between complementary and distinctive features that allow for discrimination between different partners, often in response to an effector.

The concept of conformational changes in interacting proteins is not limited to the initial process of complexation, but is often central to the function of a complex, so that rearrangements within or between subunits contribute to function-related movements or the fine-tuning of activities by mediating allosteric or cooperative effects. A prime example of cooperativity conferred by subunit rearrangements is the mammalian hemoglobin that is comprised of four monomers, each equipped with one oxygen binding site. Upon binding of oxygen to one of the four subunits, the quaternary structure is rearranged from a tense (T) form to a relaxed (R) form, which increases the affinity of oxygen to the remaining free oxygen binding sites of the complex, enabling efficient oxygen transport from the lungs to the tissue.[26, 27] Besides the ubiquitous allosteric effects, some enzymes are even more directly dependent on complex formation, in that the active site is located at the protein-protein interface with the active site residues contributed by one or both subunits to jointly catalyze one reaction. For example, in the homodimeric triosephosphate isomerase, the eponym for the TIM-barrel fold, all catalytic residues are located on one subunit, but their productive conformation is stabilized by a protruding loop from the interacting protomer.[28] Similarly, in bacterial and mammalian ornithine decarboxylases, each of the two symmetric active sites of the homodimer comprises residues from both subunits, rendering the catalytic activity of the enzyme dependent on complexation.[29, 30]

The pivotal role and overwhelming complexity of PPIs inevitably raises questions about their evolutionary origins. A fundamental concept of evolution is that new functionalities and characteristics evolve randomly by modifying and recombining existing scaffolds, initially generating a high degree of promiscuity. If a promiscuous side-functionality turns out to be beneficial or detrimental in a given environment, positive or negative selection may take place, which eventually promotes the emergence and persistence of novel features, in this case interactions.[31-33] In the light of the dense packaging of proteins within a cell, it is very likely that unspecific, short-lived and non-functional interactions occur, which increase the evolutionary potential of the participating proteins and could gradually transform into

physiologically relevant PPIs. Aside from the gain of an enzymatic or regulatory function, the formation of PPIs potentially offers further (initial) benefits such as an increase in (thermo-)stability.[34-36] In turn, fairly stable and specific PPIs, whether functional or not, pave the way for genetic fusion events in which the protomers are converted into structural domains of a larger overall fold or functional domains of a multi-enzyme complex.[37, 38] Interestingly, some proteins such as fatty acid synthases are found as either non-covalent complex or genetically fused complex in different organisms.[39] In sum, the underlying evolutionary processes of PPI formation are manifold, multidirectional and interwoven and thus are often not understood in detail.

PPIs that are beneficial to the fitness of an organism restrict the evolution of the individual subunits, as only interface modifications that maintain the PPI are permitted. On the other hand, the accumulation of various different interaction-dependent functionalities might promote the persistence of PPIs.[40] Whether interface residues are therefore generally more conserved than other residues on the protein surface is controversial.[41-44] Nevertheless, the degree of conservation correlates with the type of interaction, such that interfaces of obligate complexes evolve at a slower rate than interface residues contributing to transient interactions.[45] The slower rate in turn supports the co-evolution of the subunits.[46, 47] Moreover, conservation is not equally distributed over the whole interface, but generally lower at the rim and higher in the central part and, at the level of individual residues, correlates with the number of interactions a residue is involved in.[48, 49] In line with this, the largest share of the oligomeric binding energy is often conferred by only a small set of conserved interface residues, the so-called hotspot residues.[50, 51] Hotspot residues are defined as interface residues whose exchange to alanine leads to a difference in binding energy of more than 2 kcal/mol. The prevalence of certain residues in hotspot positions and their spatial arrangement is however still a subject of controversy.[50, 52, 53]

1.2 Protein-protein interactions as drug targets

In addition to their evolutionary implications, the discovery of hotspot residues as determinants of protein complex formation arose the interest in their exploitation as targets in drug development: The dynamic and largely flat interface area of protein complexes of around 400-5000 Å^2 [54, 55] is narrowed down to a handful of clustered residues with a distinct geometry, transforming PPIs from virtually undruggable surfaces to defined targets. Potential targets span

not only disease-related PPIs in humans,[56, 57] but also PPIs required for the survival or pathogenicity of viruses,[58] bacteria[59, 60] and parasites.[61] Extensive research has yielded many different strategies to specifically inhibit PPIs, for example by modulators that resemble the hotspot residues, including fragment-based design, macrocycles or protein domain mimicry.[62, 63] The inherent advantage of targeting PPIs instead of a substrate or ligand-binding site is its reduced susceptibility to mutational escape conferring drug resistance (**Figure 1.1**): When targeting a ligand binding site, a single mutation can be sufficient to abolish binding of the drug while maintaining the function of the protein. In contrast, a mutation of a hotspot residue might avoid inhibitor binding, but at the same time disrupts or weakens the native protein complex, which usually results in a metabolic handicap. Avoiding drug binding while maintaining complex formation thus requires simultaneous complementary modifications in the interacting polypeptide chains, which makes resistance formation significantly less probable.[60] The avoidance of resistance formation plays an exceptional role in antibiotic agents, therefore, extending the range of potential antibiotic targets to PPIs offers attractive options for more sustainable antibacterial treatments.[60, 64]

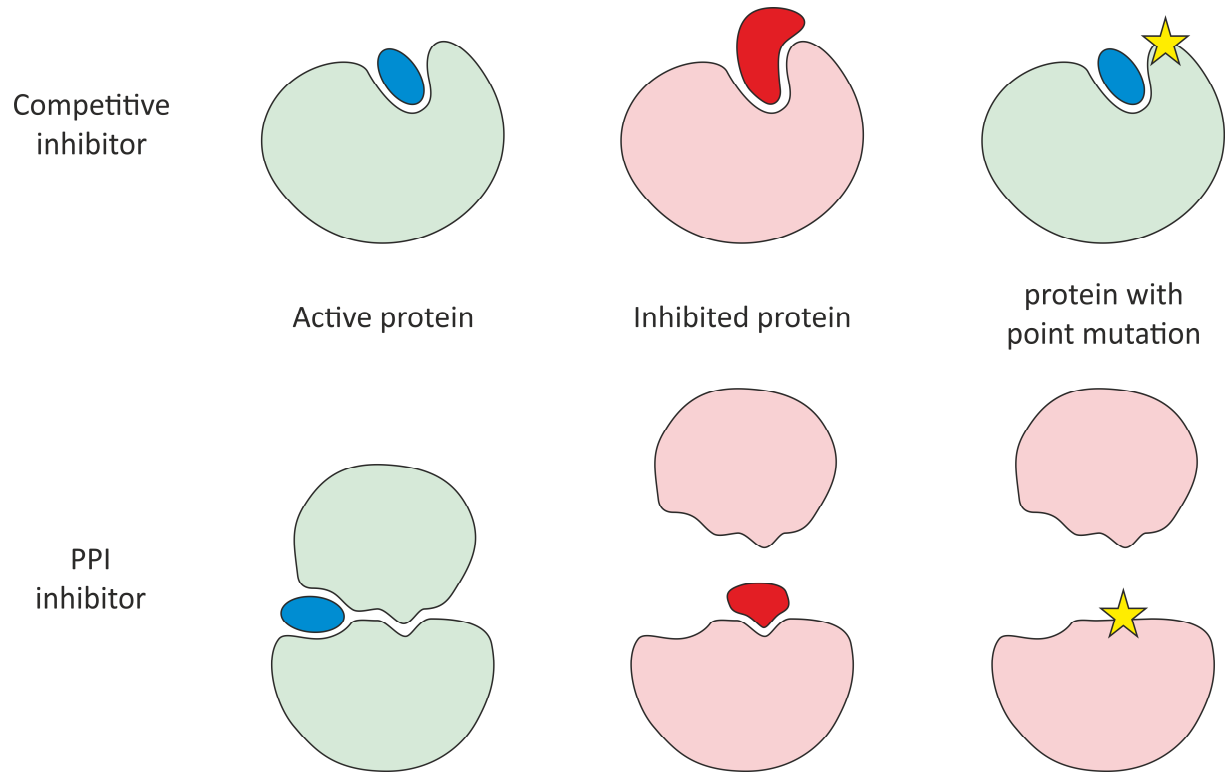

Figure 1.1: Principle of reduced resistance formation propensities in PPI inhibitors compared to competitive inhibitors. Conventional inhibitors (upper panel) bind competitively with the substrate or ligand to inactivate the target protein. However, single point mutations can quickly disrupt inhibitor binding while preserving the active site and reduce the sensitivity to the inhibitor. In contrast, PPI inhibitors (lower panel) are designed to block functionally essential subunit associations. Resistance-mediating mutations in the interface disrupt not only inhibitor binding but at the same time native complex formation and are thus less likely to persist. Light green, active proteins; light red, inactive proteins; blue, ligand; red, inhibitor; yellow, point mutation.

1.3 Glutamine amidotransferases – a versatile group of enzyme complexes

A model system for the study of PPIs are glutamine amidotransferases (GATases), which are responsible for the distribution of ammonia from the nitrogen reservoir glutamine to a range of different metabolic pathways, including the biosynthesis of nucleotides, amino sugars, amino acids and vitamins.[65] GATases minimally comprise a glutaminase and a synthase subunit, where the glutaminase hydrolyses glutamine to glutamate and ammonia, which is transferred to the active site of the synthase to aminate a specifically recognized acceptor molecule. Since an exposure of ammonia to the cytosol would lead to its protonation and prohibit further reactions, the temporal and spatial coupling of glutaminase and synthase functionalities is pivotal for the overall activity, and in many cases provided by an intermolecular channel connecting the active sites. Depending on the enzyme and the organism, different strategies were developed to ensure glutaminase-synthase association, either by forming stable and specific protein complexes with diverse quaternary structures and/or by the genetic fusion of both functionalities (**Figure 1.2**).[66, 67]

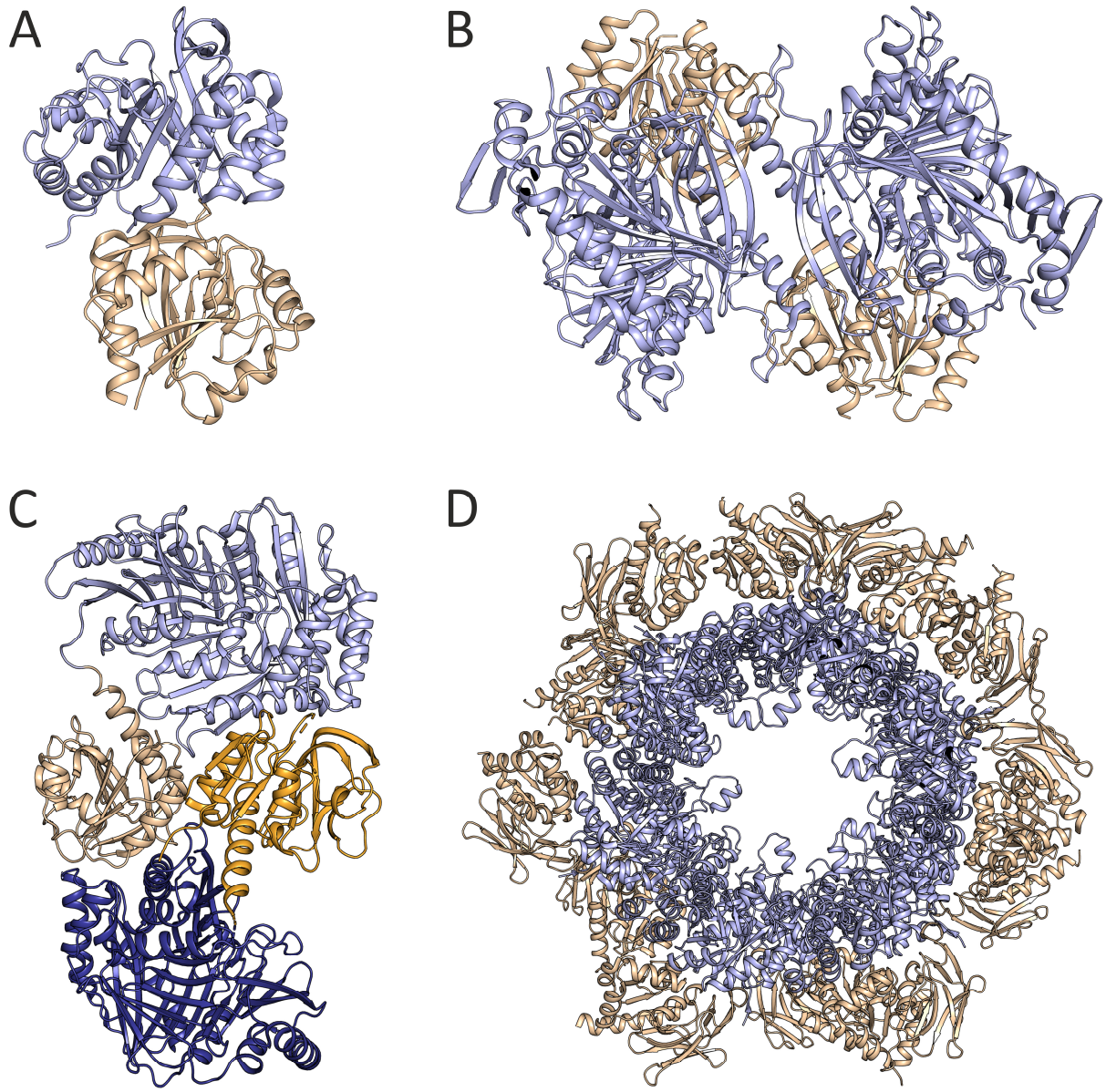

Figure 1.2: Quaternary structure of selected GATases. The association of glutaminases (wheat) and synthases (light blue) is highly diverse and varies between GATase enzymes and organisms. (A) Structure of imidazole glycerol phosphate synthase from *T. maritima*, the glutaminase and synthase subunits form a simple heterodimer (PDB-ID 7AC8).[68] (B) The anthranilate synthase from *Serratia marcescens* (PDB-ID 1I7Q) forms a dimer of heterodimers.[69] (C) Aminodeoxychorismate synthase from *Streptomyces venezuelae* (PDB-ID 8HX6) comprises two glutaminase-synthase fusion proteins (marked as bright and dark), in which the glutaminase domain from one polypeptide provides ammonia to the synthase domain of the other.[70] (D) Pyridoxal phosphate synthase from *Bacillus subtilis* (PDB-ID 2NV2) adopts a large cogwheel-like quaternary structure that consists of 12 glutaminase and synthase subunits each.[71]

Interestingly, glutaminases seem to have formed twice during evolution, so that almost all modern glutaminases belong to one of two classes, each with a highly conserved fold and active site.[72] Class I or triad glutaminases adopt an α/β-hydrolase fold with a catalytic Cys-His-Glu triad.[73-75] The reaction mechanism is similar to that observed in cysteine or serine proteases (**Figure 1.3**): The thiol group of cysteine, which is activated by the adjacent acid-base catalysts histidine and glutamate, attacks the carbamoyl group of the substrate glutamine to form a

covalent glutamyl-thioester intermediate, resulting in the abstraction of ammonia. In a second step, the thioester is hydrolyzed by an activated water molecule to release glutamate and to restore the enzyme. Both nucleophilic attacks involve a labile oxyanion intermediate state that is stabilized by two main chain amides forming the oxyanion hole. Class II or N-terminal nucleophile (Ntn) glutaminases in turn adopt an αββα-fold and are subject to auto-proteolytic activation to expose the N-terminal catalytic cysteine.[76] While the main catalytic activity is effectuated by the thiol group of cysteine activated by its free α-amino group, the reaction is in many cases supported by stabilizing or oxyanion hole-forming residues.[77]

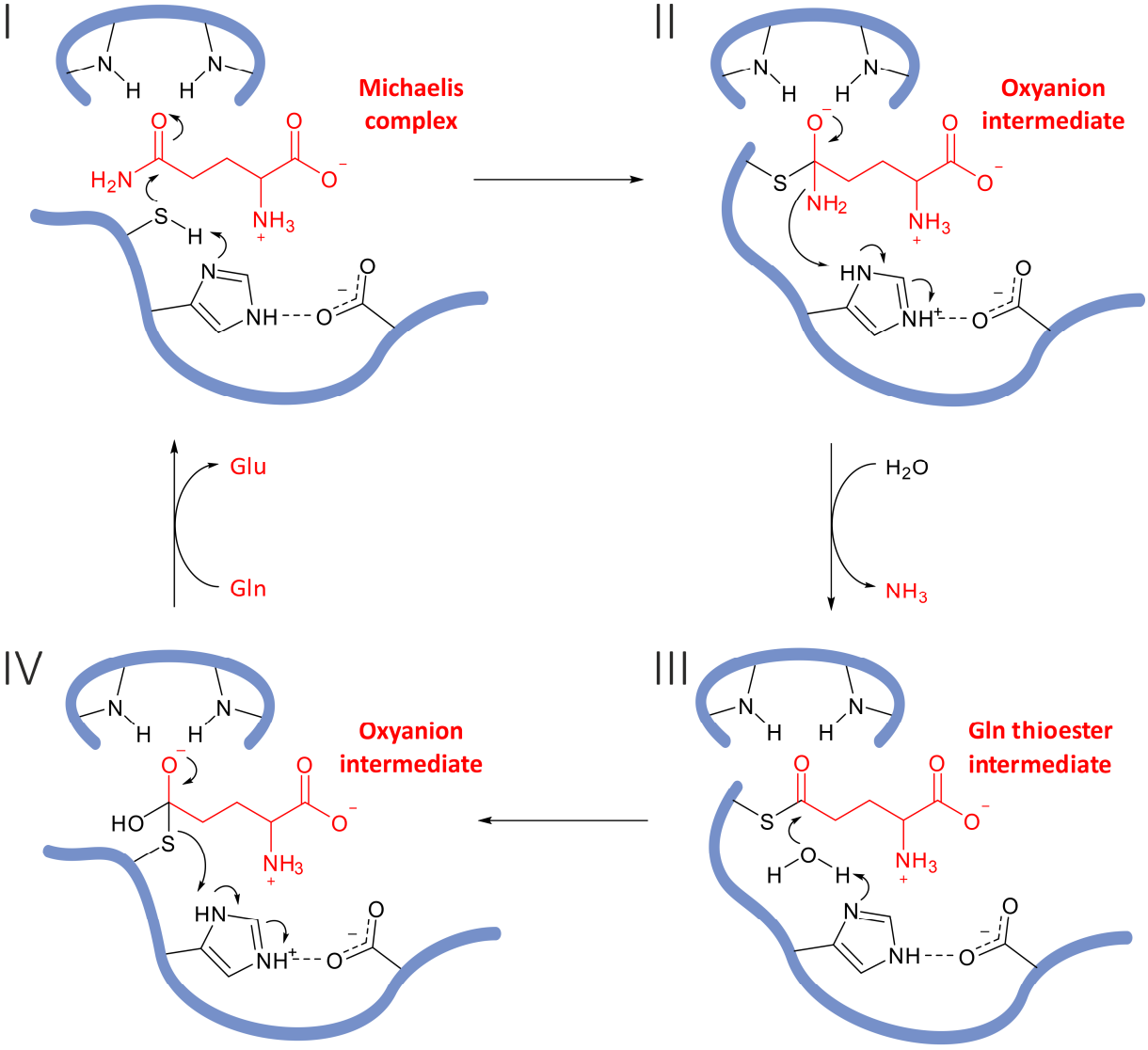

Figure 1.3: Reaction mechanism of class I glutaminases with a catalytic triad Cys-His-Glu. (I) The sulfhydryl group of the catalytic cysteine, which is deprotonated by the adjacent acid-base catalysts histidine and glutamate, attacks at the carbamoyl group of the substrate glutamine (red). (II) The tetrahedral oxyanion intermediate state is stabilized by two amides forming the oxyanion hole. (III) Upon abstraction of ammonia, a stable glutamyl-thioester intermediate is formed. (IV) Hydrolysis by an activated water molecule results in the release of glutamate and the restoration of the enzyme via a second oxyanion intermediate state.[78, 79]

To avoid the unproductive hydrolysis of glutamine and the release of toxic ammonia into the cell, the activity of the glutaminases is triggered by the presence of the respective synthase and, in most cases, the binding of acceptor substrate(s) to the active site of the synthase. In more complex GATases, the activities of both glutaminase and synthase are additionally under the control of (feedback) effectors. The underlying molecular control mechanisms vary among GATases and can influence both the turnover number k_{cat} and the Michaelis constant K_M of the glutaminase.[80] In terms of the activation mechanism, GATases usually combine a number of features from a collective toolbox in an individual manner, including the reorientation or amendment of the glutamine binding site and catalytic residues, the formation of the oxyanion hole, control of oligomerization and subunit orientation, rearrangement of disordered interface loops and formation or dilation of the ammonia channel.[68, 69, 71, 80]

In contrast to the glutaminases, the associated synthases belong to many different protein families with diverse, unrelated folds and substrates. It is thus likely that extant synthases evolved independently, starting from ammonia-dependent enzymes that improved their catalytic efficiency by recruiting one of the two glutaminase ancestors. In the course of evolution, gene duplication events and mutations could have led to the specification of the respective GATase. This hypothesis is in line with the observation that many synthases not only employ ammonia provided by their glutaminase, but can also use free dissolved ammonia at elevated pH-values.[65, 73, 81]

Of the many postulated ancestors of extant synthases, one was likely the progenitor of at least five related enzymes, the MST (menaquinone, siderophore, tryptophan biosynthetic) enzymes with a shared fold featuring two central bent β-sheets enclosed by α-helices.[69, 82-87] MST enzymes catalyze Mg^{2+}-dependent nucleophilic substitution reactions (S_N2'') on chorismate, which is produced from phosphoenolpyruvate and erythrose-4-phosphate in the shikimate pathway and represents a central metabolic node for the biosynthesis of aromatic and cyclic compounds in primary and secondary metabolism.[88] Two out of the five enzymes, salicylate synthase (SS) and isochorismate synthase (IS), use water as a nucleophile to catalyze the isomerization of chorismate to salicylate and isochorismate, respectively, which in prokaryotes represents the first step in the biosynthesis of organism-specific siderophores and the electron carrier menaquinone (**Figure 1.4**).[89, 90] The other three MST enzymes, aminodeoxychorismate synthase (ADCS), anthranilate synthase (AS) and aminodeoxyisochorismate synthase (ADICS), are GATases with an associated glutaminase and perform an amination reaction to catalyze the committed steps of folate, tryptophan and phenazine biosynthesis,

respectively (**Figure 1.4**).[91-93] In all MST enzymes except ADCS, the nucleophile (either water or ammonia) directly attacks at the C2-position of chorismate to substitute the protonated hydroxyl group at the C4-position.[87] ADCS is an exception insofar as two nucleophilic reactions take place and the attacking nucleophile varies between different organisms: First, a nucleophilic attack at the C2-position of chorismate is performed by either a catalytic lysine (for example in *E. coli*) or by ammonia (for example in *Stenotrophomonas maltophilia*), resulting in the loss of water at the C4-position. In the second step, ammonia attacks at the C4-position to release either the enzyme or the initial ammonia molecule from the reaction intermediate.[94-96] Besides their isomerization or amination activities, SS and AS enzymes have an additional lyase activity to yield the corresponding aromatized product and pyruvate, which requires separate enzymes in the other pathways, such as the pyridoxal phosphate-dependent aminodeoxychorismate lyase PabC.[82]

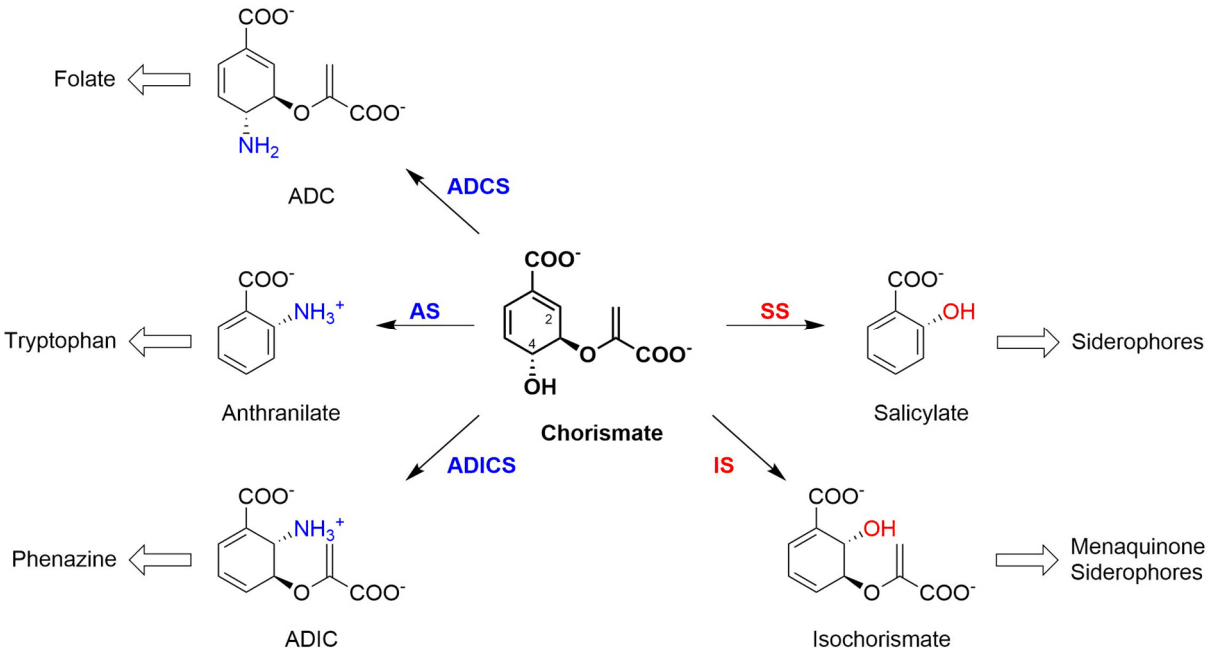

Figure 1.4: MST enzymes acting on the central metabolite chorismate. Chorismate, which is generated in the shikimate-pathway, is the substrate of at least five different MST enzymes. The ammonia-utilizing enzymes (blue), aminodeoxychorismate synthase (ADCS), anthranilate synthase (AS) and aminodeoxyisochorismate synthase (ADICS), produce aminodeoxychorismate (ADC), anthranilate and aminodeoxyisochorismate (ADIC), respectively. The water-utilizing enzymes (red), salicylate synthase (SS) and isochorismate synthase (IS), produce salicylate and isochorismate, respectively. The most common products of the respective bacterial pathways are indicated by white arrows.[82]

From the three ammonia-utilizing MST enzymes, only ADCS and AS are involved in primary metabolism and enable *de novo* biosynthesis of folate and tryptophan in bacteria, yeasts, fungi and plants, while animals rely on a dietary intake.[97] Despite the contribution of ADCS and AS to independent metabolic pathways, they are evolutionary interrelated[98] and a large fraction of

bacteria only provide one single glutaminase that serves both synthases, whereas another group of mostly γ-proteobacteria possesses two glutaminases that are specifically recognized by the respective synthases via a tailored interface add-on.[99] In these organisms, ADCS is formed by the glutaminase PabA and the synthase PabB whereas AS consists of the glutaminase TrpG and the synthase TrpE. Another hint on a shared evolutionary history is the presence of a conserved tryptophan binding site adjacent to the chorismate-binding site. While in AS, tryptophan binding is part of the feedback regulation and inhibits the activities of both the glutaminase and the synthase,[100-103] no functional role could be assigned to tryptophan binding in ADCS, where it is permanently bound and was most likely transformed into a structural element during evolution.[85] Interestingly, in another organism, *Cytophaga hutchinsonii*, the tryptophan binding site of ADCS is occupied by an intrinsic phenylalanine.[104] Similar observations have been made in the other enzymes of the MST family, in which the respective binding site is also occupied by intrinsic aromatic amino acid side chains.[105-107]

1.4 Aims of this thesis

Structures of AS from different organisms and with different ligands have been determined and mechanisms for the activation of TrpG by TrpE have been postulated.[69, 83, 103] However, whereas a structure of the ADCS complex from *Streptomyces venezuelae* has been determined, only limited insights into activation mechanisms could be gained from this structure. Therefore, in the first project described in this thesis (Chapter 2), the molecular mechanisms underlying the activation of PabA by PabB in *E. coli* were elucidated by a combined structural and functional approach and compared to the mechanisms of evolutionary related enzyme complexes.

In the second research project (Chapter 3), the functional essentiality of subunit association and the high degree of conservation of the PabA-PabB and TrpG-TrpE interfaces suggested that a bispecific PPI inhibitor could act as an antibiotic that simultaneously impedes the activities of both ADCS and AS and hence prevents the biosynthesis of folate and tryptophan. A bacteriostatic effect of ADCS and AS complex disruption could be confirmed, indicating that the glutaminase-synthase interfaces of these GATases might serve as novel antibiotic drug targets.

2 Molecular mechanism of glutaminase activation in aminodeoxychorismate synthase

2.1 Introduction

Understanding catalytic mechanisms and structure-function relationships in multi-enzyme complexes at the molecular level remains a major challenge. This also applies to the architecturally and mechanistically rich family of glutamine amidotransferases (GATases) that are responsible for the incorporation and transfer of nitrogen within numerous metabolic pathways.[65, 78, 80, 81] Typically, GATases form bi-enzyme complexes, consisting of a glutaminase subunit that hydrolyses glutamine (Gln) and a synthase subunit that incorporates the nascent ammonia into its specific substrate. Since ammonia is protonated and thus inactivated under physiological pH conditions, there is a strict requirement for transfer of ammonia from the glutaminase active site to the synthase active site sequestered from any external solvent. To achieve this, both enzymatic activities are mutually coupled: In particular, glutamine hydrolysis at the glutaminase subunit is regulated by the interaction with the synthase subunit and, in some cases, is additionally activated allosterically by substrate binding to the distal active site of the synthase subunit.[108-110]

Based on available data, the interplay of glutaminase and synthase activity occurs at multiple levels: First, there is a requirement to rearrange the glutaminase active site from a Gln accessible state to an arrangement that ensures the solvent-shielded production of reactive ammonia. This is largely achieved by well-defined glutaminase-synthase subunit (or domain) rearrangements and conformational changes in interface loops.[80, 81] Second, the activity of GAT complexes depends on a functional tunnel between the active sites. Clogged (or leaky) tunnels can produce (or release) restraints on the glutaminase active site that may generate local product inhibitory conditions.[81, 108] Next, most synthases contribute directly to the activity of their glutaminase, for example by inducing a productive orientation of the catalytic triad,[109] by supporting oxyanion hole formation,[68] or by contributing to the Gln binding pocket. Finally, there are allosteric mechanisms to synchronize glutaminase and synthase activities, induced by binding of the synthase substrate or other allosteric effectors regulating the enzymatic activity of both the glutaminase and the synthase subunit by long-range conformational changes.[80, 111]

A major challenge in the study of GATases lies in the definition of molecular mechanisms and structural rearrangements underlying the functional coupling of the two catalytic activities, glutamine hydrolysis and synthase activity. This problem was approached on the example of the class I GATase aminodeoxychorismate synthase (ADCS). ADCS, which consists of the glutaminase subunit PabA and the synthase subunit PabB, catalyses the committed step in folic acid biosynthesis, the amination of chorismate to 4-amino-4-deoxy-chorismate (**Figure 1.4**). Similar to other class I glutaminases (**Figure 1.3**), the active site of PabA from *E. coli* consists of the catalytic triad residues cysteine (aC79), histidine (aH168) and glutamate (aE170).[112] The oxyanion hole is formed by the two backbone amide protons of aG52 and aL80. To facilitate nomenclature, the small letters "a" or "b" preceding numbered residues denote residues from PabA or PabB, respectively.

Like in other GATases, the glutaminase activity of the PabA subunit is largely dependent on interactions with its synthase.[79, 110, 113] Catalytic efficiency of PabA is stimulated mainly through complex formation with the synthase PabB and, to a low extent, the turnover number is further enhanced by binding of chorismate to the active site of PabB.[114] Although amino acid residues involved in complex formation between PabA and PabB[115] and allosteric signal propagation[79] have been identified by alanine scanning approaches, elucidation of the mechanism behind glutaminase activation has been hampered by the lack of structural information. To date, several crystal structures of the PabB subunit,[85, 96, 104] the structure of an ancestral PabA subunit[79] and the structure of a fused ADCS enzyme from secondary metabolism[70] have been determined, however, structural information for an individual extant PabA subunit or the active conformation of the heterodimeric PabA-PabB complex were not available up to now.

This work describes X-ray crystal structures of the PabA subunit from *E. coli* in its apo form, of the PabA-PabB complex in its apo form and of several PabA-PabB complexes obtained in the presence of the substrates glutamine (in the form of the glutamyl-thioester intermediate) and/or chorismate. These structures reveal a drastic relative rearrangement of the PabA and PabB subunits upon glutamyl-thioester formation. In addition, a comparison of different structures allowed to identify residues in the PabA-PabB interface that change their conformation and alter their mode of interaction in the course of a catalytic cycle. By substituting eligible amino acids, their importance for complex affinity and glutaminase activity was evaluated by means of analytical gel filtration (GF), isothermal titration calorimetry (ITC), and steady-state enzyme kinetics.

By proceeding in this way, two primary molecular mechanisms for the activation of the glutaminase activity by PabB were identified. Firstly, binding of PabB reduces the degree of flexibility found in PabA interface residues, which directly affects the configuration of the catalytic triad in the active site of PabA. Secondly, Gln binding and the rearrangement of the PabA-PabB interface are coupled processes, resulting in the formation of a closed complex conformation and completion of the Gln binding pocket. On the basis of these results, a motion-dependent model for the catalytic activity of PabA is proposed, which determines the overall activity of the PabA-PabB complex.

2.2 Results

2.2.1 The glutaminase activity of ADCS depends on complexation with its synthase

The elucidation of the molecular processes underlying subunit interaction, the mutual stimulation and the overall reaction of the glutaminase PabA together with its synthase PabB requires a profound biophysical and structural characterization of the ADCS complex and its individual components. To obtain the proteins, the *E. coli pabA* and *pabB* genes were individually cloned into a pET28a vector, overexpressed in *E. coli* cells and purified by Ni-affinity chromatography. After removal of the polyhistidine-tag by TEV-cleavage, the proteins were further purified by reverse Ni-affinity chromatography and size exclusion chromatography. The attachment of a Gly_5His-linker between the sequence of the TEV cleavage site and the *pabA*-gene drastically improved the stability and solubility of PabA and increased TEV cleavage efficiency without impacting the catalytic activity of PabA, and was therefore applied for purification of all PabA proteins in this thesis.

Glutaminase activity was followed by a steady-state coupled enzymatic assay with the auxiliary enzyme glutamate dehydrogenase, which couples the hydrolysis of Gln to the spectroscopically accessible reduction of NAD^+. The activity of PabA alone, in the presence of PabB and in the presence of both PabB and its substrate chorismate (Cho) was measured. In agreement with published data,[79] the catalytic efficiency (k_{cat}/K_M^{Gln}) of PabA is greatly increased in the presence of PabB, which stimulates the turnover number of PabA more than 50-fold and decreases K_M^{Gln} by a factor of 135 (**Table 2.1**). In contrast, binding of chorismate to the active

site of PabB has only little effect on PabA activity. The k_{cat}/K_M^{Gln} value of PabA is even two-fold reduced by the presence of Cho, due to a 4-fold increased K_M^{Gln} and a two-fold increased k_{cat}. However, since the Gln concentration in *E. coli* (3.8 mM)[116] exceeds K_M^{Gln}, both in the absence (0.09 mM) and the presence (0.34 mM) of chorismate, a slight allosteric activation of PabA by chorismate can be assumed under physiological conditions.

For comparison, the stimulation profile of the homologous *E. coli* TrpG-TrpE anthranilate synthase complex, which catalyzes the transformation of Cho to anthranilate, was also analyzed. As with PabA, the catalytic efficiency (k_{cat}/K_M^{Gln}) of TrpG is increased by several orders of magnitude upon complex formation with its synthase. However, in contrast to ADCS, the presence of Cho leads to an additional 20-fold stimulation of the glutaminase activity with regard to k_{cat}/K_M^{Gln}. While the activation tendencies appear to be overall similar in both complexes, only the ADCS complex was further analyzed in this work.

Table 2.1: Stimulation of glutaminase activities by the respective synthases and chorismate in ADCS and AS.

Glutaminase	Synthase	Cho	K_M^{Gln} [mM]	k_{cat} [s^{-1}]	k_{cat}/K_M^{Gln} [$mM^{-1}s^{-1}$]
PabA	-	-	12.2 ± 0.54	$4.4 *10^{-3} \pm 6.1 *10^{-5}$	$3.6 *10^{-4} \pm 2.1 *10^{-5}$
PabA	**PabB**	-	0.09 ± 0.01	0.22 ± 0.007	2.41 ± 0.47
PabA	**PabB**	+	0.34 ± 0.03	0.37 ± 0.010	1.09 ± 0.13
TrpG	-	-	>50	>0.002	$4.8 *10^{-5} \pm 2.2*10^{-6}$
TrpG	**TrpE**	-	1.18 ± 0.04	0.17 ± 0.002	0.15 ± 0.01
TrpG	**TrpE**	+	0.29 ± 0.01	0.90 ± 0.009	3.17 ± 0.16

Glutaminase activity was followed at 25 °C in 50 mM Tricine pH 8.0, 5 mM $MgCl_2$, 150 mM KCl, 1 mM DTT, 10 mM NAD^+, 1 mg/ml GDH, varying Gln concentrations and, if indicated, 200 µM Cho. Glutaminases were added at concentrations of 0.25 µM, synthases at 1 µM. In the absence of synthases, the glutaminase concentration was increased to 5 µM.

The association of PabA and PabB, which, based on the activity assays, plays a crucial role in the activation of PabA, was analyzed by analytical gel filtration (GF) and ITC. As early works demonstrated a stabilizing effect of the substrate Gln on the complexation of PabA and PabB,[117] GF experiments were performed both in the absence and presence of Gln. ITC measurements were only conducted in the absence of Gln, since the reaction heat of Gln turnover distorts the measured ITC signals, even when using a catalytically inactive PabA variant aC79A. As expected, the wild-type proteins exhibited stable and glutamine-independent PabA-PabB complexation in GF, which is reflected in a low K_D value of 160 nM in ITC measurements

(**Table 2.3**). As described below, several enzyme variants showed Gln-dependent elution profiles, demonstrating the feasibility of this approach to evaluate PabA-PabB complex stabilization by Gln.

2.2.2 Structural characterization of the PabA-PabB complex

An in-depth analysis of the mechanistic and regulatory roles of PPIs within the PabA-PabB complex is dependent on the structural elucidation of various complex structures in the course of the enzymatic reaction. While the small size of the complex impeded structure determination via cryogenic electron microscopy, X-ray crystallography has less limitations in protein size but requires homogeneous and well-diffracting protein crystals. A thorough screening of buffers, additives and protein concentrations yielded suitable crystallization conditions that produced large PabA-PabB crystals of high quality (**Figure 2.1A**). The identity and composition of the PabA-PabB crystals was confirmed by an analysis of washed and dissolved crystals via SDS-gel electrophoresis (**Figure 2.1B**). Interestingly, the number, size and overall appearance of the crystals was significantly improved when Gln was added to the crystallization buffer, underlining the stabilizing effect of Gln on PabA-PabB complexes. Structure determination was performed by Dr. Sihyun Sung in the group of Prof. Dr. Matthias Wilmanns at the EMBL in Hamburg, who additionally established crystallization conditions for the isolated PabA subunit.

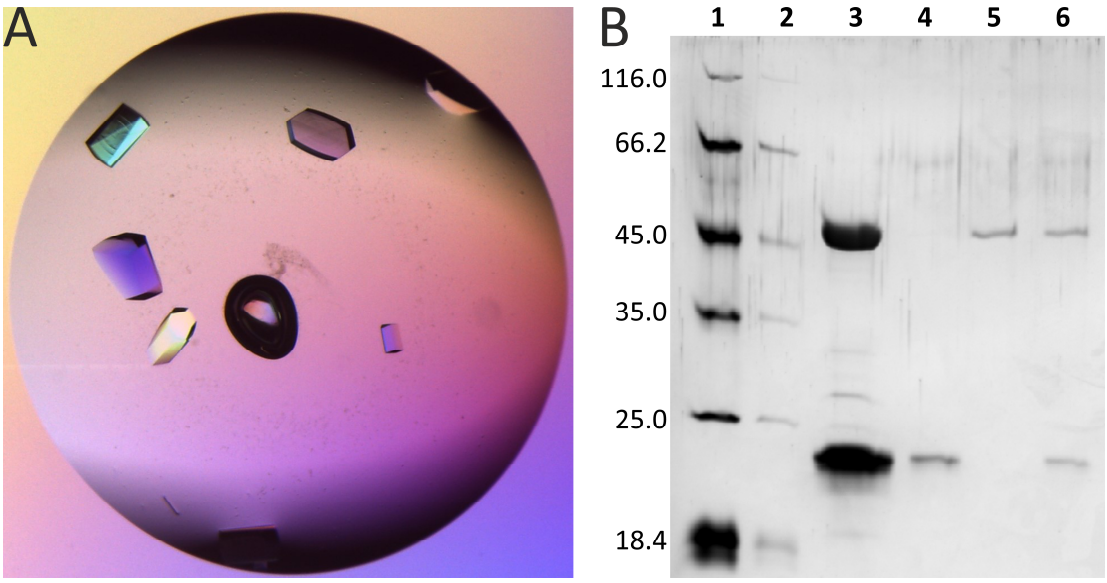

Figure 2.1: Crystals of the PabA-PabB complex and SDS-PAGE crystal analysis. (A) Exemplary microscopic image of high-quality PabA-PabB crystals obtained by a thorough screening of crystallization conditions. (B) SDS-PAGE followed by silver staining confirmed the protein content of PabA-PabB crystals. Lanes 1 and 2: Low molecular weight protein standard, respective molecular masses in kDa are indicated; lane 3: Washed and dissolved crystals; lane 4: Purified PabA; lane 5: Purified PabB; lane 6: Equimolar mixture of purified PabA and PabB.

As a result, one crystal structure of the isolated PabA subunit and four crystal structures of the PabA-PabB complex with different substrates were solved at resolutions between 1.64 Å and 2.82 Å (**Table 2.2, Figure 2.2**). The crystal structure of PabA contains three independent PabA chains without any ligands bound. All PabA-PabB crystals comprise two heterodimeric ADCS complexes, assembled by chains A/D and chains B/C, respectively. As expected, the observed PabA-PabB configurations are related to structures of other ammonia-utilizing MST enzymes, however, depending on the presence of substrates and ligands, the observed conformations displayed a remarkable degree of variability. In the PabA-PabB crystals grown without Gln, interestingly, one of the two heterodimers was formed across symmetry-related PabA and PabB subunits. To rule out any uncertainty because of experimental errors in unit cell calculation, only the heterodimer formed within the same asymmetric unit (chains B/C) was used for further analysis of these structures. Surprisingly, in the apo structure, the Gln binding pocket was not empty, but revealed an electron density corresponding to a zinc ion. Accordingly, incubation of such crystals with EDTA resulted in a very similar structure, however without the additional electron density of Zn^{2+}. An in-depth analysis about the role of this metal ion will be described in a subsequent section. Upon addition of Gln to the crystallization buffer, the glutaminase subunit of one of the heterodimers (chains A/D) displayed a glutamyl-thioester (Gln-TE) adduct covalently bound to the catalytic cysteine aC79, representing the stable catalytic intermediate state (**Figure 1.3**), whereas the PabA active site of the other heterodimer (chains B/C) was unoccupied. Furthermore, structures with bound Gln-TE exhibit a solvent molecule that interacts with the main chain carbonyl group of aY127 and the imidazole ring of aH168. Due to its proximity to the reactive carbon atom of the Gln-TE (<3 Å), this solvent molecule approximates both the expected leaving position of ammonia abstracted from the oxyanion intermediate and the position of the hydrolyzing water (**Figure 1.3**), but cannot be identified unequivocally due to the similar size and electron density distribution of ammonia and water.

Table 2.2: Summary of crystal structures solved in collaboration with Dr. Sihyun Sung.

Crystal	Resol. [Å]	Conditions	Bound Ligands	Δφ(PabA-PabB)[a]	ASA [Å^2][b]
PabA	2.82	-	Chains A, B, C: -		
PabA-PabB apo	2.45	-	Chains A/D: Trp, Zn^{2+} Chains B/C: Trp, Zn^{2+}	Reference	904
PabA-PabB EDTA	1.98	EDTA	Chains A/D: Trp Chains B/C: Trp	0	965
PabA-PabB Gln	1.86	Co-crystallized with Gln	Chains A/D: Trp, Gln-TE Chains B/C: Trp	A/D: 23.4° B/C: 7.4°	A/D: 1312 B/C: 1024
PabA-PabB Gln Cho	1.64	Co-crystallized with Gln, soaked with Cho	Chains A/D: Trp, Gln-TE, Cho, Mg^{2+} Chains B/C: Trp, Cho, Mg^{2+}	A/D: 23.2° B/C: 8.2°	A/D: 1324 B/C: 971

[a] Change of orientation of the PabB principal axis calculated with PSICO by Prof. Dr. Matthias Wilmanns, resulting from PabA-based superposition and using PabA-PabB apo as reference.
[b] Accessible surface area (ASA) as calculated by Prof. Dr. Matthias Wilmanns.

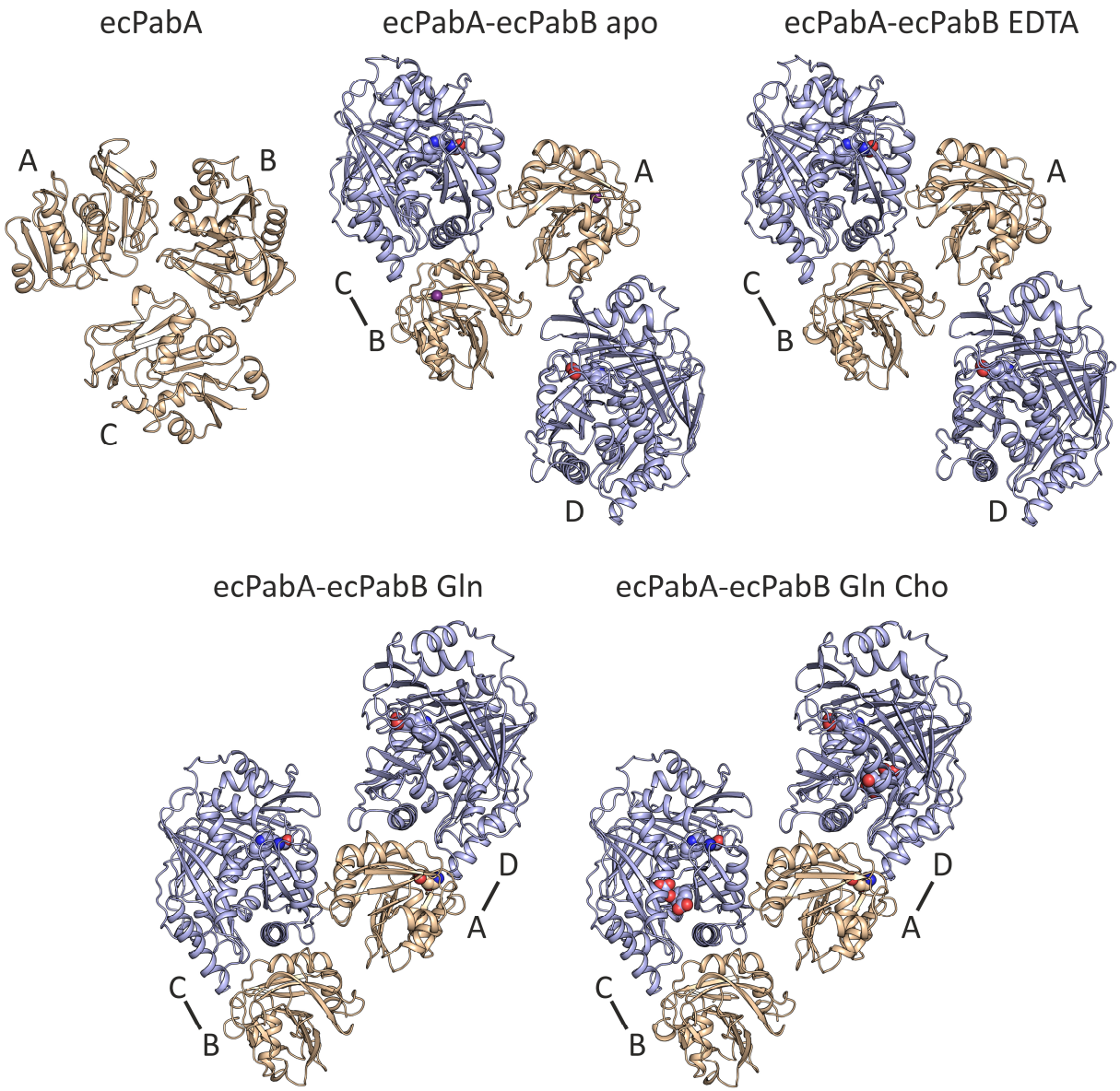

Figure 2.2: Crystal structures of *E. coli* PabA and PabA-PabB. Shown are the asymmetric units of the respective crystals. The structure of PabA comprises three individual PabA chains A, B and C per asymmetric unit. In PabA-PabB crystals grown in the absence of Gln (apo or EDTA), the second heterodimer (chains A/D) forms across adjacent asymmetric units. In PabA-PabB crystals grown in the presence of Gln (Gln and Gln Cho), both ADCS complexes (chains B/C and chains A/D) are situated within the same asymmetric unit and one of the heterodimers contained a covalent Gln-TE adduct. Glutaminase subunits are colored in wheat, synthase subunits in light blue. Bound ligands are shown as spheres. Chain indicators and subunit association are marked adjacent to the structures.

Due to the limited stability of Cho in solution, co-crystallization attempts were not successful. However, soaking crystals (grown in the presence of Gln) in a solution containing Cho resulted in PabA-PabB structures with Cho bound to both synthase subunits. As in crystals obtained without Cho, the Gln-TE was found in the glutaminase subunit of only one heterodimer (chains A/D). Similar to previous observations of related MST enzymes,[82] the benzoate moiety of Cho is complexed by a magnesium ion, which interacts with several mostly negatively charged residues via two structurally conserved water molecules (**Figure 2.3A**).

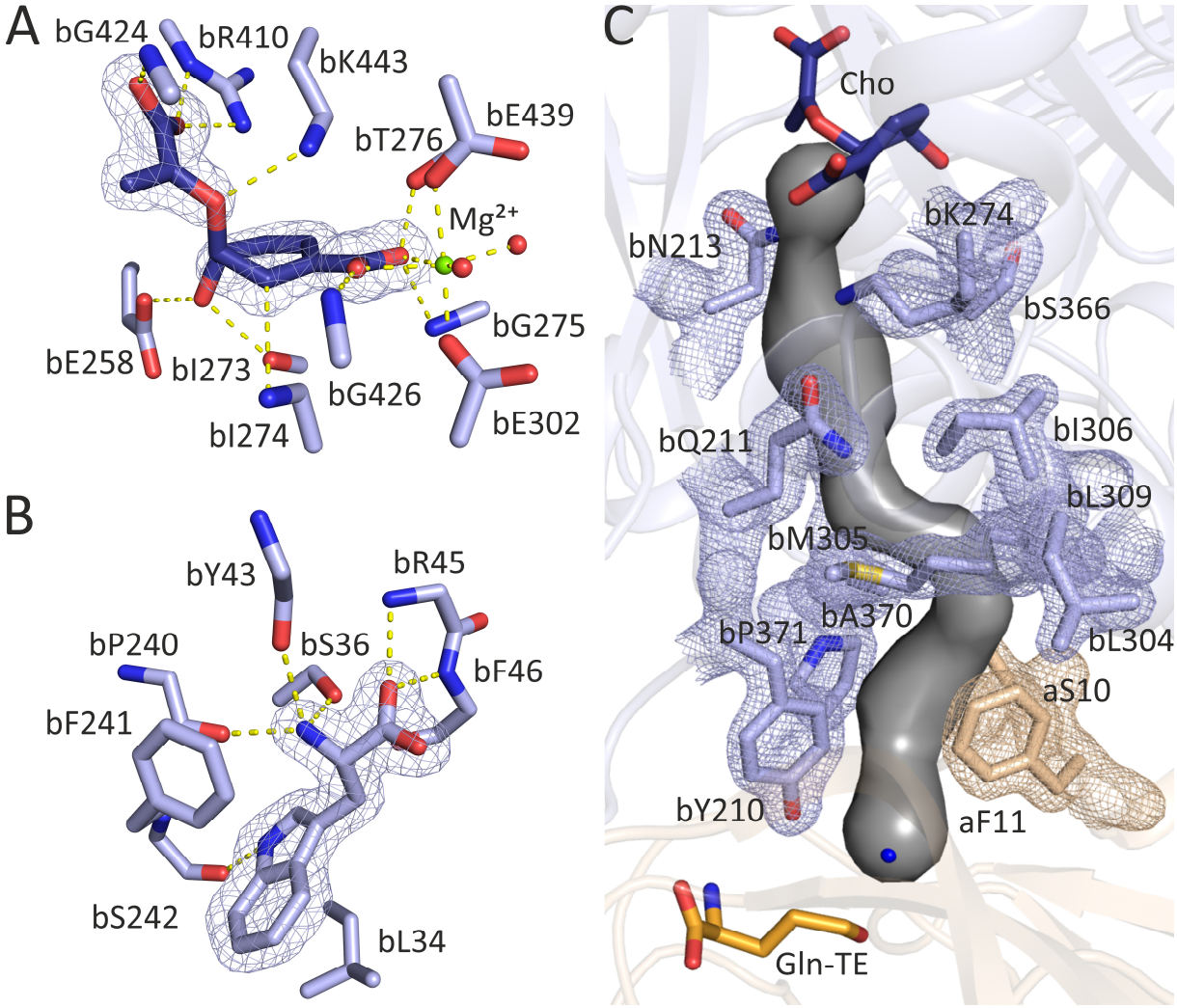

Figure 2.3: Binding sites of Cho and Trp and ammonia tunnel. (A) Chorismate (dark blue) is bound to the active site of PabB by an intricate network of PabB side chains (light blue) with a water-coordinated (red spheres) Mg^{2+} ion (green) bound to the benzoate moiety. The incomplete coverage of electron densities (blue mesh) to the modelled chorismate remains enigmatic, but is in line with previously determined Cho-binding sites in MST enzymes.[69, 107] (B) The non-covalently bound tryptophan molecule is a structural element of PabB without known functional role. (C) The ammonia tunnel connecting the Gln-TE (orange) in the active site of PabA with Cho (dark blue) in the active site of PabB was modelled using the Caver 3.0.3 plugin in PyMol with a probe radius of 0.8 Å of the PabA-PabB structure in the presence of the Gln-TE and Cho. The solvent molecule likely representing attacking water or abstracted ammonia (blue sphere) was used as the starting point. Since the ε-amino group of the catalytic K274 is not structurally resolved but modelled as intruding to the potential tunnel, it was excluded from the analysis. Electron density maps (blue or wheat mesh) are contoured at 1.5 sigma.

In line with previous observations, all complex structures revealed a tryptophan molecule bound to a structurally conserved binding site in PabB outside of the active site.[84, 95] This tryptophan molecule is thought to play a structural role and testifies for the evolutionary relationship to TrpE, in which tryptophan binding is part of a feedback control mechanism (**Figure 2.3B**).[100-103]

The active sites of PabA and PabB are connected by a mostly hydrophobic tunnel required for the solvent-excluding transport of ammonia from its production site in PabA to its incorporation site in PabB (**Figure 2.3C**). Since the glutaminase active site is close to the PabA-PabB interface, the tunnel is mainly constituted by PabB residues with several PabA residues flanking

the entrance. However, based on an analysis using the Caver tool,[118, 119] parts of this tunnel appear to be too narrow (0.8 Å) to allow unhindered transport of ammonia. This differs from observations made in other GATases but is likely compensated by side chain motions during catalysis.[120-122]

2.2.3 Glutamyl-thioester formation induces PabA-PabB subunit rearrangements

The determination of PabA-PabB structures representing different catalytic states allowed for the analysis of subunit rearrangements upon binding of the substrates and enabled conclusions on the motions accompanying the catalytic cycle. Upon binding of Cho to the active site of PabB, no significant alterations of the PabA-PabB arrangement and only minor side chain reorientations close to the active site of PabB were detected, in agreement with its minor effect on the catalytic activity of PabA (**Figure 2.4D**, **Table 2.1**, **Table 2.2**). In contrast, the presence of the Gln-TE in the active site of PabA induced a major change of the principal PabA-PabB subunit axis orientation by approximately 23°, when using the PabA-PabB apo structure as a reference (**Table 2.2, Figure 2.4A-C**). The obtained crystal structures illustrate at least two states of the PabA-PabB complex, now referred to as the open complex state in PabA-PabB apo and the closed complex state with bound Gln-TE. Rearrangements in the course of the catalytic cycle have direct consequences on the size of the interface between the two subunits, which is consistently increased upon formation of the Gln-TE. More specifically, it is extended from an area of around 1000 $Å^2$ in the absence of the Gln-TE to about 1300 $Å^2$ in the presence of Gln-TE (**Table 2.2**). This interface expansion leads to complete sealing of the PabA active site, which is a prerequisite for solvent-shielded Gln-TE binding. Interestingly, the PabA-PabB complexes void of Gln-TE but obtained in the presence of Gln (Chains B/C) displayed a rotational movement of approximately 8° using the same PabA-PabB apo reference, indicating that they represent a catalytic state just prior to or subsequent to formation of the Gln-TE. The presence of both states within the same Gln-grown crystals further supports a relative movement of the subunits during catalysis.

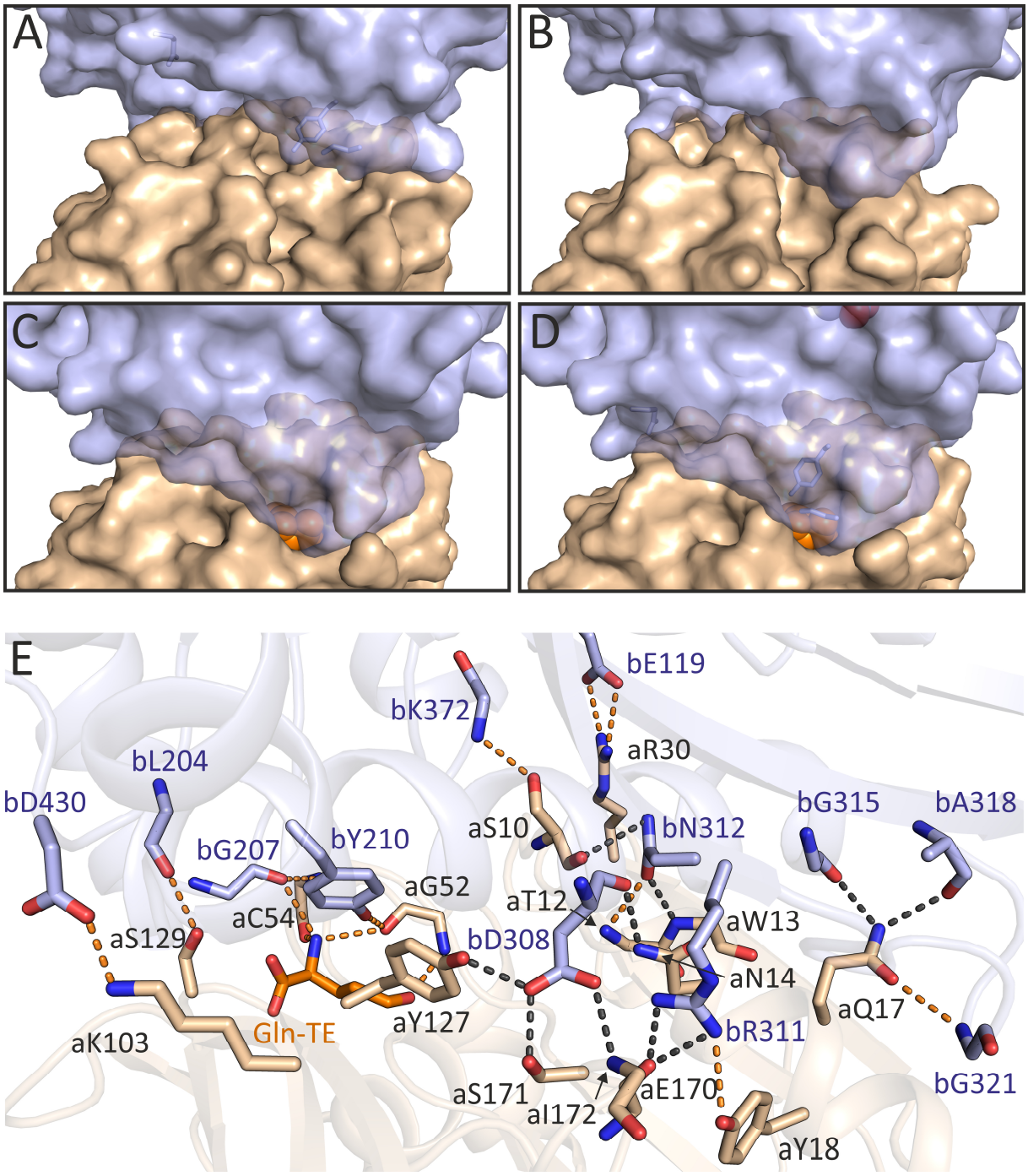

Figure 2.4: PabA-PabB subunit rearrangements upon Gln-TE formation. PabA subunits and residues are colored in wheat, PabB subunits and residues are colored in light-blue, the Gln-TE is colored in orange. (A) The interface region in PabA-PabB apo (chains B/C) represents the open complex state. Sticks representing bE119, bG207 and bY210 are shown to facilitate spatial orientation. (B) The interface region in PabA-PabB without Gln-TE despite its presence in the crystallization buffer (PabA-PabB Gln chains B/C, same observations in PabA-PabB Gln Cho chains B/C) displays a small increase in interface area due to an 8° rotational movement of PabB. (C) PabA-PabB Gln (chains A/D) is in the closed complex state, exhibiting a drastically increased interface area due to a Gln-TE-induced PabB rotational movement of 23° that results in the sequestration of the Gln-TE (orange spheres) in its binding pocket. (D) The additional presence of Cho (spheres) in PabA-PabB Gln Cho crystals (chains A/D) has no further impact on subunit orientations. Sticks representing bE119, bG207 and bY210 are shown to facilitate spatial orientation. (E) The formation of the Gln-TE induces additional molecular interactions between PabA and PabB. Gln-TE independent interactions are marked as grey dashes, Gln-TE-induced interactions are marked as orange dashes.

At a molecular level, clusters of PabA-PabB interface residues can be identified, that either interact in a Gln-TE-independent manner or only come into contact upon Gln-TE-induced subunit rearrangements (**Figure 2.4E**). The former includes aS10, aW13, aN14, aQ17, aY127, aE170, aS171 and aI172, that interact with bD308, bR311, bN312, bG315 and bA318. Upon formation of the Gln-TE, additional interactions are formed between the PabA residues aT12, aY18, aR30, aG52, aC54, aK103 and aS129 and the PabB residues bE119, bL204, bG207, bY210, bG321, bK372 and bD430. Interestingly, the majority of PabA residues contributing to this expanded PabA-PabB interface are located at the N-terminal segment of PabA. The conformational changes are most visibly illustrated by a long-range movement of residue bE119 from the PabB subunit, which is located in 10-13 Å distance from any PabA residues in different ADCS structures without Gln-TE. In the presence of Gln-TE however, the same residue forms a salt bridge with aR30 from the PabA subunit (**Figure 2.4A, D, E, Figure 2.5A**).

2.2.4 Model for glutamine binding and turnover

To analyze the functional implications and the role of selected interface residues in the observed PabA-PabB subunit rearrangement upon Gln-TE formation, the effect of selected representative amino acid exchanges on complex affinity and glutaminase activity was investigated. The first pair of residues, aR30 and bE119, is located at the edge of the PabA-PabB interface distant from the active site and interacts via a salt bridge only when the Gln-TE is bound to PabA (**Figure 2.4A, D, E, Figure 2.5A**). Therefore, respective mutations are expected to affect the subunit rearrangement without a direct impact on the active site of PabA. Charge-reversing side chain substitutions (aR30E, bE119R) and a shortened side chain (bE119D) were introduced, which were expected to shift the PabA-PabB conformational equilibrium in the presence of Gln to the open complex state. All three variants aR30E, bE119R and bE119D formed relatively stable and Gln-independent complexes with the respective wild-type partner on the GF column, in line with only minor decreases in PabA-PabB affinity in ITC measurements (**Table 2.3**). These observations confirm that the aR30-bE119 salt bridge is not mandatory for initial PabA-PabB complex formation. At the same time, all three variants displayed wild-type-like glutaminase turnover numbers k_{cat}, but drastically increased K_M^{Gln} values (**Table 2.3**). The impact on K_M^{Gln} scales with the introduced change of functional groups: While charge-preserving shortening of the side chain in variant bE119D results in a moderate 5-fold increase of K_M^{Gln}, the introduction of an electrostatic repulsion, as for the variants aR30E or bE119R, leads to a 20-fold increase in K_M^{Gln} values. Given that both aR30 and bE119 are not directly

involved in Gln-TE binding, this data demonstrates that the controlled closure of the PabA-PabB complex is crucial for Gln binding and thus glutaminase activity.

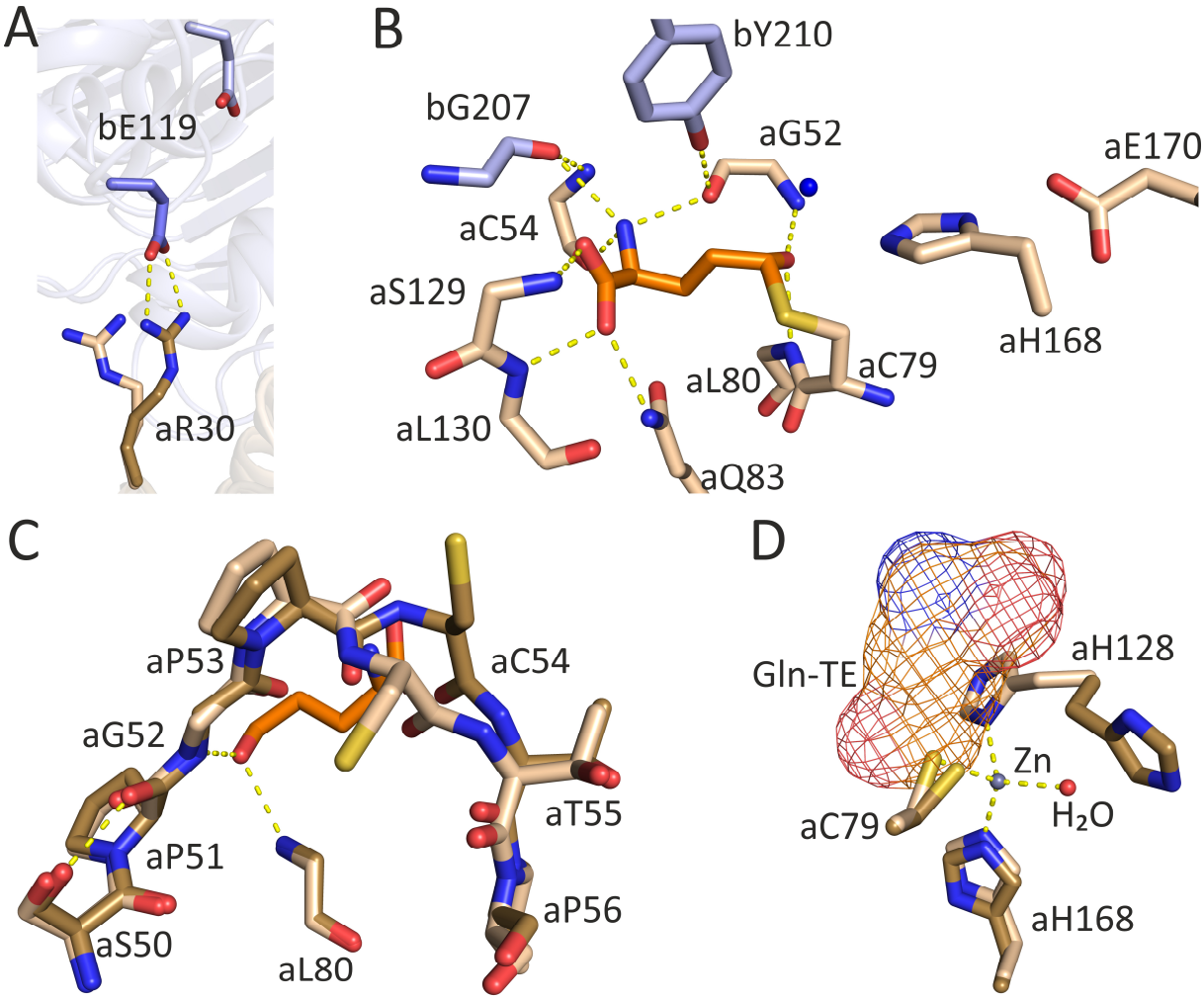

Figure 2.5: The impact of Gln-TE formation on selected residues. PabA residues are colored in wheat, PabB residues are colored in light-blue, the Gln-TE is colored in orange. Light colors represent the apo state, dark colors represent the Gln-TE bound state. (A) Upon formation of the Gln-TE, a salt bridge between aR30 and bE119 is formed as a consequence of the rotational movement of PabB. (B) The Gln-binding pocket (with Gln-TE covalently attached to the active site residue aC79) is formed by residues of both PabA and PabB. (C) While the formation of the Gln-TE induces a flip in aC54, which is in close proximity to the oxyanion hole forming residues aG52 and aL80, the conformation of the oxyanion hole itself is unchanged. (D) The structure of PabA-PabB apo displays a zinc coordinated in the PabA active site with unknown function. In the absence of zinc, aH128 flips from a position partially blocking the Gln binding site (displayed as mesh) to another conformation that does not hinder binding of Gln.

Table 2.3: Effects of mutations in PabA or PabB on PabA-PabB assembly and the catalytic activity of PabA.

PabA/PabB	ITC [a]	GF [b]		Catalytic activity [c]		
	K_D [µM]	-Gln	+Gln	K_M^{Gln} [mM]	k_{cat} [s^{-1}]	k_{cat}/K_M^{Gln} [$mM^{-1}s^{-1}$]
wt/wt	0.16 ± 0.06	+	+	0.34 ± 0.03	0.37 ± 0.010	1.09 ± 0.13
aR30E/wt	0.38 ± 0.20	+	+	6.42 ± 0.58	0.51 ± 0.014	$7.9 *10^{-2} \pm 9.3 *10^{-3}$
aS50A/wt	0.16 ± 0.03	+	+	2.58 ± 0.18	0.66 ± 0.013	0.26 ± 0.02
aP53A/wt	0.18 ± 0.07	+	+	0.65 ± 0.02	0.41 ± 0.004	0.63 ± 0.03
aC54A/wt	0.18 ± 0.12	+	+	0.36 ± 0.04	0.45 ± 0.011	1.24 ± 0.16
aC54G/wt	0.06 ± 0.02	+	+	0.33 ± 0.02	0.43 ± 0.007	1.28 ± 0.11
aY127A/wt	> 8	-	+	0.17 ± 0.02	0.02 ± 0.000	0.14 ± 0.01
aY127A, aS171A/wt	n. b.	-	+/-	0.22 ± 0.01	0.01 ± 0.000	$5.5 *10^{-2} \pm 4.0 *10^{-3}$
aH128A/wt	0.37 ± 0.07	+/-	+/-	29.8 ± 1.73	0.28 ± 0.006	$9.2 *10^{-3} \pm 7.5 *10^{-4}$
aS171A/wt	0.92 ± 0.71	+/-	+	0.05 ± 0.00	0.08 ± 0.001	1.46 ± 0.08
wt/**bE119D**	0.84 ± 0.06	+	+	1.71 ± 0.05	0.59 ± 0.005	0.34 ± 0.01
wt/**bE119R**	0.54 ± 0.04	+/-	+/-	8.07 ± 0.83	0.48 ± 0.014	$6.0 *10^{-2} \pm 7.9*10^{-3}$
wt/**bS206G, bD208G, bC209G**	n. b. [d]	+	+	9.57 ± 0.39	0.43 ± 0.006	$4.5 *10^{-2} \pm 2.4*10^{-3}$
wt/**bG207P**	1.70 ± 0.60	+/-	+/-	18.7 ± 1.01	0.11 ± 0.002	$5.7 *10^{-3} \pm 4.3 *10^{-4}$
wt/**bY210A**	5.50 ± 2.90	-	+/-	2.73 ± 0.31	0.80 ± 0.028	0.29 ± 0.04
wt/**bY210F**	0.53 ± 0.10	+	+	1.48 ± 0.08	0.75 ± 0.011	0.51 ± 0.03
wt/**bD308A**	n. b.	-	-	8.57 ± 1.29	0.11 ± 0.005	$1.3 *10^{-2} \pm 2.5 *10^{-3}$
wt/**bD308E**	1.70 ± 0.48	-	+/-	0.19 ± 0.01	0.29 ± 0.005	1.54 ± 0.12
wt/**bD308N**	n. b.	-	-	2.63 ± 0.30	0.10 ± 0.003	$3.6 *10^{-2} \pm 5.5 *10^{-3}$
wt/**bR311A**	n. b.	-	-	3.94 ± 0.44	0.39 ± 0.010	0.10 ± 0.01
aH128A/bS206G, bD208G, bC209G				<50	>0,03	$5.4 *10^{-4} \pm 2.7 *10^{-5}$
aH128A/bG207P				<50	>0,006	$9.5 *10^{-5} \pm 3.9 *10^{-6}$
aH128A/bY210A				<50	>0,08	$1.5 *10^{-3} \pm 5.3 *10^{-5}$

[a] K_D values were determined via ITC in 50 mM Tris/HCl pH 7.5, 50 mM KCl, 5 mM $MgCl_2$ using a MicroCal PEAQ-ITC instrument (Malvern) at 25 °C, standard errors were calculated from 2 technical replicates. n. b., no binding detectable. To prevent background signal originating from substrate turnover, all ITC measurements were performed in the absence of Cho and Gln.

[b] PabA-PabB complexation deduced from retention volumes as determined by analytical GF. Analytical GF was performed on a Superdex 200 column equilibrated with 50 mM Tris/HCl pH 7.5, 50 mM KCl, 5 mM $MgCl_2$, 2 mM DTT and, if indicated, 5 mM Gln. Due to the limited stability and availability of Cho, all GF measurements were performed in the absence of Cho. The GF elution profiles are shown as Supplemental data (**Figure S2.1**). +, PabB exclusively found in complex with PabA; -, no PabA-PabB complex detected; +/-, fraction of PabB in complex.

[c] Steady-state kinetic measurements of glutaminase activity were performed at 25 °C in 50 mM Tricine pH 8.0, 5 mM $MgCl_2$, 150 mM KCl, 1 mM DTT, 10 mM NAD^+, 1 mg/ml GDH, 200 µM Cho and varying Gln concentrations. PabA was added at concentrations of 0.25 µM or 0.5 µM, PabB at a 4-fold molar excess over PabA.

[d] It is unclear why this variant shows no binding signal in ITC while complexation is unambiguous in analytical GF.

Next, amino acid exchanges of residues which are directly involved in the formation of the Gln binding pocket were analyzed structurally and biophysically. Interestingly, along with the relative motion of the PabB subunit upon Gln-TE formation, two residues of PabB, bG207 and bY210, approach the active site of PabA (**Figure 2.4A, D, E, Figure 2.5B**). In this state, bG207 interacts with the α-amino group of the Gln-TE directly as well as via the backbone amine of aC54. The side chain conformation of aC54 is changed in the presence of Gln-TE with the sulfhydryl group pointing towards PabB in the Gln-TE bound state and in the opposite direction in the apo state (see below). bY210 in turn is part of the same loop as bG207 and its hydroxyl group interacts with the backbone carbonyl of aG52, a residue that participates in oxyanion hole formation via its backbone amine. Furthermore, bY210 is in close proximity to the electron density that likely represents leaving ammonia or attacking water. The Gln-TE also forms specific interactions with the main chain carbonyl groups of PabA residues aG52 and aC54 and interacts with the side chain amido group of aQ83 as well as with the main chain amido groups of aS129 and aL130.

Since the observed dihedral angle of bG207 in the presence of the Gln-TE would be non-permissive for residues other than glycine, a variant in which bG207 is mutated to proline was generated. bG207P exhibits compromised PabA-PabB complex formation capacity, both in the absence and presence of Gln (**Table 2.3**). While complex formation in the absence of Gln is 10-fold reduced as estimated by ITC, the diminishment of Gln binding affinity during PabA catalysis is 55-fold, reducing substrate turnover to residual levels. The amplified loss of glutaminase activity hence seems to be due to a combined effect of weakened PabA-PabB assembly and loss of bG207-mediated interaction with the bound Gln-TE. This is most likely a consequence of the reduced conformational flexibility of proline instead of glycine in this position. To verify this hypothesis and to increase the overall loop flexibility around bG207, a triple variant bS206G, bD208G, bC209G was produced. This variant formed stable and Gln-independent heterodimers, allowing to analyze the isolated effect of altered flexibility of

the bG207 backbone carbonyl atom on Gln-TE binding. Kinetic measurements revealed a 28-fold increase in K_M^{Gln} with unchanged k_{cat}, confirming that the correct orientation and degree of backbone flexibility in bG207 is required for Gln-TE binding. Side chain removal of bY210 (bY210A) reduces PabA-PabB complex affinity 35-fold in the absence of Gln, which is however partially reversed by Gln. Yet, the K_M^{Gln} value of this variant is only 8-fold increased, indicating that transient initial PabA-PabB complex formation is strengthened in the closed complex state upon Gln-TE formation. Another ADCS variant, in which only the *p*-hydroxyl group of the bY210 phenyl side chain was removed (bY210F), formed a stable complex with PabA and has only a small impact on Gln binding, as indicated by a 4-fold increase in K_M. In summary, these data indicate that the aromatic ring of bY210 plays a role in PabA-PabB complex formation, whereas its hydroxyl group is less involved. Increasing the flexibility of PabB loop bS206-bC209 by introducing glycine residues does not impact complex formation capacities, while the restriction of its conformational space by the introduction of a proline instead of glycine reduces the affinity for the PabA subunit. Furthermore, disturbing the conformation of bG207 largely impacts Gln binding, proving its direct participation in the Gln binding pocket. Together with residues from PabA, these interactions at the non-catalytic end of the Gln-TE provide an intricated network, which positions the catalytic center of the Gln-TE at very high spatial precision. In this closed complex arrangement, the entire exposed Gln-TE surface not interacting with PabA residues (25 $Å^2$) is buried by interactions with residues of the PabB subunit, demonstrating that the Gln binding site is formed by residues from both PabA and PabB, while the catalytic triad is provided exclusively by PabA residues. In sum, Gln induces the relative movement of PabB, which then completes the binding pocket to lock Gln in the active site until hydrolysis to glutamate and ammonia took place. The exact mechanism of subsequent complex opening remains elusive, but is most likely based on the delicate equilibrium between open and closed complex state.

Next, a PabA sequence segment (aS50-aP56), that is involved both in Gln-dependent interactions with PabB (aC54-bG207) and in oxyanion hole formation (aG52), was investigated (**Figure 2.5B, C**). While no Gln-TE induced conformational changes of the oxyanion hole forming residues aG52 and aL80 could be observed, specific conformational changes were identified in the adjacent residue aC54 and its peptide bonds, which adopts a strained conformation in the presence of the Gln-TE (**Figure 2.5C**). However, no function could be assigned to this rearrangement, since variants with reduced restraints on the peptide bonds (aC54G, aC54A, aP53A) displayed unchanged catalytic parameters and complexation

properties, with the exception of a mild 2-fold increase in K_M in variant aP53A (**Table 2.3**). The conformational changes of aC54 and its peptide bonds rather seem to be part of the Gln-TE induced binding pocket formation than a causality for the formation of the oxyanion hole. To analyze whether aS50, which interacts via its side-chain hydroxyl group with the peptide bond between aP51 and the oxyanion-hole forming aG52, has an impact on the peptide bonds' amide-iminol-tautomery equilibrium, an aS50A variant was generated. This variant had an 8-fold increased K_M^{Gln} (**Table 2.3**), indicating that aS50 is involved in Gln binding.

2.2.5 A zinc ion binding to the active site of PabA

Interestingly, the PabA-PabB apo structure revealed a metal ion bound to the Gln binding pocket of PabA. This metal is found exclusively in the apo complex structure crystallized in the absence of Gln. The metal ion displayed a tetrahedral coordination with the catalytic residues aC79 and aH168 as well as aH128 and a water molecule and overlaps with the binding site of Gln (**Figure 2.5D**). An analysis by X-ray fluorescence spectroscopy conducted by Dr. Sihyun Sung identified the metal as zinc, which is in accordance with the observed coordination geometry.[123, 124] Since zinc was not consciously added at any stage during purification and crystallization, the most plausible explanation for its presence is its extraction from the expression host. Incubation of PabA-PabB apo crystals with 1 mM EDTA resulted in a loss of the electron density assigned to Zn^{2+}. Concomitantly, aH128 flips from an orientation blocking the PabA active site to an insufficiently resolved conformation, in which it most likely integrates into an alternative interaction network (see below). The conformation of aH168 is virtually unchanged and aC79 seems to gain the freedom to adopt two (similar) conformational states (**Figure 2.5D**). As expected, the conformations closely resembled the geometries observed in the structures void of Gln-TE despite the addition of Gln. Overall, the elimination of Zn^{2+} exerts no global structural effects on the PabA-PabB complex but induces conformational changes at the active site of PabA.

To confirm and quantify Zn^{2+}-binding to the PabA-PabB complex in solution, inductively coupled plasma-optical emission spectrometry (ICP-OES) experiments were performed in collaboration with Vanessa Tomanek in the group of Prof. Dr. Axel Dürkop (Faculty for Chemistry and Pharmacy, University of Regensburg). ICP-OES allows for the highly sensitive quantification of various trace elements via analysis of specific atomic emissions based on standards with known concentrations.[125] To avoid interference with signals of other metals,

purified PabA and PabB were brought into a metal-free buffer (50 mM Tris/HCl pH 7.5) using a desalting column and mixed equimolarly to yield a final concentration of 11 µM PabA-PabB complex. All three tested methods to eliminate organic components during sample preparation, namely (i) acidification with 2 % HNO_3 followed by centrifugation, (ii) ashing overnight, followed by dissolution of remains in 32 % HNO_3, and (iii) evaporation at 145 °C overnight, followed by dissolution of remains in 32 % HNO_3, yielded zinc concentrations of 0.04-0.41 µM (**Table 2.4**), indicating that only one out of 25-250 PabA molecules coordinates zinc in solution.

Table 2.4: Quantification of zinc in PabA-PabB by ICP-OES with different methods of sample preparation.

Sample preparation	c(Zn) [µM]	c(PabA-PabB) [µM]	Zn/PabA-PabB molar ratio
Acidification - centrifugation	0.085	11	0.008
Ashing	0.041	11	0.004
Evaporation	0.409	11	0.037

Potential functional implications of Zn^{2+} on the catalytic activity of PabA could not be directly assessed, since even low concentrations (0.5 mM) of $ZnCl_2$ led to complete precipitation of PabA and major aggregation of PabB. Therefore, glutaminase activity after removal of Zn^{2+} was investigated, using EDTA as a chelating agent of divalent cations. However, 1 mM or 10 mM EDTA did not alter the low basal activity of isolated PabA (**Table 2.5**). The determination of catalytic parameters in the presence of PabB necessitates comprehensive controls to exclude any interfering effect of Mg^{2+} deprivation by EDTA. While the sum of experiments clearly confirms the requirement of Mg^{2+} for binding of Cho, no further variation of catalytic parameters upon addition of EDTA and thus removal of Zn^{2+} could be observed. Moreover, in line with the unchanged catalytic activity of the PabA-PabB complex, its dissociation constant K_D was also unaffected by the presence of EDTA (0.16 µM ± 0.06 µM without EDTA vs 0.17 µM ± 0.13 µM with 1 mM EDTA).

Table 2.5: Effects of chorismate, EDTA and $MgCl_2$ on the catalytic activity of PabA.

PabB	Cho	EDTA	$MgCl_2$	K_M^{Gln} [mM]	k_{cat} [s^{-1}]	k_{cat}/K_M^{Gln} [$mM^{-1}s^{-1}$]
-	-	-	+	12.2 ± 0.54	$4.4 *10^{-3} \pm 6.1 *10^{-5}$	$3.6 *10^{-4} \pm 2.1 *10^{-5}$
-	-	+	-	10.5 ± 0.76	$4.4 *10^{-3} \pm 9.6 *10^{-5}$	$4.1 *10^{-4} \pm 3.9 *10^{-5}$
+	-	-	-	0.09 ± 0.005	0.20 ± 0.003	2.35 ± 0.17
+	-	-	+	0.09 ± 0.015	0.22 ± 0.007	2.41 ± 0.47
+	-	+	-	0.08 ± 0.002	0.19 ± 0.001	2.42 ± 0.08
+	-	+	+	0.09 ± 0.005	0.23 ± 0.003	2.58 ± 0.17
+	+	-	-	0.07 ± 0.005	0.14 ± 0.003	1.98 ± 0.18
+	**+**	**-**	**+**	**0.34 ± 0.032**	**0.37 ± 0.010**	**1.09 ± 0.13**
+	+	+	-	0.08 ± 0.002	0.15 ± 0.001	1.91 ± 0.07
+	**+**	**+**	**+**	**0.27 ± 0.010**	**0.31 ± 0.003**	**1.13 ± 0.05**

Steady-state kinetic measurements of glutaminase activity were performed at 25 °C in 50 mM Tricine pH 8.0, 150 mM KCl, 1 mM DTT, 10 mM NAD^+, 1 mg/ml GDH, 0.25 µM PabA, varying Gln concentrations and, if indicated, 1 µM PabB, 200 µM Cho, 1 mM EDTA, 5 mM $MgCl_2$. Changes in catalytic parameters are induced by the simultaneous presence of both Cho and $MgCl_2$ (marked bold) and are due to the allosteric regulation of glutaminase activity by Mg^{2+}-dependent Cho binding. This means that Cho or $MgCl_2$ in the absence of the respective other component do not affect the activity of PabA. Likewise, EDTA has no effect on PabA glutaminase activity.

The conflicting results on Zn^{2+}-binding in the PabA-PabB complex obtained via X-ray structure determination and X-ray fluorescence on the one hand and ICP-OES and functional assays on the other hand are enigmatic. A potential explanation would be the inadvertent presence of zinc in the crystallization buffer, which is supported by its absence in the structure of the isolated PabA subunit, that has been solved under different conditions. Alternatively, since crystallization, ICP-OES and the functional characterization were performed with different protein purification batches, naturally deviating compositions of the poorly defined culture medium for protein overexpression could explain differences in the PabA-PabB metal content. Nevertheless, a metal-binding site appears to be present at the active site of PabA that, even without known functional implications, adds to the knowledge of metal-binding properties of enzymes and may just as well represent an evolutionary relict or adventitious feature.

The PabA residue aH128, which coordinates Zn^{2+} in the PabA-PabB apo structure, is structurally not resolved in the PabA-PabB structure acquired in the presence of EDTA and is found in an alternative orientation in all structures determined in the presence of Gln (**Figure 2.5D**). In that manner, it protrudes into the Gln binding site in the apo state, but undergoes a

Gln-dependent flip that renders the Gln binding pocket accessible. For a better understanding of this side chain reorientation, a mutant devoid of the imidazole side chain, aH128A, was generated and analyzed. While the turnover number k_{cat} was virtually unchanged, K_M^{Gln} was almost 100-fold increased and even exceeded the K_M^{Gln} of the isolated PabA subunit (**Table 2.1**, **Table 2.3**). However, the structural data revealed no direct interactions of aH128 with the Gln-TE and PabA-PabB complex formation of the variant was only slightly impaired. To inquire on the molecular mechanism of aH128As drastically reduced substrate binding affinity, interdependent effects with the PabB residues bG207 and bY210, which act on the N-terminal amino group of the Gln-TE intermediate, were investigated. However, combinations of the aH128A variant with respective PabB variants demonstrated an additive (independent) decrease of catalytic efficiency with overall extremely reduced activities. Accordingly, aH128 appears to contribute to substrate binding by an alternative mechanism, for example via backbone restraints on the neighboring aS129 and aL130 main chains, which interact with the carboxy-group of the Gln-TE. The observed flexibility of aH128 prior to Gln-TE formation again points toward an auto-induced shaping of the Gln binding pocket.

2.2.6 PabB induces a catalytically competent active site conformation in PabA

Superposition of the three individual PabA chains in the PabA crystal revealed distinct differences in electron densities assigned to residues of the catalytic triad. Accordingly, in the absence of PabB, three different side chain orientations were observed for aH168 and aE170 and even the small side chain of aC79 displayed two different conformations (**Figure 2.6B**, upper panel). In contrast, the PabA structures obtained in complex with PabB revealed only one conformation for the catalytic residues (**Figure 2.6B**, lower panel). Remarkably, the formation of the Gln-TE at aC79 did not trigger any further reorientation, thus, the state observed in the PabA-PabB apo structure probably represents the catalytically active side chain conformation. Therefore, based on the variability of electron density, PabB seems to stabilize the catalytically active side chain conformation in PabA via specific interface interactions.

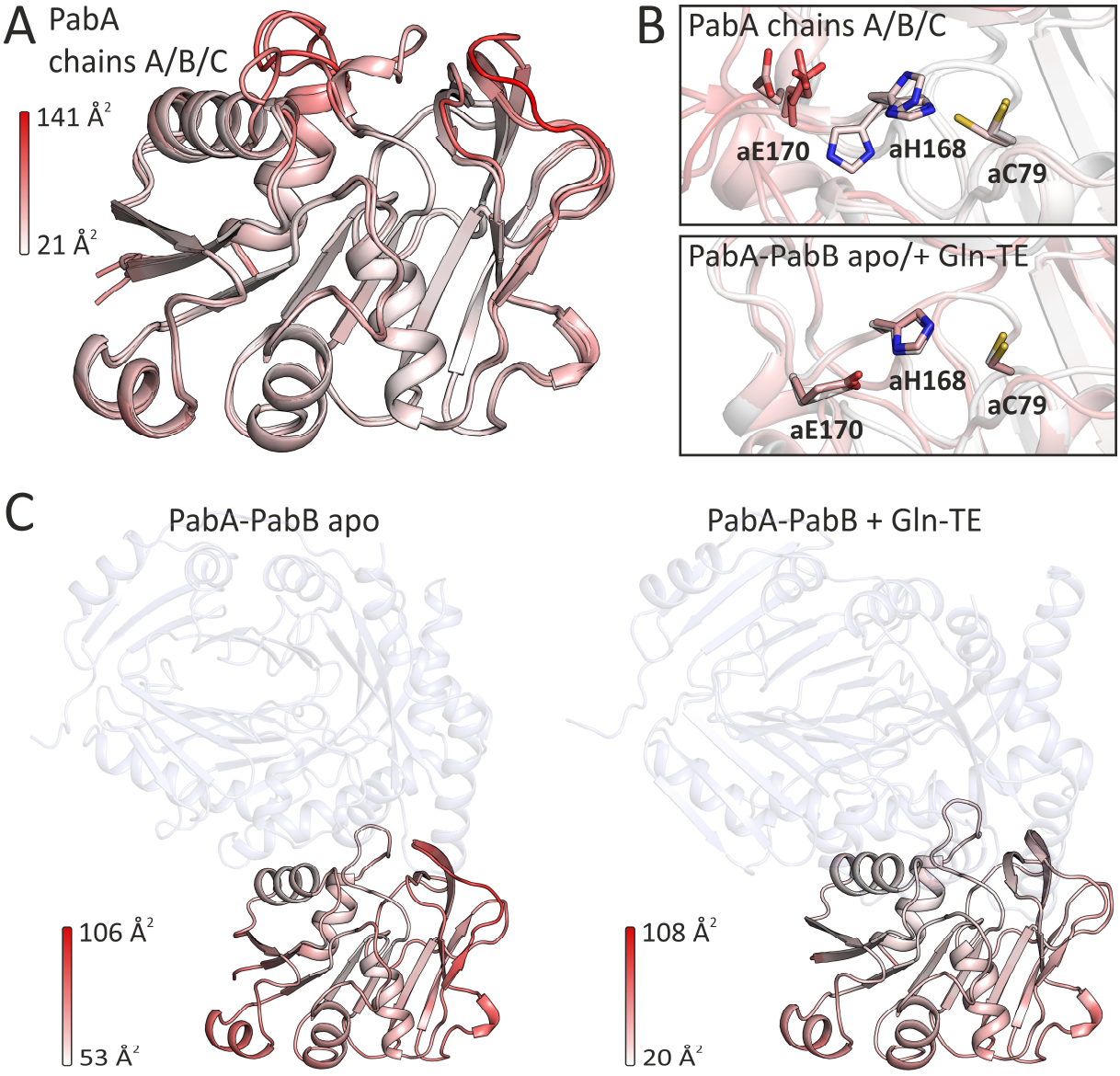

Figure 2.6: Conformational variability of PabA in its apo form and in complex with PabB. (A) Superposition of the three PabA chains found in the PabA crystal. The intensity of the coloring (by B-factor) correlates with the flexibility. Regions with a higher degree of flexibility are predominantly found at the interface to PabB and, strikingly, include the catalytic residues aH168 and aE170. (B) The reorientation and rigidification of the PabA catalytic triad aC79-aH168-aE170 upon complexation with PabB is illustrated by the comparison of side chain conformations in separate PabA chains A, B and C (upper panel) with the conformations found in the PabA-PabB complex irrespective of bound Gln-TE (lower panel). (C) Flexibility, as indicated by B-factors of the PabA subunit in complex with PabB in the absence and presence of the Gln-TE, as indicated. The region of PabA that interacts with PabB, which is extended in the presence of the Gln-TE, experiences a distinct loss of flexibility. Color bars indicate the applied B-factor minima and maxima to account for overall differences of crystal B-factors.

For an overall comparison of flexibilities in the isolated PabA subunit and PabA in complex with PabB, B-factors were analyzed. The B-factor, also called Debye-Waller factor, describes the spread of electron density for each atom and reflects both static disorders and vibrational motions. Static disorders include varying conformational states, positions and orientations between molecules in different unit cells as well as crystal defects resulting for example from radiation damage. Vibrational motions in turn describe the relative movements of atoms in the

protein crystal. In high-resolution crystals, B-factors can be carefully used as an indicator of flexible (high B-factor) or rigid (low B-factor) regions within proteins.[126, 127] The isolated PabA subunit displays several regions with elevated B-factors that accumulate at the interface towards PabB (**Figure 2.6A**). Intriguingly, one of those regions contains the catalytic residues aH168 and aE170. After formation of the PabA-PabB complex, the PabA regions that interact with PabB exhibit a reduction of B-factors, indicating decreased flexibility due to stabilizing interactions with PabB. In line with this, the stabilized region is further extended by the closing of the complex upon Gln-TE formation (**Figure 2.6C**). Overall, the data indicate that the reduction of flexibility in PabA due to interactions with PabB comes with the stabilization of the catalytically competent conformation of the catalytic triad and contributes to the activation of PabA by PabB.

Two residues of PabB, bD308 and bR311, are particularly close to the catalytic residues aH168 and aE170 and their side chains reach out into distinct PabA surface pockets in the center of the PabA-PabB interface (**Figure 2.4E**). Residue bD308 interacts with the side chains of aY127 and aS171, with the backbone of aI172 and, via its own backbone, with aN14 and was previously found to play a major role in complex formation.[115] Residue bR311 interacts with bD308 and the main chain carbonyl group of the catalytic residue aE170. Side chain replacement by alanine in each of the two PabB residues causes PabA-PabB disassembly in GF experiments, even in the presence of Gln (**Table 2.3**). To test the specific role of bD308 further, this residue was also mutated into an isosteric mutant bD308N, in which the steric properties but not the negative charge of its side chain remains preserved, and into bD308E, where the charge is maintained but the side chain is extended by one methylene group. As observed for the bD308A variant, the bD308N variant did not form a stable complex with PabA, demonstrating that the side chain carboxylate group is essential for PabA-PabB assembly. In the bD308E variant, PabA-PabB assembly could be partly restored, however only when Gln was added. The observed degree of complexation closely correlated with the ability of the different PabB variants to stimulate the glutaminase activity of PabA (**Table 2.3**). Except for the bD308E mutant, all tested bD308 and bR311 variants displayed a 10- to 80-fold reduction of glutaminase catalytic efficiency with the major impact on K_M^{Gln} (8-25-fold increase) rather than k_{cat} (< 4-fold decrease). The finding that these PabB residues are not a part of the glutaminase active site but are nevertheless essential for Gln binding could be a result of both the disrupted PabA-PabB complex formation and the loss of specific stabilizing interactions around the catalytic triad of PabA.

When changing the PabA residues interacting with bD308, namely aY127 and aS171, or a combination of both to alanine, no or only partial complex formation was observed in the absence of Gln in GF and ITC experiments. However, the addition of Gln restored PabA-PabB complexation of the single variants and improved complexation of the double variant (**Table 2.3**). Interestingly, these variants displayed an increased level of substrate binding but 5- to 30-fold decreased turnover numbers (**Table 2.3**). In line with the sequential and structural proximity of aY127 and aS171 to the catalytic residues aH168 and aE170, the kinetic parameters of the mutants suggest that these residues, similar to aH128, play roles in the formation of a catalytically competent glutaminase active site conformation. Since the k_{cat} values of bD308A and bD308N show the same tendency as the k_{cat} values of aY127A and aS171A, it seems probable that the carboxylate group of bD308 (which directly interacts with aY127 and aS171) is involved in the formation of the active site conformation via those two residues. Whether the observed kinetic effects are solely due to the reduction in PabA flexibility cannot be judged based on the present data, since all mutations prevented not only single, potentially stabilizing interactions, but also weakened the overall PabA-PabB complexation. Nevertheless, the structural and biochemical data suggest a crucial role of PabB to generate a catalytically competent conformation of the glutaminase catalytic triad, irrespective of the presence of Gln. Moreover, while the Gln-independent PabA-PabB assembly is already involved in the PabA active site conformation via the interactions of bD308 and bR311, it is more sensitive to mutations of interface residues than the closed complex in the presence of Gln, confirming that Gln significantly contributes to PabA-PabB complex stabilization. Furthermore, no significant conformational changes of any PabB segments involved in the PabA-PabB interface were detected. Hence, all observed conformational changes in PabA are caused by PabB binding and the overall PabA-PabB subunit rearrangement upon Gln-TE binding.

2.3 Discussion

The central question regarding GATases is how glutamine hydrolysis and synthase activity are functionally coupled. In particular, the activity of the glutaminase subunit requires adjustment to the synthase turnover to avoid the wasteful consumption of glutamine and the release of toxic ammonia. A profound understanding of the underlying mechanistic and structural processes and the relevant inter- and intramolecular motions is lacking in many GATases and only few generally applicable concepts have been identified up to now. In this work, mechanistic investigations were performed on the example of the ADCS (PabA-PabB) complex by a combined structural and functional approach. In this system, activation of the PabA glutaminase activity is mainly achieved through complex formation with the synthase subunit PabB, whereas allosteric activation through the PabB substrate chorismate seems to play a minor role.

A comparison of structures of the isolated PabA subunit and the PabA-PabB complex indicated that complex formation reduces the degree of conformational freedom at the interface region of PabA, thereby stabilizing the productive orientation of the catalytic triad within the PabA active site. In particular, the structures of separate PabA subunits indicate significant deviations of the catalytic triad (aC79, aH168, aE170) from a catalytically competent arrangement. In contrast, all ADCS complex structures irrespectively of any bound ligands display aH168 and aE170 in a proper arrangement to allow polarization of aH168 by aE170. Accordingly, the substitution of PabB side chains directly or indirectly interacting with the PabA catalytic triad resulted in a loss of PabA-PabB complex affinity, which was accompanied by reduced Gln binding affinities.

Furthermore, structural data revealed significant PabA-PabB rearrangements upon formation of the glutamyl-thioester reaction intermediate, characterized by a 23° rigid body rotation. This corresponds to a shift from an open complex state in the apo structures to a closed complex state in the structures with bound Gln-TE intermediate. Interestingly, the shared Gln binding pocket, comprising residues from both PabA and PabB, is formed exclusively in the closed complex state. Perturbations of the apparent equilibrium between open and closed state therefore drastically reduce the affinity of the PabA-PabB complex towards Gln. Moreover, the Gln-TE induced closure of the PabA-PabB complex induces an extension of the PabA-PabB interface with additional molecular interactions, which increases complex affinity. This finding is supported by an increased sensitivity for PabA-PabB disassembly in the absence of Gln, and,

along the same lines, the ability of Gln to restore artificially weakened PabA-PabB complexation.

The individual effects of Gln binding and the formation of the covalent Gln-TE intermediate cannot be distinguished based on the available structural and biophysical data. However, these two reaction steps induce multiple conformational changes on both large and small scales to transform the PabA-PabB complex from a state that allows substrate access to a state that fully encloses the reactive intermediate state and directs the produced ammonia to the active site of PabB. This implies a motion-dependent mechanism of action in which a catalytic cycle comprises both the open and the closed complex state.

In the following, the findings will be discussed in comparison to known structures and activation mechanisms for other class I glutamine amidotransferase complexes. The PapAB enzyme from *S. venezuelae* is the only other ADCS enzyme for which structural information of a glutaminase-synthase complex is available.[70] As other *Streptomyces* species, *S. venezuelae* features two ADCS enzymes, the primary PabA-PabB heterodimeric enzyme complex, and a fusion protein PapAB which is linked to the biosynthesis of chloramphenicol and other species-specific antibiotics.[128-130] The structural data revealed that the PapAB enzyme from *S. venezuelae* forms a dimeric intertwined quaternary structure, in which the glutaminase domain of one protomer interacts with the synthase domain of the other protomer (**Figure 1.2C**). This structure has been solved in an apo state and in a Cho-bound state, but provides no information on bound Gln intermediates.[70] Rather, the glutaminase active site cysteine appears to be oxidized to cysteine sulfonic acid. In this system, binding of chorismate to one of the synthase domains is linked to conformational changes to the interacting glutaminase domain, which impact the ammonia tunnel, the oxyanion hole, the glutaminase active site and molecular interactions at the glutaminase-synthase interface. In contrast, the effects of Cho on the PabA-PabB complex of *E. coli* described in this work are minor and restricted to the direct environment of the Cho-binding site. Since the intertwined quaternary structure of the *S. venezuelae* ADCS fusion protein complex differs considerably from the quaternary structure observed in *E. coli*, it appears reasonable that subunit communications involved in allostery and mutual catalytic activation also differ. In line with this, in anthranilate synthase (AS) complexes from various organisms, deviations in quaternary structures are also linked to different mechanisms of cooperativity.[69, 83, 103]

The closest homolog to ADCS enzymes is the AS TrpG-TrpE complex which catalyzes the committed step in tryptophan biosynthesis (**Figure 1.2B**). The two synthase subunits in ADCS and AS, PabB and TrpE respectively, are homologs, both converting the substrate chorismate and possessing highly similar three-dimensional structures.[69, 83, 103] As with PabA, the main activation of the TrpG activity takes place at the level of synthase complex formation, however, binding of chorismate to the active site of TrpE also plays a role (**Table 2.1**). Currently, a direct comparison of a TrpG apo structure with the structure of the TrpG-TrpE apo complex or structural analysis on the isolated effect of Gln are not possible because the corresponding structures are not available. However, a comparison of two TrpG-TrpE complex structures from the γ-proteobacterium *Serratia marcescens*, one structure with bound inhibitor tryptophan representing an inactive state (PDB-ID: 1I7S) and the other structure in presence of Cho and bound Gln-TE intermediate representing the active conformation (PDB-ID: 1I7Q), allows to draw conclusions about the conformational changes that accompany regulation of glutaminase activity.[69] In this case, two β-sheets in TrpG become largely disordered in the presence of tryptophan and appear to move in such a way as to disrupt the correct orientation of residues that are necessary for Gln binding. However, no relevant subunit rearrangements were observed. In another context, the analysis of constitutively active TrpG mutant enzymes (T129Y and T129F from *T. maritima*) revealed that glutaminase stimulation is linked to a distance reduction of the functional residues in the catalytic triad.[109] Overall, in the AS complex, activation of glutaminase activity also appears to proceed via fine-tuning of the orientation of catalytic residues within the glutaminase active site, whereby the molecular mechanisms seem to be distinctly different from the ones identified within the PabA-PabB complex. It would be of particular interest to investigate how the observed differences in PabA and TrpG activation by PabB and TrpE translate into those AS and ADCS enzymes which share the same glutaminase subunit.[99]

Another related GATase, ADICS, forms intertwined heterodimers similar to those observed in the *S. venezuelae* ADCS complex.[107] A comparison of an apo structure and a structure containing the Gln-TE and Cho also reveals a large substrate-induced subunit rearrangement. However, this apparent movement is restricted to reorientations of the functional units in relation to each other, while the interaction within the functional glutaminase-synthase units does not change considerably. Furthermore, the Zn^{2+} binding site observed in the PabA-PabB apo structure is in a similar position as observed in a structure of ADICS. In contrast to ADCS, however, Gln-TE formation and Zn^{2+} binding was not mutually exclusive in ADICS. While

Zn^{2+} could potentially act as a Lewis acid to enhance catalysis,[123] Zn^{2+} in fact was shown to decrease the catalytic activity of ADICS. Moreover, in ADICS, no conformational changes upon Zn^{2+} binding were observed. Thus, functional implications, if existing, would probably differ between the systems. Due to the high degree of conservation of the cysteine and histidine residues coordinating the Zn^{2+} ion, this metal ion might as well represent a fortuitous evolutionary feature.

Another class I GATase for which the structural changes associated with allosteric activation of glutaminase activity are very well characterized is the imidazole glycerol phosphate synthase which consists of the glutaminase subunit HisH and the synthase subunit HisF (**Figure 1.2A**).[68, 108, 131, 132] A remarkable property of the *T. maritima* HisH-HisF complex is that while HisH is initially not activated by binding of HisF, it shows an increase in Gln turnover by over three orders of magnitude upon binding of the synthase substrate, making this bienzyme complex one of the most tightly allosterically regulated GATases known to date.[108, 110, 133] Structural and mutational analysis of the HisH-HisF complex from *T. maritima* indicates a direct involvement of two HisF residues in the formation of the glutaminase active site and emphasizes the importance of the formation of a specific and tight protein-protein interface of the two subunits for the coupling of the two catalytic activities.[108] Upon conversion from the inactive to the active conformation induced by binding of both substrates, four significant structural rearrangements have been observed:[68] An active site loop closes over the HisF active site, then the hydrophobic core in HisF is remodelled. In consequence, there appears a closing motion at the HisH-HisF interface and finally these events prime the HisH active site for the formation of the oxyanion hole. It has been proposed that the reorganization of the glutaminase oxyanion hole in the presence of both substrates is a central aspect in the allosteric coupling of the glutaminase and synthase reactions.[68, 131, 132] In contrast, in ADCS, the glutaminase active site oxyanion hole is in an active conformation regardless the addition of any substrates.

In contrast to the HisH-HisF complex and similar to ADCS, the glutaminase activity of pyridoxal 5′-phosphate synthase from *Bacillus subtilis* is increased in the presence of its synthase, but experiences no further activation upon binding of the substrates of the synthase.[134] It was shown that the presence of the synthase induces conformational changes in the glutaminase subunit which lead to the formation of the oxyanion hole and changes in the glutamine binding site. Furthermore, an N-terminal helix of the synthase is involved in both sealing of the glutaminase binding site and the transient assembly of 12 glutaminase-synthase complexes to an unusual macromolecular cogwheel (**Figure 1.2D**).[71, 135]

The structural and mechanistic comparison of GATases inevitably raises the question of how unproductive hydrolysis of Gln is avoided under physiological conditions. While the case of HisH seems clear, in which glutaminase activity depends on the presence of the synthase substrate at the HisF active site, TrpG and PabA display significant activities even without Cho bound to the respective synthase. As the major activating effect is conferred by high affinity complexation with TrpE and PabB, respectively, it is tempting to speculate about additional, so far unidentified regulatory mechanisms. For example, on the level of enzyme kinetics, a ligand or protein might specifically inhibit complex formation (and thus glutaminase activity) at low cellular Cho concentrations to couple Gln hydrolysis to the presence of Cho. This would be supported by the finding that the negative charge of one single conserved residue (bD308 in PabB) is crucial for PabA-PabB and TrpG-TrpE complex formation, but not for HisH-HisF complex formation.[115] This conserved aspartate residue would thus make a plausible target for an inhibiting ligand or protein. Another plausible mode of regulation would be a tight control of gene expression of one or both subunits, in a way that the formation of the complex is regulated via protein levels in the cell. However, the variable operon organization of both folate and tryptophan biosynthetic genes between prokaryotes[128, 136] renders a general mechanism of gene expression control unlikely. In line with this, the regulation of expression of tryptophan biosynthetic genes in response to cellular tryptophan levels is distinctly different in *E. coli* and *B. subtilis*.[137-139] In contrast, no such feedback control mechanism is known for folate biosynthesis.

Overall, there appears to be no unifying general mechanism of glutaminase-synthase communication in class I GATases. Instead, molecular mechanisms for activity control appear to have evolved after the functional specification from the shared enzyme ancestor, adapted to the requirements of the respective metabolic pathway and organism. In light of the restricted evolutionary space of protein-protein interfaces, the high degree of diversity is even more astonishing. Acquiring detailed mechanistic knowledge about further GATases thus has the potential to provide additional insight in the often unclear evolutionary relations within this class of enzymes.

2.4 Material and Methods

2.4.1 Cloning and mutagenesis

The genes for ecPabA, ecPabB, ecTrpGD and ecTrpE were available from a previous study[99] and were cloned into a pET28a vector with an N-terminal His_6-Tag followed by a TEV cleavage site. TrpG is present in *E. coli* as a fusion protein with TrpD and was purified as such. For reasons of clarity, however, it will only be referred to as TrpG. The solubility and stability of PabA was increased by the addition of an N-terminal Gly_5His-Tag via site-directed mutagenesis. PabA and PabB variants were also produced by site-directed mutagenesis.

2.4.2 Gene expression and protein purification

Gene expression and protein purification were performed essentially as described.[79] In brief, *E. coli* BL21-Gold (DE3) cells were transformed with the respective plasmid and grown in 3-6 L Luria broth medium supplemented with 50 µg/ml kanamycin at 37 °C to an OD_{600} of 0.6. Expression was induced by 0.5 mM IPTG, followed by overnight shaking at 25 °C. Cells were harvested, resuspended in 50 mM Tris/HCl pH 7.5, 300 mM KCl, 10 mM imidazole and 2 mM DTT, and lysed by sonication.

Proteins were purified via Ni^{2+} affinity chromatography by applying the soluble lysate to a HisTrap excel column (5 ml, GE Healthcare). Proteins used for crystallization were cleaved with TEV protease to remove the His_6-Tag (TEV protease to protein mass ratio: 1 to 50) while dialyzing against 3 L 50 mM Tris/HCl pH 7.5, 50 mM KCl at 4 °C overnight, followed by reverse Ni^{2+} affinity chromatography. All proteins were further purified by preparative gel filtration on a Superdex75 pg HiLoad 26/600 column (320 ml, GE Healthcare). Protein concentrations were determined spectrophotometrically at 280 nm, with molar extinction coefficients calculated via ExPASy ProtParam.

2.4.3 Purification of chorismate

Cho was purified by Dr. Sandra Schlee from culture supernatant of *E. coli* KA12 cells (graciously provided by Prof. Dr. Donald Hilvert and Prof. Dr. Peter Kast, ETH Zürich) as described previously.[140] After removing the cells by centrifugation, the supernatant was

acidified with HCl (5 M) to pH 1.5 and extracted with ethylacetate (2 x 180 ml). The combined extracts were washed with saturated brine (360 g/l NaCl) and ethylacetate was removed *in vacuo*, yielding a small volume of crude Cho. The crude material was loaded on 50 g C18 reverse phase silica and eluted with 10 mM ammoniumacetate (pH 6.0), 10 ml fractions were collected and for each fraction absorption spectra were recorded. Fractions containing Cho in sufficient concentration and purity (ε_{275}(Cho) = 2630 M^{-1} cm^{-1}) were combined and lyophilized. The resulting lyophilizate was dissolved in a small volume of sterile water, aliquoted, and stored at -80°C. Sample purity was assessed by analytical reverse phase HPLC and total turnover by anthranilate synthase in an enzymatic assay.

2.4.4 Analysis of PabA-PabB complex formation by analytical gel filtration

Analytical GF was applied to assess the ability of subunit variants to form a heterodimeric PabA-PabB complex in the presence and absence of the substrate Gln.[79] PabA and PabB subunits were mixed in an equimolar ratio to final concentrations of 50 µM each in GF buffer (50 mM Tris/HCl pH 7.5, 50 mM KCl, 5 mM $MgCl_2$, 2 mM DTT and, where indicated, 5 mM Gln). As controls, the isolated wt subunits were also applied at 50 µM under the same measuring conditions. Samples were applied to a Superdex200 increase 10/300 GL column (GE Healthcare) equilibrated with GF buffer with or without Gln at 25 °C at a flow rate of 0.3 ml/min. Protein elution was followed by absorbance measurements at 280 nm. Calibration was performed with the Cytiva LMW and HMW calibration kits and confirmed the deduced oligomerization states.

2.4.5 Analysis of PabA-PabB complex formation by ITC

ITC measurements were performed to quantify PabA-PabB complex affinities. PabA and PabB subunits were dialyzed (Spectra/Por® 1 Dialysis Membrane, MWCO 6-8 kDa) overnight at 4 °C against a 1000-fold volume excess of degassed ITC buffer (50 mM Tris/HCl pH 7.5, 50 mM KCl, 5 mM $MgCl_2$). Experiments were performed using a MicroCal PEAQ-ITC instrument (Malvern) at 25 °C with a reference power of 10 µcal/s. A total of 19 or 23 injections of 1 or 2 µl 250 µM PabB were titrated from a rotating syringe (750 rpm) into the isothermal chamber containing 300 µl 25 µM PabA with a delay time of 150 s between injections. Enthalpy differences were obtained by integrating the heat pulses of each injection and plotted against the PabB/PabA ratio. From the resulting isotherm, the binding stoichiometry N, dissociation

constant K_D and thermodynamic parameters ΔH and ΔS were calculated using the MicroCal PEAQ-ITC Analysis Software (Fit: One set of sides, Version 1.41, Malvern).

2.4.6 Steady-state enzyme kinetics

The glutaminase activities of ecTrpG and ecPabA were measured essentially as described.[79, 140] In brief, glutaminase activity was followed under steady-state conditions by a coupled enzymatic assay with glutamate dehydrogenase (GDH), coupling turnover of Gln to the production of α-ketoglutarate and the conversion of NAD^+ to NADH ($\Delta\varepsilon_{340\,nm} = 6220\ M^{-1}\ cm^{-1}$), which can be continuously monitored spectroscopically. Measurements were carried out in 50 mM Tricine pH 8, 5 mM $MgCl_2$, 150 mM KCl, 1 mM DTT, 10 mM NAD^+, 1 mg/ml GDH, 200 µM Cho and varying Gln concentrations. Glutaminases were added at concentrations of 0.25 µM or 0.5 µM, synthases at a 4-fold excess over the glutaminase. In the absence of synthases, the glutaminase concentration was increased to 5 µM. Measurements were conducted at 25 °C in 96-well plates using a plate reader (Tecan Infinite M200 Pro). To calculate glutaminase activity k_{app}, the initial slope of the reaction time course was corrected by the substrate-free baseline, transformed to v_i ($v_i = \frac{slope}{\Delta\varepsilon * 0.45\ cm}$) and normalized by the glutaminase concentration. To obtain the Michaelis-Menten parameters k_{cat} and K_M, k_{app} was plotted against the Gln concentration and a hyperbolic fit was applied to the resulting plot using the Origin 2020 software ($k_{app} = \frac{k_{cat} * [Gln]}{K_M + [Gln]}$). The reported values are an average of a biological duplicate, each with at least two technical replicates.

2.4.7 Crystallization

PabA-PabB crystals were grown at 18 °C in 24-well plates by combining 2 µl volumes of 8.25 mg/ml protein and reservoir solution at a 1:1 ratio, using the hanging-drop vapor diffusion method. The reservoir solution contained 0.1 M MES (pH 6.5) and 1.5 M magnesium sulfate heptahydrate. For PabA-PabB structure determination in the presence of Gln, the reservoir solution was supplemented with 0.2 M Gln. After four days, crystals of mixed sizes were observed. Crystals larger than 50 µm in length were collected from the initial crystallization drop and washed with the reservoir solution 5 to 6 times. Subsequently, the washed crystals were crushed with a seed bead (JBS Beads-for-Seeds, CO-501) in 500 µl of precipitant and serially diluted 10-, 100- and 1000-fold. A macro-seeding method was employed to obtain

crystals of sufficient size for X-ray diffraction experiments and data collection. Crystals of a size of at least 300 x 200 x 100 μm^3 were obtained after 3-4 days of macro-seeding using the hanging-drop vapor-diffusion method. For PabA-PabB structure determination in the presence of Cho, 14.4 mM Cho was added to ADCS crystals co-crystallised in the presence of Gln. For PabA-PabB structure determination in the absence of zinc, 1 mM EDTA was added to PabA-PabB crystals without Gln added. All crystals were transferred into paratone-N oil as a cryoprotectant and flash-frozen in liquid nitrogen for storage, prior to X-ray data collection.

The separate PabA subunit was crystallized at 18 °C from 2 µl protein solution at 16.5 mg/ml and 2 µl reservoir solution comprising 0.2 M sodium formate, 20 % (v/w) PEG-3350, and 0.2 M Gln, employing the hanging drop vapor diffusion method. Small crystals were observed after one week. The cover glass was then transferred to new reservoir solutions with incrementally increased precipitant concentrations filled with 1 ml of 25%, 30%, 35% and 40% (v/w) PEG-3350 every second day for sequential dehydration. The dehydrated crystals were subsequently fast frozen in liquid nitrogen.

2.5 Supplemental data

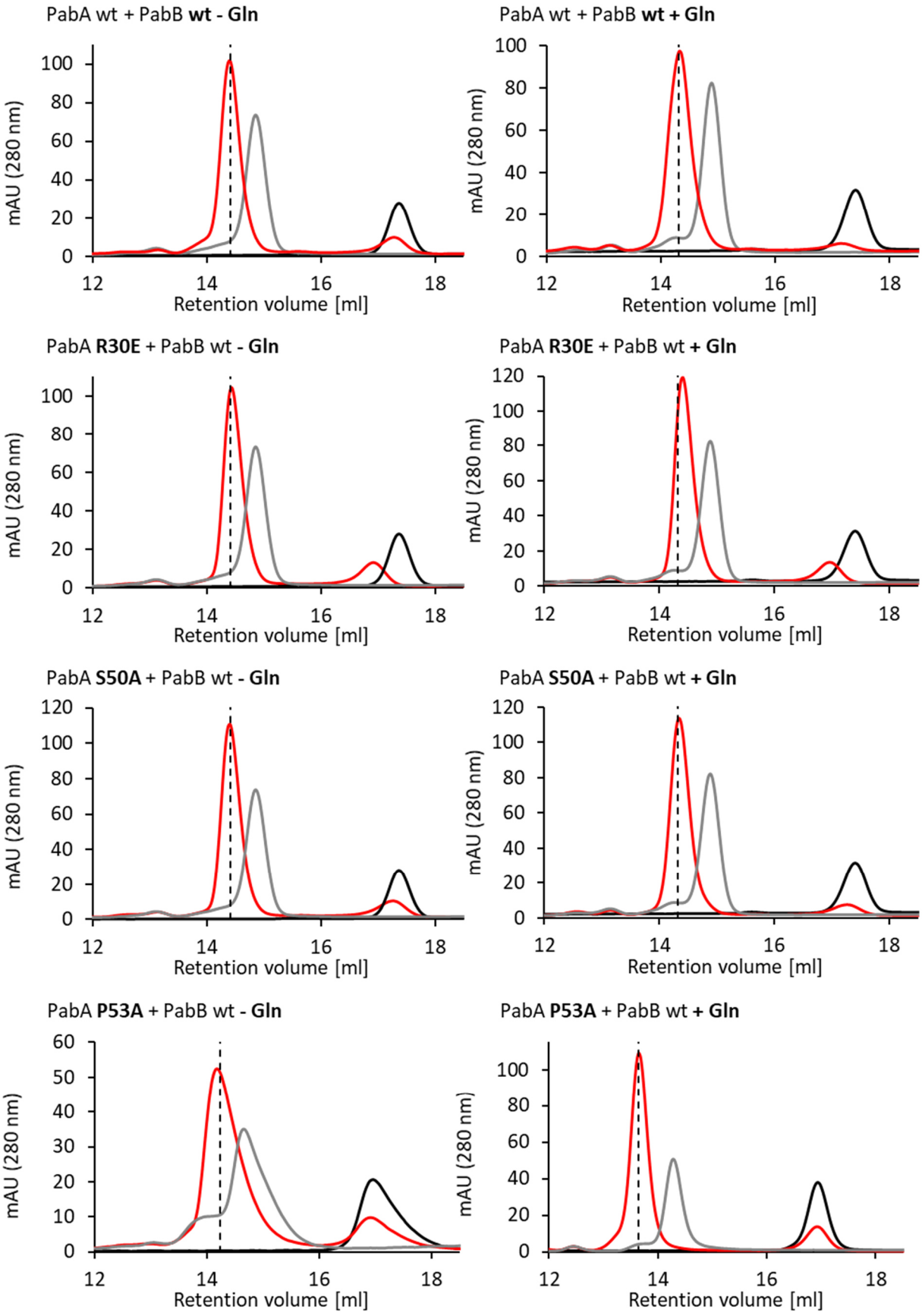

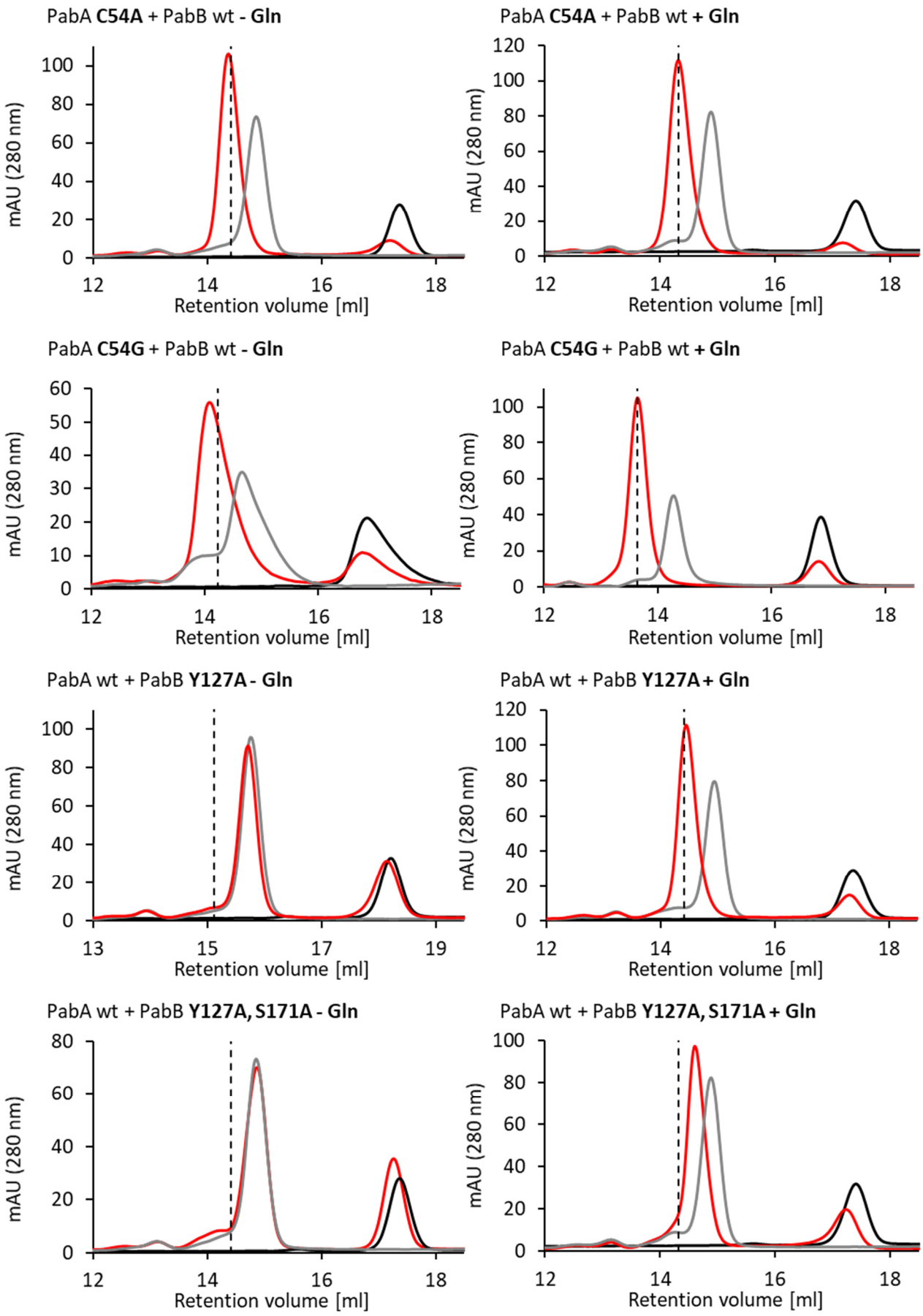
PabA **C54A** + PabB wt **- Gln**
PabA **C54A** + PabB wt **+ Gln**
PabA **C54G** + PabB wt **- Gln**
PabA **C54G** + PabB wt **+ Gln**
PabA wt + PabB **Y127A - Gln**
PabA wt + PabB **Y127A + Gln**
PabA wt + PabB **Y127A, S171A - Gln**
PabA wt + PabB **Y127A, S171A + Gln**
mAU (280 nm)
Retention volume [ml]

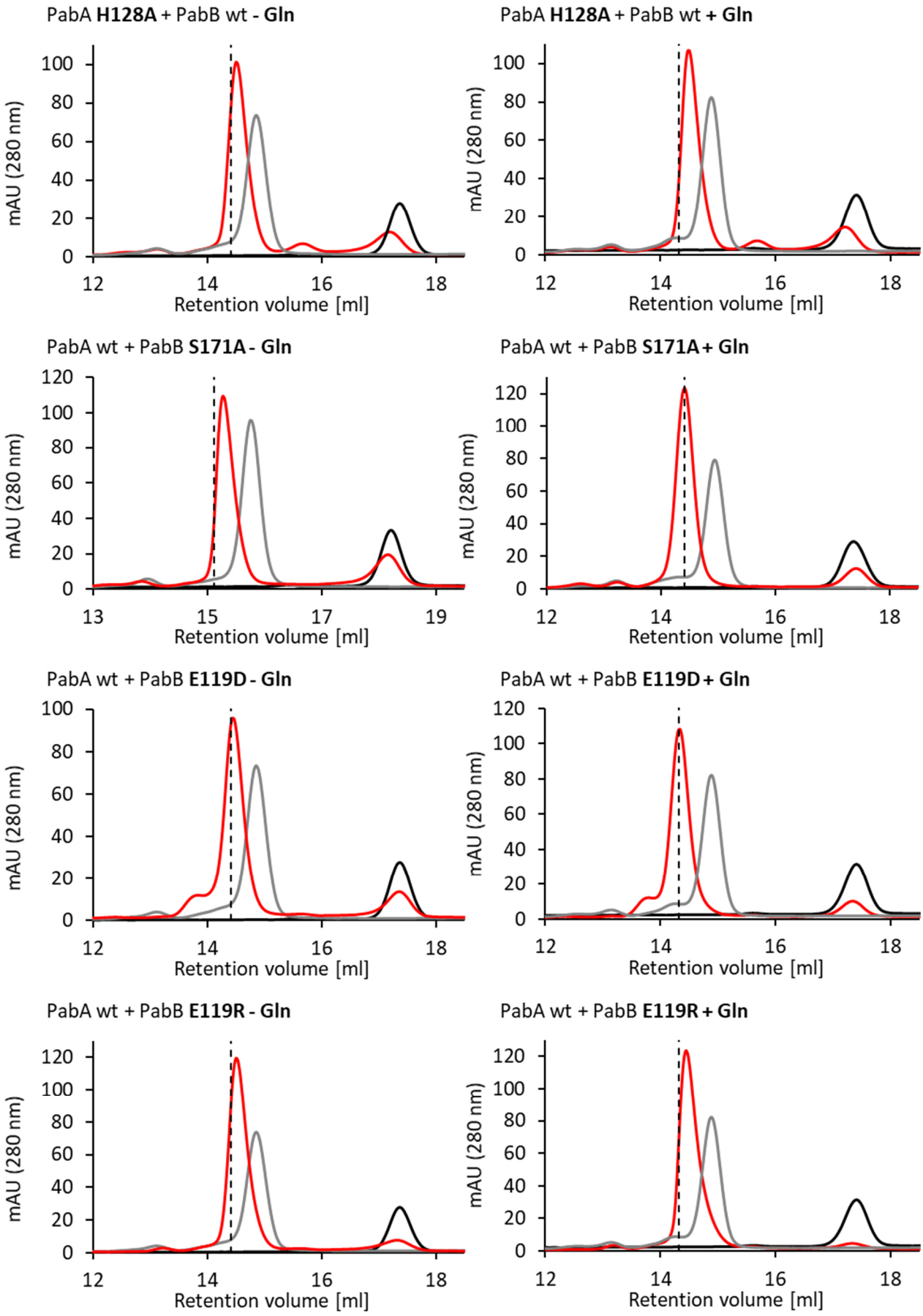
PabA H128A + PabB wt - Gln
PabA H128A + PabB wt + Gln
PabA wt + PabB S171A - Gln
PabA wt + PabB S171A + Gln
PabA wt + PabB E119D - Gln
PabA wt + PabB E119D + Gln
PabA wt + PabB E119R - Gln
PabA wt + PabB E119R + Gln
mAU (280 nm)
Retention volume [ml]

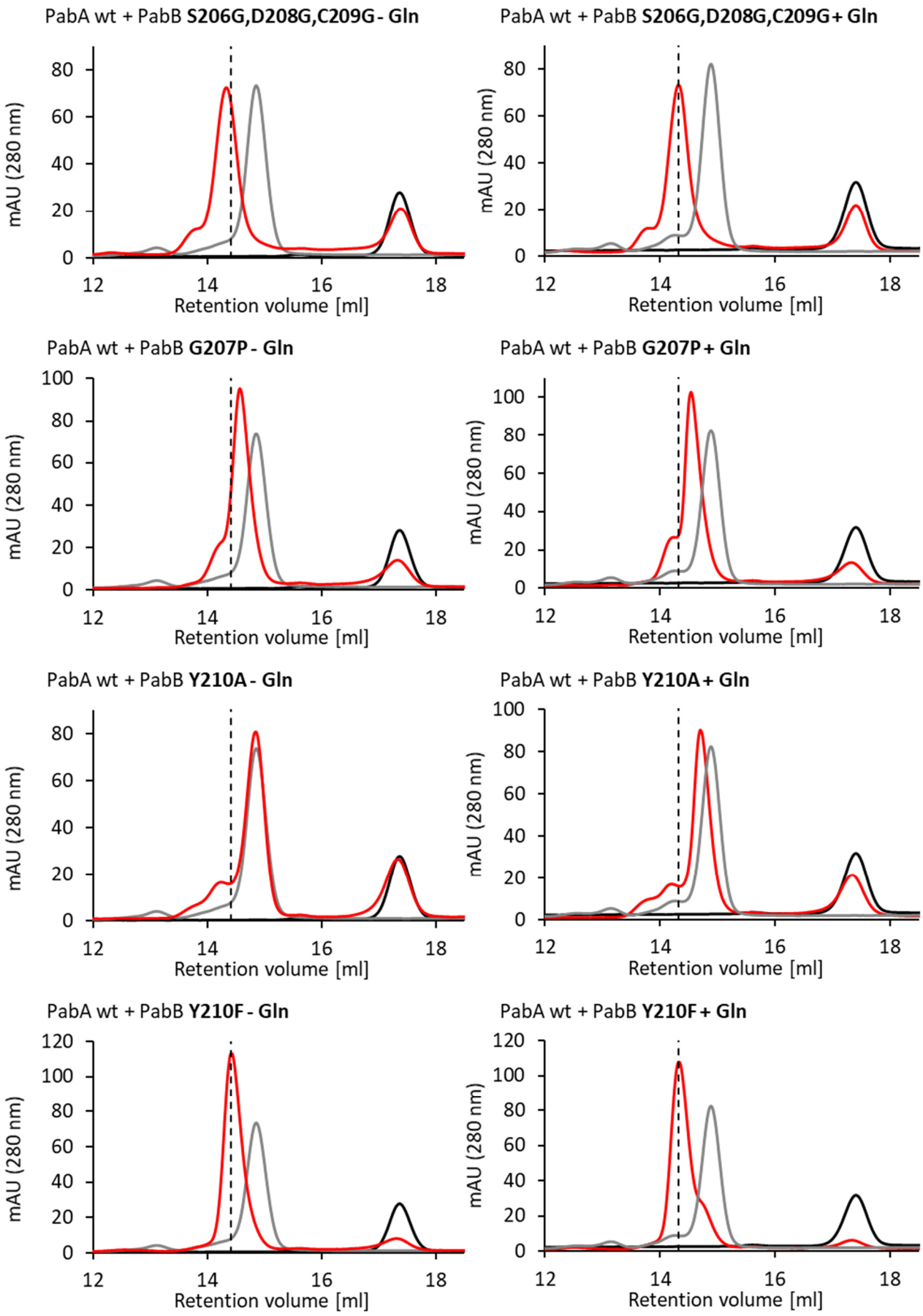
PabA wt + PabB S206G,D208G,C209G - Gln
PabA wt + PabB S206G,D208G,C209G + Gln
PabA wt + PabB G207P - Gln
PabA wt + PabB G207P + Gln
PabA wt + PabB Y210A - Gln
PabA wt + PabB Y210A + Gln
PabA wt + PabB Y210F - Gln
PabA wt + PabB Y210F + Gln
mAU (280 nm)
Retention volume [ml]

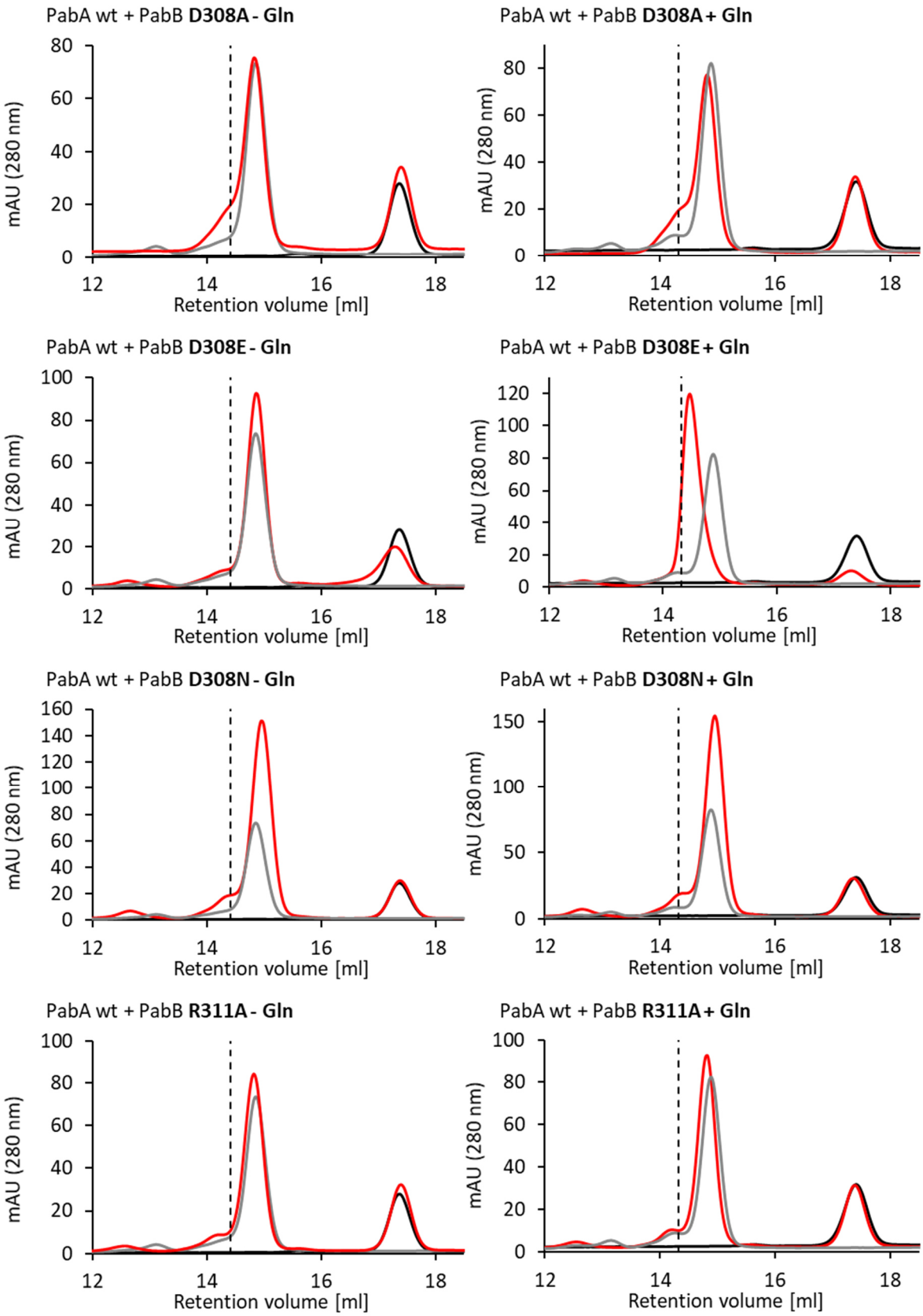

Figure S2.1: Elution profiles from analytical GF of PabA and PabB variants. Analytical GF was performed on a Superdex 200 column equilibrated with 50 mM Tris/HCl pH 7.5, 50 mM KCl, 5 mM $MgCl_2$, 2 mM DTT and, if indicated, 5 mM glutamine (Gln). Dashed line, retention volume of the wt PabA-PabB complex; black, wt PabA; grey, wt PabB; red, variant as indicated above each graph + respective wt interaction partner.

3 Validation of aminodeoxychorismate synthase and anthranilate synthase as novel targets for bispecific antibiotics inhibiting conserved protein-protein interactions

3.1 Abstract

Multi-resistant bacteria are a rapidly emerging threat to modern medicine. It is thus essential to identify and validate novel antibacterial targets that promise high robustness against resistance-mediating mutations. This can be achieved by simultaneously targeting several conserved function-determining protein-protein interactions in enzyme complexes from prokaryotic primary metabolism. Here, we selected two evolutionary related glutamine amidotransferase complexes, aminodeoxychorismate synthase and anthranilate synthase, that are required for the biosynthesis of folate and tryptophan in most prokaryotic organisms. Both enzymes rely on the interplay of a glutaminase and a synthase subunit that is conferred by a highly conserved subunit interface. Consequently, inhibiting subunit association in both enzymes by one competing bispecific inhibitor has the potential to suppress bacterial proliferation. We comprehensively verified two conserved interface hotspot residues as potential inhibitor binding sites *in vitro* by demonstrating their crucial role in subunit association and enzymatic activity. For *in vivo* target validation, we generated genomically modified *Escherichia coli* strains in which subunit association was disrupted by modifying these central interface residues. The growth of such strains was drastically retarded on liquid and solid minimal medium due to a lack of folate and tryptophan. Remarkably, the bacteriostatic effect was observed even in the presence of heat-inactivated human plasma, demonstrating that accessible host metabolite concentrations do not compensate for the lack of folate and tryptophan within the tested bacterial cells. We conclude that a potential inhibitor targeting both enzyme complexes will be effective against a broad spectrum of pathogens and offer increased resilience against antibiotic resistance.

3.2 Importance

Antibiotics are indispensable for the treatment of bacterial infections in human and veterinary medicine and are thus a major pillar of modern medicine. However, the exposure of bacteria to

antibiotics generates an unintentional selective pressure on bacterial assemblies that over time promotes the development or acquisition of resistance mechanisms, allowing pathogens to escape the treatment. In that manner, humanity is in an ever-lasting race with pathogens to come up with new treatment options before resistances emerge. In general, antibiotics with novel modes of action require more complex pathogen adaptations as compared to chemical derivates of existing entities, thus delaying the emergence of resistance. In this contribution, we use modified *Escherichia coli* strains to validate two novel targets required for folate and tryptophan biosynthesis that can potentially be hit by one and the same bispecific protein-protein interaction inhibitor and promise increased robustness against bacterial resistances.

3.3 Introduction

Since the discovery of sulfonamides and penicillin, antibiotics have become indispensable for the treatment of bacterial infections. Through decades of their application, however, resistances have developed against the commonly used agents and their derivatives, culminating in the emergence of multidrug-resistant pathogens that cause protracted or even life-threatening infections. According to the World Health Organization (WHO, https://www.who.int/news-room/fact-sheets/detail/antimicrobial-resistance accessed on 9 February 2024) and the World Bank, the spread of multi-drug resistant bacteria is associated with increased morbidity, mortality, and healthcare cost.[141, 142] In 2017, the WHO published a list of 12 pathogen families featuring a particularly high threat to public health, in which resistant *Acinetobacter baumannii*, *Pseudomonas aeruginosa*, and *Enterobacteriaceae* such as *Escherichia coli* were considered as most critical.[143] The preliminary climax was the appearance of an *E. coli* strain in China harboring the *mcr-1* gene that enables bacteria to withstand the last resort antibiotics of the polymyxin group. Within 12 months, this resistance gene has spread across the globe, has mutated, and has been transferred to other bacteria.[144] Hence, without fast and decisive action, the community is heading toward a post-antibiotic era, in which even common infections and minor injuries could become fatal. To preserve our ability to fight bacterial infections effectively, we must not only minimize the emergence and spread of resistances through a more careful use of antibiotics in humans and agricultural livestock, but also increase our efforts to develop new antibiotic agents against so-far unexploited targets.

Most currently used classes of antibiotics act by inhibiting a single enzyme target that catalyzes a key step of bacterial cell wall and membrane biosynthesis, or bacterial DNA, RNA, or protein

synthesis. These "traditional" antibiotics have only been incrementally modified during the past decades, mostly to overcome the resistance noted with earlier analogs of these classes.[145, 146] To counteract resistance development more sustainably, there is an urgent need for antibiotics with novel modes of action. A large and highly diverse group of new antibiotic targets comes into play when exploiting bacterial protein-protein interactions (PPI) occurring in enzyme complexes. Compared to a single enzyme whose active site is inhibited, targeting PPIs within enzyme complexes reduces the probability of resistance formation, as compatible interface mutations must occur simultaneously at all interacting subunits to prevent binding of the antibiotic while preserving function-determining wild-type interaction (**Figure 1.1**). However, in contrast to the usually deep binding pocket that makes up the active site of an enzyme, protein-protein interfaces tend to be large and flat and were thought to present few salient interactions that could serve as targets. This problem is mitigated by the finding that the major subunit binding energy in many PPIs is conferred by individual hotspot residues, which are surrounded by solvent-occluding amino acids.[50, 147] By mimicking or targeting such hotspot residues or regions, several compounds have been identified that inhibit selected PPIs and are used as lead compounds or drugs against various diseases.[57, 60, 64, 148]

Protein complexes that qualify as antibiotic targets must be essential for the growth, toxicity, and/or the survival of bacteria and, at the same time, should have no homologous human counterparts that could provoke off-target effects. Two such enzyme complexes are aminodeoxychorismate synthase (ADCS) and anthranilate synthase (AS) that catalyze the first steps of folate and tryptophan biosynthesis, respectively. Both ADCS and AS are bi-enzyme complexes that belong to the class of glutamine amidotransferases (GATases).[81] The functional unit of GATases comprises a glutaminase subunit (PabA in ADCS and TrpG in AS) that hydrolyzes glutamine to produce glutamate and ammonia, which is transferred through an inter-molecular channel to the associated synthase subunit (PabB in ADCS and TrpE in AS). There, ammonia is incorporated into the substrate of the synthase (chorismate for both PabB and TrpE), yielding specific products (4-amino-4-deoxychorismate for ADCS; anthranilate for AS). In both systems, the catalytic activities of the synthases and the glutaminases depend on the formation of functional heteromeric PabA-PabB (ADCS) or $TrpG_2$-$TrpE_2$ (AS) complexes.

Here, we aimed to test whether the disruption of ADCS and AS complex formation impacts bacterial growth and therefore qualifies their PPIs as antibiotic targets. For this purpose, we confirmed by *in silico* and *in vitro* validation that putative hotspot residues of the *E. coli* glutaminases ecPabA and ecTrpG and their homologs from *P. aeruginosa* are pivotal for

complex formation and enzymatic activity. The essentiality of complex formation was then demonstrated by introducing these hotspot mutations to the genomic DNA of *E. coli* BW25113. The modified bacterial strains, which exhibit impaired ADCS and AS complex formation, showed drastically retarded growth on liquid and solid minimal media and in the presence of human plasma, which was fully restored upon the addition of a folate precursor and tryptophan. The observed bacteriostatic effect validates the ADCS and AS enzyme complexes as novel targets for the development of bispecific antibiotically active agents with high resilience against the development of antibiotic resistance.

3.4 Results

3.4.1 *In silico* and *in vitro* validation of interface hotspot residues in the ADCS and AS complexes

Besides their similar catalytic activities, ADCS and AS also display remarkable structural similarities (**Figure 3.1A**), including highly conserved interface interactions. Specifically, a central aspartate residue of the synthase (ecPabB: D308; ecTrpE: D367) interacting with opposing tyrosine and serine residues of the glutaminase (ecPabA: Y127, S171; ecTrpG: Y132, S173) was found to be crucial for the formation of glutaminase-synthase complexes (**Figure 3.1B**).[115] Moreover, a phylogenetic analysis of a large set of AS and ADCS sequences showed that these putative hotspot residues are almost ubiquitously conserved in the bacterial kingdom (695 AS and ADCS sequences, non-redundant filtered set)[115] and also occur in pathogens on the WHO priority list, e.g. *P. aeruginosa* and *Staphylococcus aureus*. The conservation of putative interface hotspot regions between ADCS and AS enables the implementation of a further level of protection against resistance formation insofar as one and the same PPI inhibitor could block both glutaminase-synthase interactions, thereby preventing the biosynthesis of folate as well as tryptophan (**Figure 3.1C**).

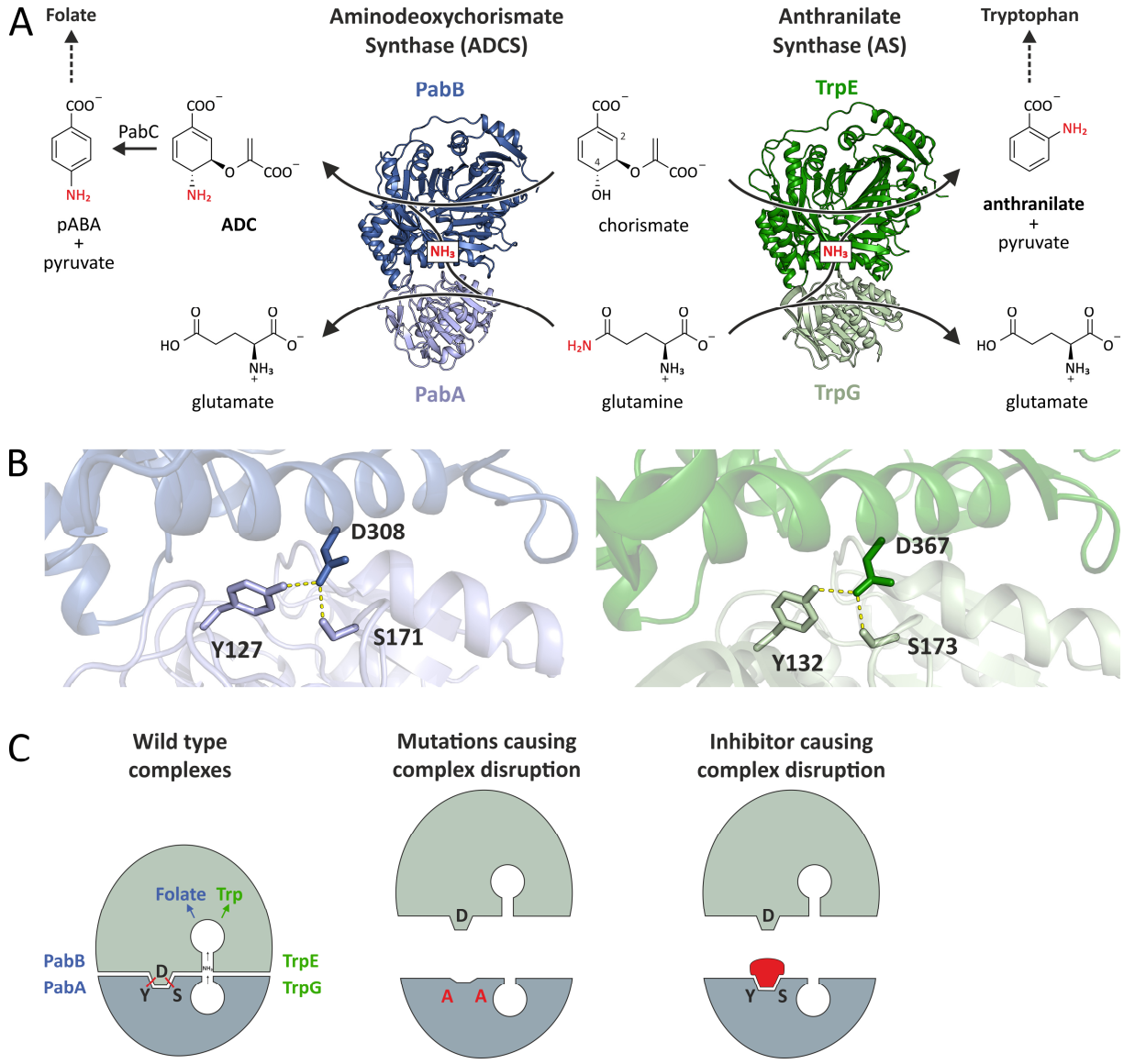

Figure 3.1. Reaction scheme and hotspot interface residues in ADCS and AS. (A) ADCS (homology model of the enzyme from *E. coli*)[79] consists of a glutaminase subunit PabA (light blue), and a synthase subunit PabB (blue). AS (crystal structure of the enzyme from *Serratia marcescens*, PDB-ID: 1I7Q)[69] is organized as a dimer of heterodimers (one heterodimer shown here) comprising the glutaminase subunit TrpG (light green) and the synthase subunit TrpE (green). The homologous complexes share the same fold and have r.m.s.d. values of 1.5 Å and 1.1 Å when superimposing the synthase or glutaminase subunits, respectively. The glutaminases hydrolyze glutamine to produce nascent ammonia, which is channeled to the respective synthase active site. In PabB, ammonia is incorporated at the C4 position of chorismate to produce 4-amino-4-deoxy-chorismate (ADC), which is further processed by the aminodeoxychorismate lyase PabC to pyruvate and para-amino-benzoate (pABA), a precursor of folate. TrpE catalyzes the incorporation of ammonia at the C2 position of chorismate and a subsequent lyase reaction to yield pyruvate and anthranilate, a precursor of tryptophan. (B) The positions of putative hotspot residues in the PPI of ADCS (left panel) and AS (right panel) are shown. (C) Schematic representation of the functional ADCS/AS complex with putative hotspot interface residues (left panel) and disruption of complex formation by the introduction of hotspot mutations (middle panel) or a putative PPI inhibitor (right panel).

To demonstrate that the formation of the ADCS and AS complexes is essential for bacterial growth, we mimicked the prospective disruption of complex formation by exchanging the *bona fide* hotspot residues required for glutaminase-synthase interaction. Corroborating previous findings, computational alanine scanning with the online tool Robetta,[149, 150] using a homology model of the ecPabA-ecPabB complex[79] and the TrpG-TrpE complex structure from *S. marcescens*,[69] showed that the D308A exchange in ecPabB and the D367A exchange in smTrpE (corresponding to D367A in ecTrpE) by far yielded the largest complex-destabilizing effects of all interface residues, with ΔΔG values of 12.25 kcal mol^{-1} and 8.19 kcal mol^{-1}, respectively (**Table S3.1**). Furthermore, *in silico* mutations of the residues tyrosine and serine in the glutaminase subunit, residues that form polar interactions with the opposing aspartate residue in the synthase subunit, also indicated significant complex destabilization: in the case of ecPabA, for Y127A a ΔΔG of 4.96 kcal mol^{-1} and for S171A a ΔΔG of 5.27 kcal mol^{-1} were calculated, whereas in the case of smTrpG residues, for Y133A (corresponding to ecTrpG Y132A) a ΔΔG of 2.96 kcal mol^{-1} and for S175A (corresponding to ecTrpG S173A) a ΔΔG of 3.68 kcal mol^{-1} were calculated (**Table S3.1**).

Based on these findings, we decided to impede ADCS and AS subunit association by generating the glutaminase double mutants ecPabA Y127A, S171A and ecTrpG Y132A, S173A. For *in vitro* analysis, the corresponding genes were produced by site-directed mutagenesis and overexpressed in *E. coli*, and the resulting recombinant proteins were purified from the soluble cell extract by metal chelate affinity chromatography using an N-terminal hexahistidine tag and subsequent preparative size exclusion chromatography (SEC). The purified glutaminase subunits and their corresponding mutants were then tested for their functional and physical interactions with the respective synthases ecPabB and ecTrpE. To this end, the turnover numbers (k_{cat}) of ADCS and AS with saturating concentrations of the synthase substrate chorismate and the glutaminase substrate glutamine were determined by steady-state kinetics. Moreover, glutaminase-synthase interactions were quantified by activity titrations in turnover assays to determine an apparent dissociation constant K_D^{app}. In addition, complex formation capacities were analyzed by analytical SEC. The results are shown in **Table 3.1, Figure S3.1** and **Figure S3.2**. Noticeably, there was no turnover activity of the double mutant ecPabA Y127A, S171A with ecPabB, which prevented the determination of complex affinities in activity titrations. This result indicated that, due to interrupted complex formation, no ammonia was delivered from the glutaminase to the synthase active site. In line with this conclusion, SEC experiments did not detect a stable complex between ecPabA Y127A, S171A and ecPabB

(**Figure S3.2**). In contrast, a slow conversion of chorismate to anthranilate was detected in the presence of ecTrpG Y132A, S173A and ecTrpE. However, the k_{cat} value was around 500-fold lower than that of the wild-type AS complex. Moreover, K_D^{app} was about 50-fold increased and SEC indicated that only a fraction of the subunits was engaged in complex formation. A plausible interpretation of these results is that the ecTrpG Y132A, S173A mutant transiently interacts with ecTrpE. Hence, the destabilization of the glutaminase-synthase complexes by the double alanine substitutions is less pronounced for the ecTrpG-ecTrpE system than for the ecPabA-ecPabB system, in accordance with the smaller ΔΔG values deduced from the *in silico* alanine scan.

We then tested the broader applicability of our approach by analyzing ADCS and AS mutants of the pathogen *P. aeruginosa* that is known to be an important cause of infection, especially in patients with compromised host defense mechanisms, and readily develops antibiotic resistances.[151, 152] This organism features one shared glutaminase paPabA for both synthases, paPabB and paTrpE. Generation and analysis of a paPabA double mutant with homologous amino acid exchanges revealed characteristics that are similar to the ones observed for the *E. coli* proteins: a mixture of paPabA Y127A, S176A with paPabB under saturating concentrations of chorismate and glutamine did not lead to detectable formation of ADC, and neither activity titrations nor SEC provided indications of complex formation (**Table 3.1**, **Figure S3.1** and **Figure S3.2**). Analogous to the measurements with the ecTrpG double mutant, a slow conversion of chorismate to anthranilate was detected with paPabA Y127A, S176A and paTrpE; however, the k_{cat} value was about 130-fold lower than that of the wild-type AS complex. Moreover, K_D^{app} was about 60-fold increased and SEC experiments did not detect a stable complex. Hence, paPabA Y127A, S176A and paTrpE seem to form a transient complex similar to ecTrpG Y132A, S173A with ecTrpE. We conclude that the same hotspot region as in *E. coli* is crucial for promoting subunit association and thus synthase activity. Hence, it is very likely that a potential PPI inhibitor would equally disrupt complex formation in the ADCS and AS of *P. aeruginosa* and *E. coli*.

Table 3.1: Turnover number and complex formation of synthases with wild-type and double mutant glutaminases at 25 °C.

Synthase	Glutaminase	Synthase activity (k_{cat} [s^{-1}])[a]	Complex affinity (K_D^{app} [nM])	Complex formation (SEC)[d]
ecPabB[b]	**ecPabA**	0.35 ± 0.01	35.9 ± 2.7	+
ecPabB[c]	**ecPabA Y127A, S171A**	Not detectable	Not detectable	-
ecTrpE[b]	**ecTrpG**	1.57 ± 0.02	32.7 ± 1.3	+
ecTrpE[c]	**ecTrpG Y132A, S173A**	<0.003[e]	>1730[e]	±[f]
paPabB[b]	**paPabA**	0.41 ± 0.01	41.5 ± 2.2	+
paPabB[c]	**paPabA Y127A, S176A**	Not detectable	Not detectable	-
paTrpE[b]	**paPabA**	3.85 ± 0.07	73.5 ± 3.3	+
paTrpE[c]	**paPabA Y127A, S176A**	0.03 ± 0.001	4360 ± 235	-

[a] Synthase activity was measured in 100 mM TEA, pH 8.5, 5 mM $MgCl_2$, 1 mM DTT, 200 µM chorismate, and 20 mM glutamine, PabB reactions additionally contained 2 µM bsPabC as an auxiliary enzyme.
[b] 0.05 µM synthase was titrated with 0.002-2 µM glutaminase.
[c] Between 0.25 and 2 µM synthase was titrated with 0.02-20 µM glutaminase.
[d] Glutaminase and synthase were mixed to a final concentration of 50 µM each and applied to a Superdex200 increase 10/300 GL column (GE Healthcare); elution was performed using 50 mM Tris/HCl, pH 7.5, 50 mM KCl, 5 mM $MgCl_2$, and 2 mM DTT.
[e] Values represent an estimation since residual activities were at the lower limit of detection.
[f] Partial AS complex formation was observed.

3.4.2 *In vivo* validation of ADCS and AS as targets for a PPI inhibitor

Based on the finding that the described hotspot mutations prevent functional and physical glutaminase-synthase interactions *in silico* and *in vitro*, we attempted to validate ADCS and AS as novel targets for a PPI inhibitor *in vivo*. To this end, *E. coli* gene deletion strains (Δec*pabA* or Δec*trpG*) and strains containing the hotspot mutations (ec*pabA* Y127A, S171A or ec*trpG* Y132A, S173A) were generated by homologous recombination. The effect of the genomic mutations on the growth of *E. coli* was analyzed in liquid and solid M9 minimal medium. To test whether growth deficiencies of the strains with hotspot mutations are due to reduced enzymatic activities caused by disruption of complex formation, control experiments in the presence of the folate precursor para-amino-benzoate (pABA) and tryptophan, respectively, were performed (**Figure 3.2**). Indeed, growth curves in liquid M9 medium indicated that hotspot mutations cause growth defects. In case of ec*pabA* Y127A, S171A, growth reduction amounts to around 70% within 18 h of incubation, similar to what is observed in the absence of the ec*pabA* gene (Δec*pabA*). In the case of ec*trpG* Y132A, S173A, growth is reduced by about 35% within 18 h, which is less pronounced than the 70% growth reduction observed for the Δec*trpG* strain. The stronger effect of the hotspot mutations in ecPabA Y127A, S171A compared to ecTrpG Y132A, S173A is in line with the *in vitro* results (**Table 3.1**). The addition of pABA and Trp to the culture medium restored the growth of all mutant strains to wild-type levels.

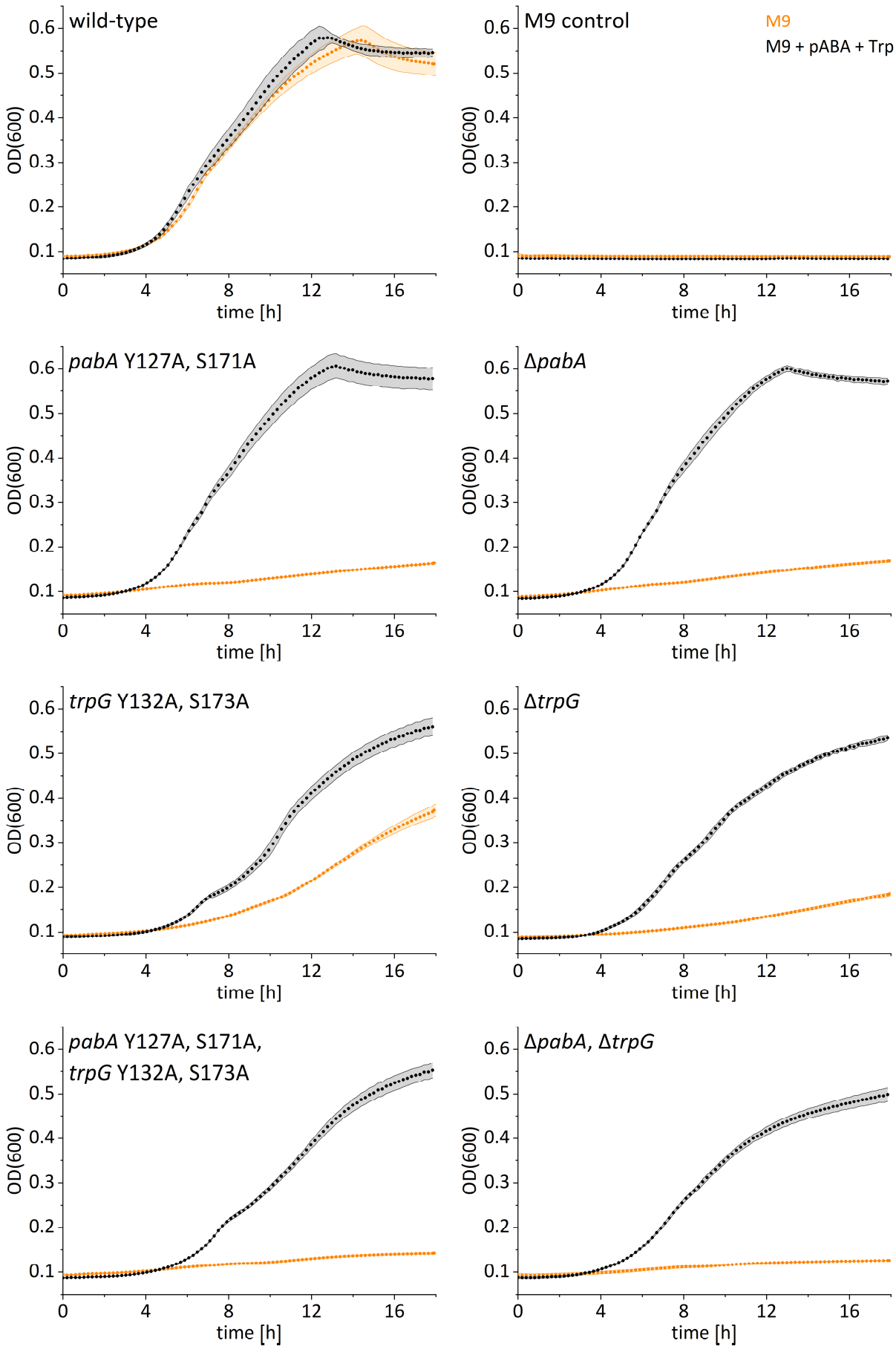
wild-type
M9 control
M9
M9 + pABA + Trp
pabA Y127A, S171A
ΔpabA
trpG Y132A, S173A
ΔtrpG
pabA Y127A, S171A,
trpG Y132A, S173A
ΔpabA, ΔtrpG
OD(600)
time [h]
0.1
0.2
0.3
0.4
0.5
0.6
0
4
8
12
16

Figure 3.2: Growth in liquid M9 minimal medium of *E. coli* strains with genomic manipulations of ec*pabA* or/and ec*trpG*. Growth curves of indicated strains were observed at 37°C in the absence (orange circles) and presence (black circles) of 100 nM pABA and 10 µM tryptophan (Trp), SDs are shown as orange or gray frames. "wild-type" represents the *E. coli* strain with unmodified *pabA* and *trpG* genes as positive control, "M9 control" indicates non-inoculated medium, "Δ*pabA*" and "Δ*trpG*" denote genomic deletions of the respective gene, "*pabA* Y127A, S171A" and "*trpG* Y132A, S173A" denote the introduction of hotspot mutations into the respective gene. Hotspot mutations resulted in a significant reduction of bacterial growth, which could be fully restored by the addition of pABA and Trp.

To gain further insights into the phenotypic effects caused by the mutations, growth analyses were also performed on solid M9 minimal medium (**Figure 3.3**). Under these conditions, the hotspot mutations increase the time required for the formation of visible colonies from one day to two days and slow down the increase in colony size, which corresponded to observations for the respective deletion mutants. The addition of pABA and tryptophan to the plates restored the growth of all mutant strains to wild-type levels, indicating that the observed growth phenotype was caused by a lack of folate and/or tryptophan.

A particular advantage of a common PPI inhibitor of ADCS and AS would be its ability to simultaneously block the biosynthesis of both folate and tryptophan. To mimic this effect, an *E. coli* strain containing the combined genomically encoded hotspot mutations ec*pabA* Y127A, S171A plus ec*trpG* Y132A, S173A was generated. The consequences of those mutations for the growth of *E. coli* were also analyzed on liquid and solid M9 minimal medium (**Figure 3.2** and **Figure 3.3**). On liquid medium, growth inhibition was comparable to what was observed for ec*pabA* Y127A, S171A; however, on solid medium, the combination of ec*pabA* and ec*trpG* hotspot mutations further delayed the formation of visible colonies to 4 days, in line with results obtained for the respective double deletion mutant Δ*pabA* Δ*trpG*. These findings underline the benefit of targeting two enzyme complexes at once. Again, the addition of pABA and tryptophan restored growth to wild-type levels.

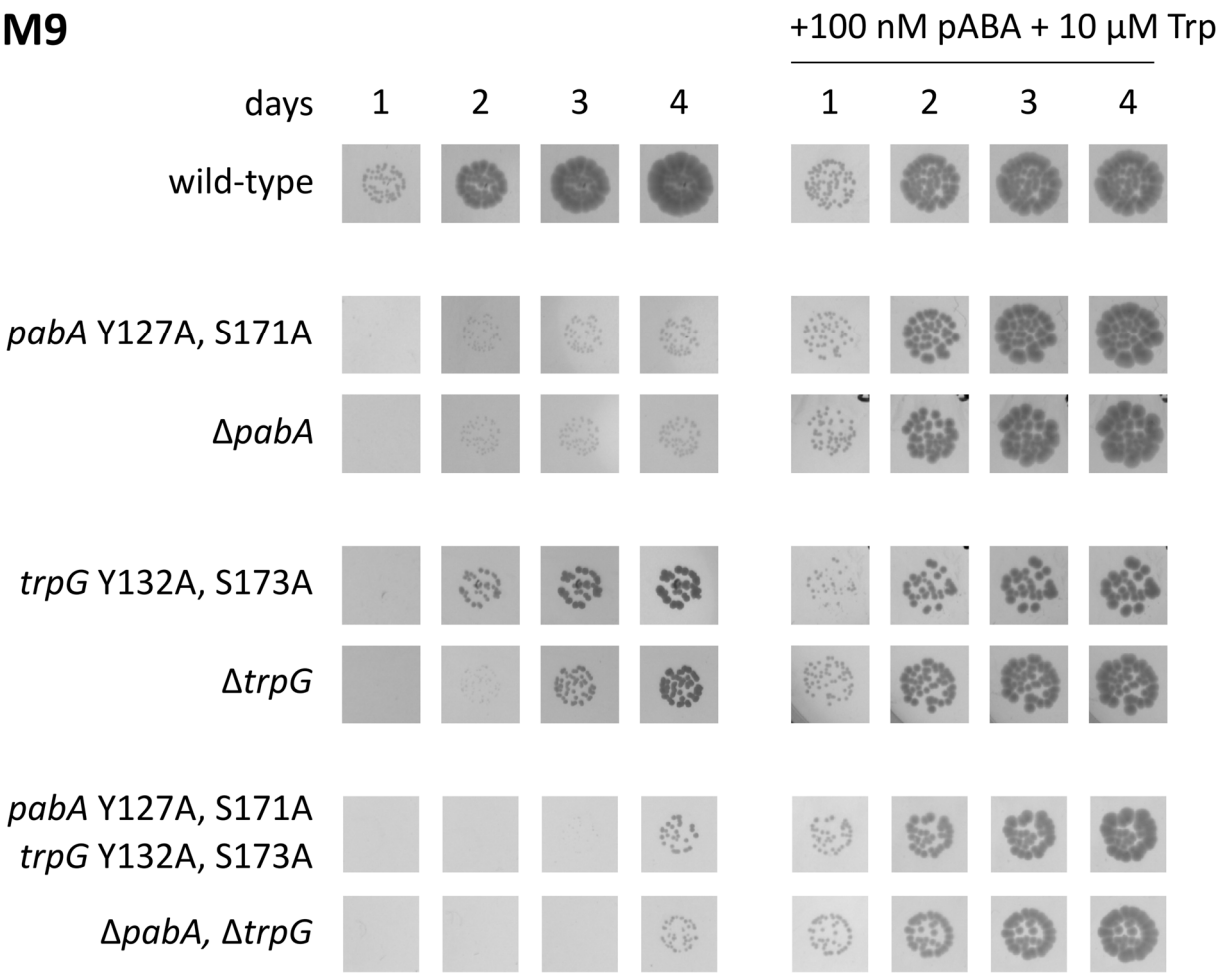

Figure 3.3: Growth on solid M9 minimal medium of *E. coli* strains with genomic manipulations of ec*pabA* or/and ec*trpG*. Colony formation velocity at 37°C of an *E. coli* wild-type control strain (wild-type, line 1) is compared with strains containing genomic manipulations of ec*pabA* (lines 2 and 3), ec*trpG* (lines 4 and 5), and the combined manipulations (lines 6 and 7). The addition of pABA and tryptophan (Trp) is indicated. Shown are growth plates after incubation for 1, 2, 3, and 4 days. Hotspot mutations resulted in a significant delay of bacterial growth, which could be fully restored by the addition of pABA or Trp.

For further *in vivo* validation, the growth of the *E. coli* strain containing genomic mutations ec*pabA* Y127A, S171A plus ec*trpG* Y132A, S173A or the double deletion strain Δ*pabA* Δ*trpG* was analyzed on solid M9 minimal medium supplemented with heat-inactivated human plasma at a share of 20% and 50% (**Figure 3.4**). The results show that even under these conditions the combined hotspot mutations drastically increase the time required for the formation of visible colonies compared to the wild-type control; actually, even after 6 days, only small colonies were visible, in accordance with observations for the double deletion strain. The addition of pABA and tryptophan again restored growth to wild-type levels. Addition of heat-exposed pABA and tryptophan equally restored growth of genetically modified strains (**Figure S3.3**), so we can exclude a potential disintegration of pABA or tryptophan in human plasma in the course of these experiments.

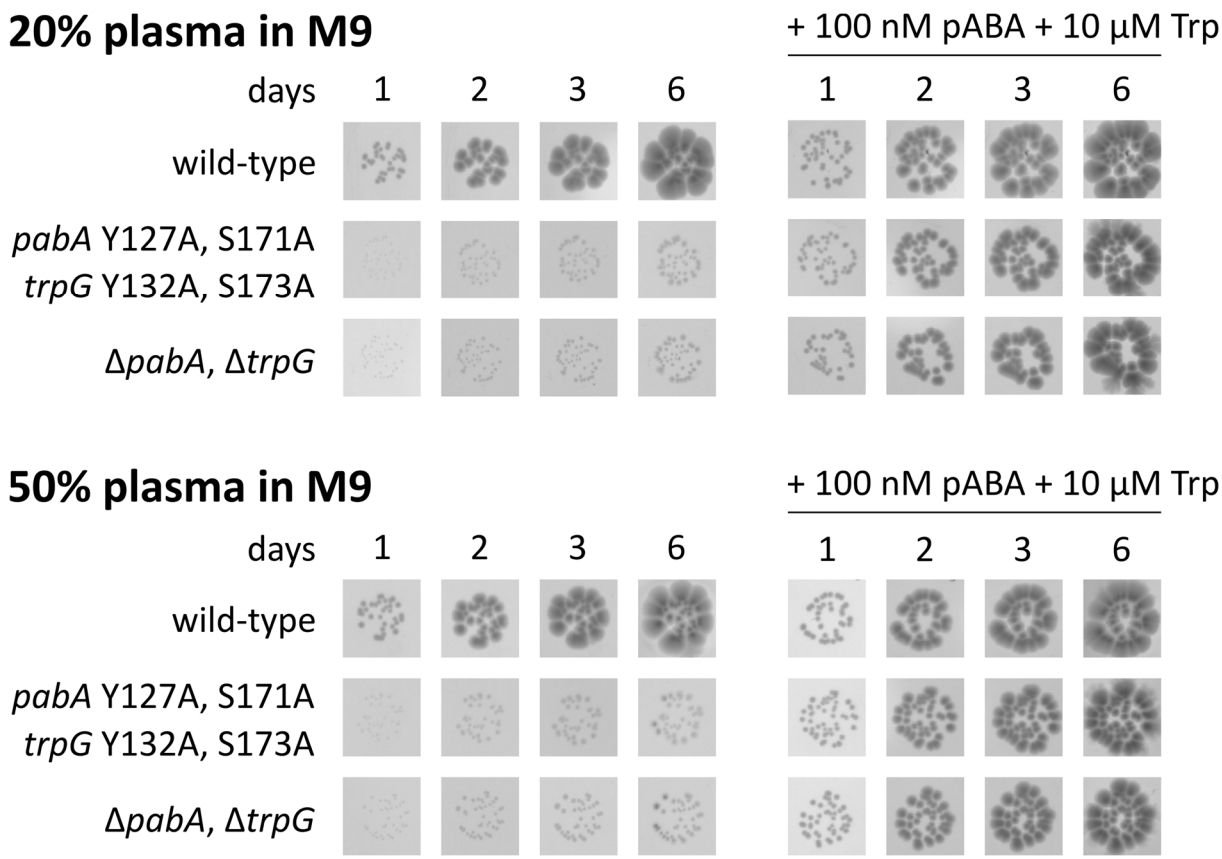

Figure 3.4 Growth of *E. coli* strains with genomic manipulations of ec*pabA* or/and ec*trpG* on solid M9 minimal medium supplemented with heat-inactivated human plasma. Colony formation velocity at 37°C of an *E. coli* wild-type control strain (wild-type) is compared with a strain containing genomic manipulations of ec*pabA* and ec*trpG* (*pabA* Y127A, S171A, *trpG* Y132A, S171A) and the double deletion mutant (Δ*pabA* Δ*trpG*). The addition of pABA and tryptophan (Trp) is indicated. Shown are growth plates after incubation for 1, 2, 3, and 6 days. Hotspot mutations resulted in a significant delay of bacterial growth, which could be fully restored by the addition of 100 nM pABA and 10 µM Trp.

3.5 Discussion

The identification and validation of new targets for antibiotics with novel modes of action remains a challenging endeavor. In this work, we selected two homologous enzyme complexes, ADCS and AS, that catalyze the committed steps of two essential metabolic pathways, folate and tryptophan biosynthesis, respectively. Importantly, the activity of both enzymes depends on the formation of functional glutaminase-synthase complexes, which makes it possible to control enzymatic activity with specific PPI inhibitors. Due to the high similarity of ADCS and AS subunit interfaces, which manifests in conserved interface hotspot residues, specific PPI inhibitors might have the potential to impair both enzyme activities, ADCS (PabA-PabB) and AS (TrpG-TrpE), simultaneously. With the analysis described in this work, we present a thorough target validation of the two enzyme complexes. In the first step, we could show that complex formation indeed depends on a set of well conserved hotspot residues: An aspartate

residue of the synthases interacting with tyrosine and serine residues of the glutaminases. Respective alanine substitution mutants of the glutaminases did not form stable complexes with their synthases and, accordingly, showed no ADCS activity and just residual AS activity *in vitro*.

Introducing the identified hotspot mutations into genomically encoded *E. coli* PabA or TrpG glutaminases revealed distinct growth phenotypes on liquid and solid medium, in all likelihood due to impaired association with their respective synthase PabB or TrpE. Impeding the AS complex led to the phenotype of tryptophan bradytrophs, with cells showing regular colonies, however with retarded growth that was fully restored upon supplementation of tryptophan. The disruption of ADCS complex formation on the other hand generated pABA auxotrophs with a small-colony phenotype. Small-colony variants have previously been observed for a broad range of bacteria, are characterized by a slowed metabolism (colonies were about one-tenth the size of the respective wild-type species), and are frequently associated with a deficiency in electron transport or the biosynthesis of thymidine.[153] Since tetrahydrofolic acid is required as a cofactor for thymidylate synthase and ADCS is needed for the production of folate, the similarity of phenotypes is plausible. In line with this, thymidine-dependent small-colony variants of *S. aureus* have been found in patients with chronic infections under long-term treatment with antifolates (trimethoprim-sulfamethoxazole) targeting reactions in folate biosynthesis downstream of ADCS.[154]

In vivo simultaneous complex disruption of both ADCS and AS further delayed the emergence of small colonies, indicating synergistic growth defects when targeting the two independent metabolic pathways. Simultaneous inactivation of the ADCS and AS complexes should reflect the mode of action of a bispecific PPI inhibitor. However, we observed that relatively low concentrations of pABA and tryptophan in the medium (100 nM and 10 µM, respectively) were sufficient to restore growth in strains with genomic mutations. Therefore, we were concerned that metabolite concentrations in the host cellular environment might already be sufficient to restore growth. The human metabolome database indicates blood concentrations of roughly 20-90 µM tryptophan and 5-30 µM pABA (www.hmdb.ca; accessed on 15 December 2023). Remarkably though, even in the presence of physiological concentrations of human plasma, bacterial growth of the mutant strains was drastically reduced, indicating that the available concentrations of exogenous metabolites are not sufficient to meet the demand of *E. coli*. It is likely, that the scarcity of tryptophan is even enhanced in the local environment of infections, where interferon gamma induces the expression of indoleamine-2,3-dioxygenases that

catabolize tryptophan. As a consequence, local tryptophan levels are depleted, which leads to starvation of the intruding pathogen.[155-157] For a final assessment of *in vivo* efficacy, comprehensive experiments with different pathogens in mammalian tissue culture and living organisms are needed to address local tissue conditions. Promising insights have however already been provided in previous studies,[158-160] which demonstrated that deletion of *pabA* or *pabB* genes drastically reduces the virulence and growth of *Listeria monocytogenes*, *Streptococcus pneumoniae*, and even the fungus *Aspergillus fumigatus* in mice.

In this context, it is worth mentioning that antifolates have been used for decades in the treatment of bacterial infections by targeting dihydropteroate synthase (sulfonamides)[161] or dihydrofolate reductase (trimethoprim),[162, 163] which catalyze reactions in the folate biosynthetic pathway downstream of ADCS. To overcome the fast development of resistances against these compounds, the sulfonamide sulfamethoxazole and trimethoprim are frequently applied in combination to achieve a synergistic inhibitory effect with an extended spectrum of activity.[164-166] As a matter of fact, co-targeting the biosynthesis of pABA has been shown to drastically increase the efficiency of sulfonamides and related substances (that bind competitively with pABA to dihydropteroate synthase) in *Mycobacterium tuberculosis.* Through such an approach, it was possible to restore susceptibility in a p-aminosalicylic acid resistant strain.[167, 168] Therefore, a specific inhibitor of ADCS and AS could potentially be used as an amendment to the existing sulfamethoxazole-trimethoprim treatment.

Similar to sulfonamides, an inhibitor targeting ADCS and AS is expected to function as a broad-spectrum antibiotic. Despite the obvious advantages of narrow antibiotics, namely the decreased risk of resistance formation and the preservation of commensal bacteria, in practice, the development of pathogen-specific antibiotics is scientifically challenging and comes with a further reduction of the already low economic incentive. Furthermore, it necessitates quick and reliable diagnostic tools for the identification of the pathogen prior to the treatment.[169, 170] The required time for the closure of this diagnostic and economic gap can be bridged by versatile antibiotics that are applicable for the treatment of multiple multi-resistant infections.

A logical continuation of the target validation presented in this work, would be the development of high-affinity PPI inhibitors that disrupt complex formation by mimicking hotspot interactions in the interfaces of ADCS and AS. To develop such PPI inhibitors, several approaches are conceivable. On the one hand, the rational design of small molecules or peptides that are modelled based on the hotspot region in the synthase interface is promising. On the

other hand, “randomized” approaches, including fragment screenings or phage display, might lead to success.[171, 172] For example, the inordinate interaction of p53 and MDM2 (murine double minute 2) has been shown to be a part of the pathophysiology of many cancer types.[173-175] A number of different PPI inhibitors have been developed by various approaches that bind to the relatively flat interface of MDM2 with affinities up to several orders of magnitude above p53.[176] The transfer into clinical application has proven difficult and the most successful compound to date just recently failed in a phase III study.[177] Nevertheless, ongoing clinical trials with various alternative compounds raise optimism for successful approval.[178] In another study, recombinant peptide libraries allowed for the identification of a peptide agonist that binds with high affinity to the flat binding site of the thrombopoietin receptor (TpoR), which natively interacts with the glycoprotein hormone thrombopoietin. The clinical application of the Fc-dimerized peptide (romiplostim) as a treatment of immune thrombocytopenia relies on its activating effect on TpoR to initiate the production of platelets. It was shown biophysically and structurally that the peptide binds competitively with thrombopoietin, and binding of both ligands relies on the same surface amino acid side chain of TpoR.[179, 180] With a potential clinical indication, competitive inhibitors could therefore be designed analogously to this or similar targets.

In targeting ADCS and AS, depending on the type and the intrinsic properties of the identified inhibitor, different decorations or modifications need to be considered to avoid cytotoxicity and to improve its stability and cellular uptake. In this context, the potential differential ability of the active ingredient to access the cytoplasm of gram-positive vs gram-negative or intracellular vs extracellular pathogens may dictate the spectrum of activity.[181-183]

3.6 Material and Methods

3.6.1 Computational alanine scanning

Computational alanine scannings were performed using the Robetta web tool with default parameters.[149, 150] Input protein complex structures were a homology model of PabA-PabB from *E. coli*[79] and the crystal structure of $TrpG_2$-$TrpE_2$ from *S. marcescens* (PDB-ID: 1i7q).[69]

3.6.2 Cloning and protein purification

The genes encoding ecPabA, ecPabB, ecTrpGD, ecTrpE and bsPabC were available from a previous study,[99] and the genes for paPabA, paPabB and paTrpE were codon-optimized for expression in *E. coli* and synthesized (ThermoFisher Scientific). The genes were cloned into a pET28a vector with an N-terminal His_6-Tag followed by a TEV cleavage site. TrpG is present in *E. coli* as a fusion protein with TrpD and was purified as such. For simplicity, however, it is referred to as ecTrpG. The solubility and stability of PabA enzymes were increased by the addition of an N-terminal Gly_5His-Tag via site-directed mutagenesis. Hotspot mutations of ecPabA, ecTrpG, and paPabA were introduced by site-directed mutagenesis. Gene expression and protein purification were performed essentially as described.[79] *E. coli* BL21-Gold (DE3) cells were transformed with the respective plasmid and grown in 3-8 L Luria broth medium supplemented with 50 µg/ml kanamycin at 37 °C to an OD_{600} of 0.6. Expression was induced by 0.5 mM IPTG, followed by overnight shaking at 25 °C. Cells were harvested, resuspended in 50 mM Tris/HCl, pH 7.5, 300 mM KCl, 10 mM imidazole, and 2 mM DTT, and lysed by sonication. Proteins were purified via Ni^{2+} affinity chromatography by applying the soluble lysate to a HisTrap excel column (5 ml, GE Healthcare). When possible, proteins were cleaved with TEV protease to remove the His_6-Tag (TEV protease to protein mass ratio: 1 to 50) while dialyzing against 3 L 50 mM Tris/HCl, pH 7.5, 50 mM KCl at 4 °C overnight, followed by reverse Ni^{2+} affinity chromatography. All proteins were further purified by preparative gel filtration on a Superdex75 pg HiLoad 26/600 column (320 ml, GE Healthcare). Protein concentrations were determined spectrophotometrically at 280 nm, with molar extinction coefficients calculated via ExPASy ProtParam.

3.6.3 Activity titrations

Enzymatic turnover of the synthase substrate chorismate was determined continuously under steady-state conditions.[99] Activity of ecTrpE and paTrpE was followed by the fluorescence of anthranilate (excitation at 313 nm and emission at 390 nm); the activity of ecPabB and paPabB was quantified in a coupled enzymatic assay with the aminodeoxychorismate lyase PabC from *B. subtilis*, coupling the turnover of chorismate to the production of pABA, which can be monitored by fluorescence spectroscopy (excitation at 290 nm and emission at 350 nm). All measurements were conducted at 25 °C in 96-well plates using a plate reader (Tecan Infinite M200 Pro) in the presence of 100 mM TEA, pH 8.5, 5 mM $MgCl_2$, 1 mM DTT, 200 µM

chorismate,[140] 20 mM glutamine and, in the case of PabB reactions, 2 µM bsPabC. Apparent K_D-values between wild-type glutaminases and synthases were estimated by titrating 0.05 µM synthase with 0.002-2 µM glutaminase. For glutaminases with hotspot mutations, concentrations were increased to 0.25-2 µM synthase and 0.02-20 µM glutaminase.

Chorismate turnover was calculated from fluorescence units using total turnover calibration curves that were linear between 0.5 and 50 µM chorismate. To obtain synthase activity k_{app}, the initial slope of the reaction time course was corrected by the glutaminase-free baseline and normalized by the synthase concentration. The turnover number k_{cat} and the apparent dissociation constant K_D^{app} were obtained by plotting k_{app} against the glutaminase concentration and applying a sigmoidal fit to the resulting plot using the Origin 2020 software ($k_{app} = \frac{k_{cat} * [Glutaminase]^2}{(K_D^{app})^2 + [Glutaminase]^2}$). The reported values are an average of a biological duplicate, each with two technical replicates, errors represent SDs.

3.6.4 Analysis of glutaminase-synthase complex formation

Analytical size exclusion chromatography was applied to assess the ability of wild-type and mutant glutaminases to associate with their respective synthase, essentially as described.[79] PabA and PabB subunits were applied individually at 50 µM or mixed in an equimolar ratio to final concentrations of 50 µM each. Samples were applied to a Superdex200 increase 10/300 GL column (GE Healthcare) operated on an ÄKTAmicro system (GE Healthcare). The column was equilibrated with 50 mM Tris/HCl pH 7.5, 50 mM KCl, 5 mM $MgCl_2$, and 2 mM DTT at 25 °C. Protein elution was performed at a flow rate of 0.3 ml/min and was followed by absorbance measurements at 280 nm. Calibration was performed with the Cytiva LMW and HMW calibration kits.

3.6.5 Genomic modification of *E. coli*

Chromosome engineering in *E. coli* was based on the λ Red recombination system, which is expressed by *E. coli* DY329 in a temperature-dependent manner.[184, 185] Linear DNA constructs for homologous recombination were flanked by 50 nucleotide extensions corresponding to regions upstream and downstream of the target locus. To generate deletion mutants Δ*pabA*, Δ*trpG*, and Δ*trpRLEGD*, the linear DNA construct comprises a resistance cassette from the pKD3 (chloramphenicol) or pKD4 plasmid (kanamycin).[184] For the generation of wild-type

controls and hotspot-mutated strains, a chloramphenicol resistance cassette was fused with the respective wild-type or hotspot-mutated *pabA* or *trpRLEGD* sequence and was introduced to Δ*pabA* or Δ*trpRLEGD* strains bearing kanamycin resistance to ensure full integration of the modified sequence.

E. coli DY329 cells were grown at 30 °C to an OD of 0.4-0.6, then shaken at 37 °C for 15 min to induce recombinase genes. Subsequently, they were shaken on ice and thoroughly washed with ice-cold ddH_2O. The electrocompetent cells were transformed with 100-300 ng of the respective linear DNA construct by electroporation (2500 V, 25 µF, 200 Ohm), grown overnight at 30 °C and then screened on selective LB plates. The success of genomic modifications was confirmed by colony PCR and Sanger sequencing.

As *E. coli* DY329 is vulnerable to temperatures higher than 30 °C, modifications made to genomic DNA of *E. coli* DY329 were transferred to *E. coli* BW25113 by P1 transduction, which enables the transfer of chromosomal regions up to a length of 100 kb from one bacterial strain to another.[186] P1-donor lysates were generated by infecting modified *E. coli* DY329 cells with P1 phages in LB medium amended with 0.2% glucose and 5 mM $CaCl_2$. Upon lysis, 10% chloroform was added to lyse surviving cells, followed by centrifugation to yield the donor lysate in the supernatant. 800 µl of an *E. coli* BW25113 (recipient) overnight culture in LB medium amended with 2.5 mM $CaCl_2$ was infected with 400 µl donor lysate for 25 min at 37 °C without shaking. After halting the infection with 5 ml saline (145 mM NaCl and 50 mM trisodium citrate), cells were grown for 1 h at 37 °C and then screened on selective LB plates. The success of genomic modifications was again confirmed by colony PCR and Sanger sequencing.

To facilitate the generation of strains in which both *pabA* and *trpG* were mutated, the chloramphenicol resistance cassette (which is flanked by FLP recognition target sites) was excised from Δ*pabA*-Cam, *pabA* Y127A, S171A-Cam, and *pabA* wt-Cam BW25113 strains by FLP (encoded on the pCP20 plasmid) as described previously.[184, 187] P1 donor lysates conferring the desired *trpG* modifications (fused to the chloramphenicol resistance cassette from pKD3) were then applied to the respective Cam-sensitive *pabA*-modified strains as described above. The success of genomic modifications was again confirmed by colony PCR and Sanger sequencing.

3.6.6 Growth assays on liquid and solid medium

While all investigated strains held a chloramphenicol resistance cassette, growth assays were performed in the absence of any antibiotics to avoid potential influence on proliferation.[188] Overnight cultures were grown at 37 °C in M9 medium supplemented with 30 µg/ml chloramphenicol, 100 nM pABA and 10 µM Trp. Cells were harvested and washed thoroughly with 0.9% NaCl to remove any excess supplements. For growth assays in liquid medium, 1 ml M9 medium (where indicated, amended with 100 nM pABA and 10 µM Trp) was inoculated to an OD_{600} of 0.01 in a sterile 24-well plate. Bacterial growth at 37 °C and 140 rpm was followed by measuring OD_{600} values in a plate reader (Tecan Infinite M200 Pro). Errors represent SDs of triplicates. To observe growth on solid medium, the washed cells were diluted to an OD_{600} of 1 x 10^{-5}, and drops of 5 µl were placed on solid M9 medium (where indicated, amended with 100 nM pABA and 10 µM Trp) and incubated at 37 °C. Measurements were performed at least in duplicates with reproducible effects. Human plasma was kindly provided by Prof. Dr. Dr. André Gessner (University Hospital Regensburg) and was heat inactivated at 56 °C for 30 min prior to its addition to M9 minimal medium with 1.5% agar.

3.7 Acknowledgement

This work was supported by the grant 16GW0257 from the German Ministry for Education and Research (Bundesministerium für Bildung und Forschung). We thank Jeannette Ueckert and Sonja Fuchs for expert technical assistance, André Gessner (University Hospital Regensburg) for providing human plasma samples, and Maximilian Plach and Matthias Wilmanns for comments on the manuscript.

3.8 Supplemental data

Table S3.1: Computational alanine scanning using a homology model of the ecPabA-ecPabB complex and the TrpG-TrpE complex structure from *Serratia marcescens*. All interface residues with a calculated ΔΔG>2 kcal/mol are listed. Homologous residues between ecPabA-ecPabB[79] and smTrpG-smTrpE[69] are listed in the same column, dashed lines indicate direct interactions between listed residues as observed in the structures. Residues highlighted in blue or green comprise the deduced hotspot residues from ecPabA-ecPabB or smTrpG-smTrpE, respectively.

PabB						Y210		**D308**		R311	N312					
ΔΔG(complex) (kcal/mol)						2.10		**12.25**		7.30	2.19					
PabA			Q17		H101		**Y127**		**S171**							
ΔΔG(complex) (kcal/mol)			3.21		2.99		**4.96**		**5.27**							
TrpE				E159		F262		**D367**		R370	N371	D372	Q488			
ΔΔG(complex) (kcal/mol)				2.05		2.95		**8.19**		3.84	3.69	3.93	2.87			
TrpG	F13	N16		R32	H107		**Y133**		**S175**							
ΔΔG(complex) (kcal/mol)	2.10	2.58		2.02	4.46		**2.96**		**3.68**							

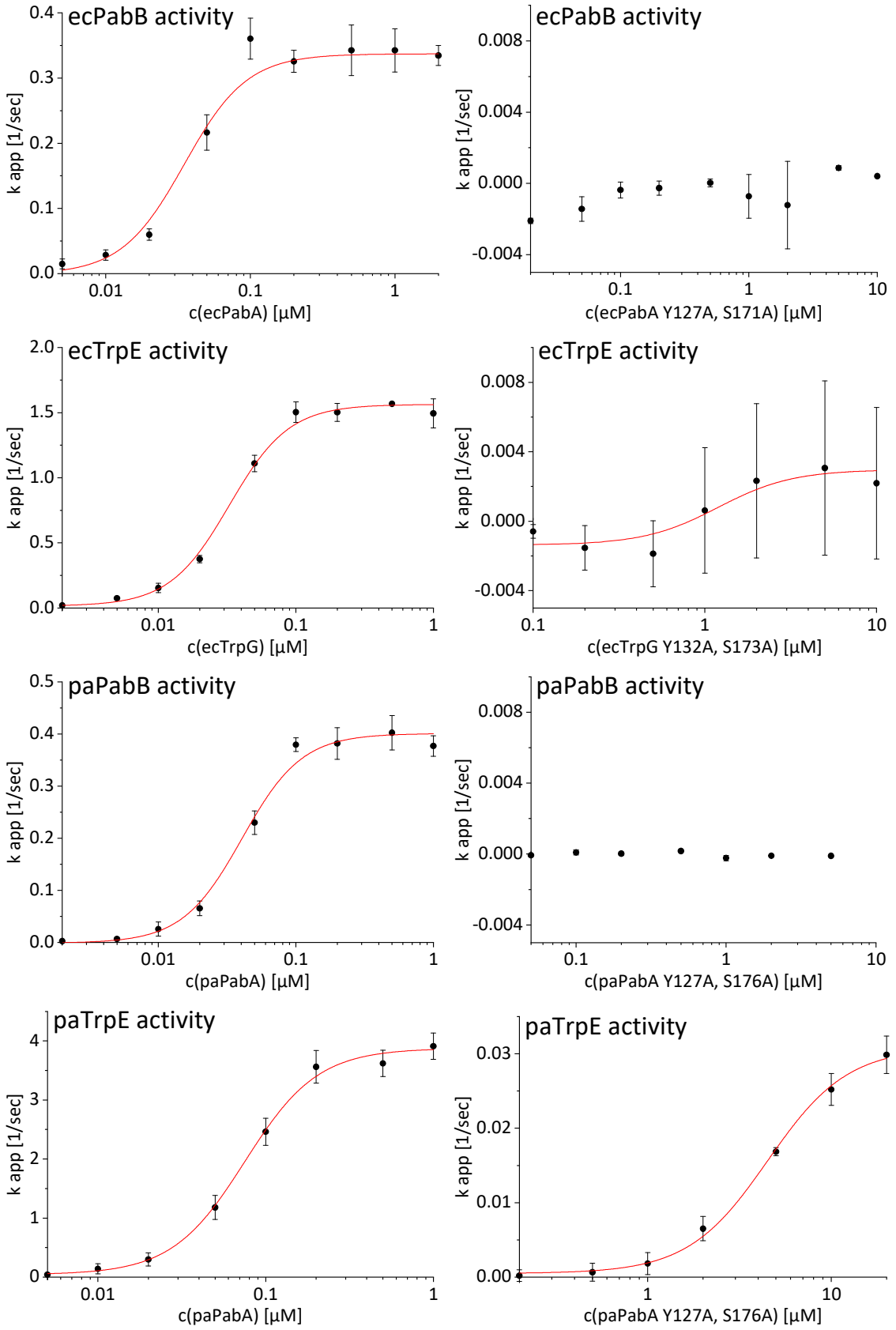

Figure S3.1: Activity titrations monitoring glutaminase-dependent synthase activities. Apparent turnover numbers at 25 °C of the indicated synthases are plotted against the concentration of wild-type glutaminases (left column) or glutaminases with hotspot mutations (right column). Error bars indicate standard deviations, red lines represent the applied sigmoidal fit. Glutaminases with hotspot mutations do not or only marginally stimulate the activity of PabB or TrpE, respectively.

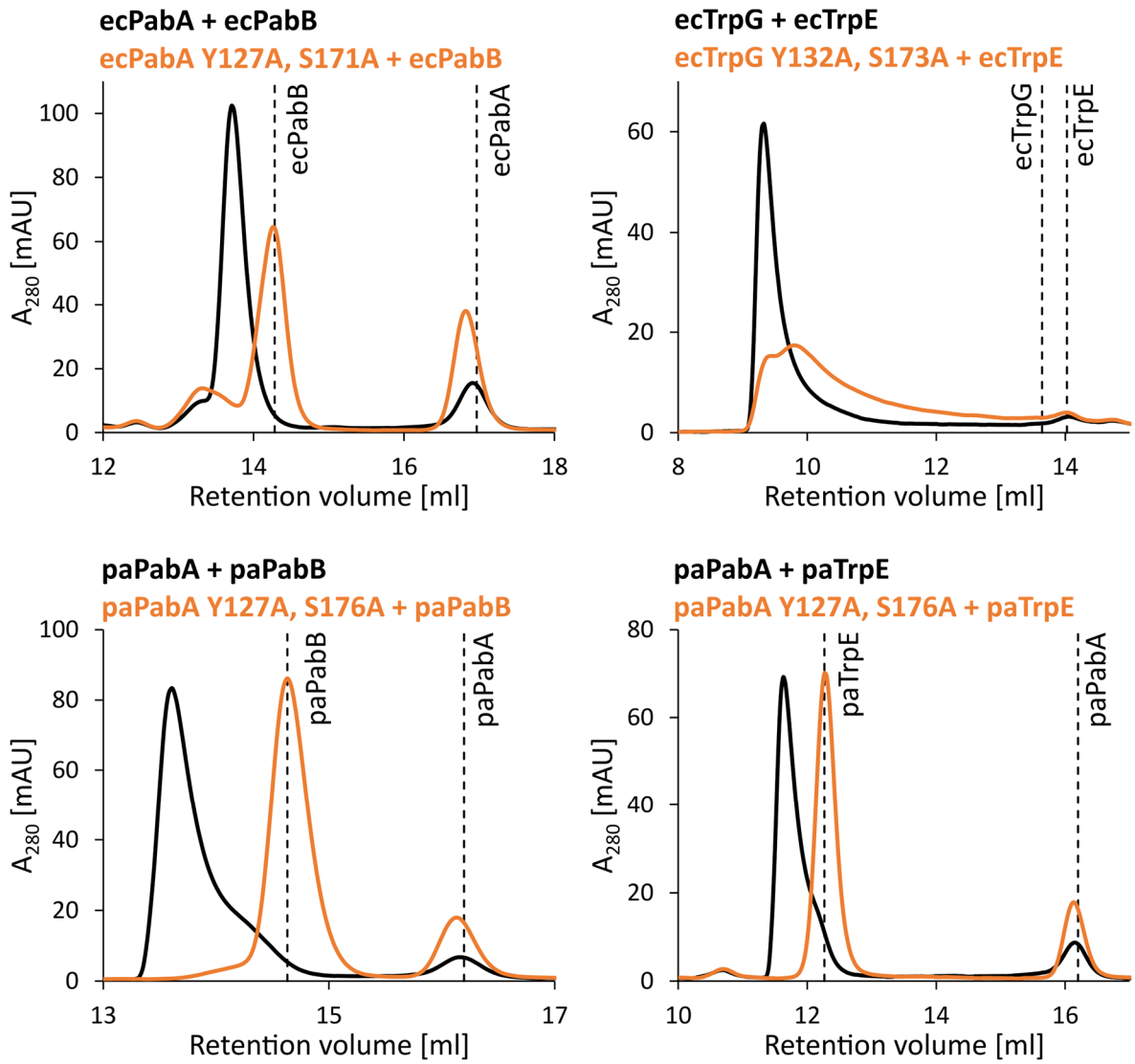

Figure S3.2: Assessment of glutaminase-synthase association by analytical size exclusion chromatography. Retention volumes of the isolated glutaminase and synthase subunits are marked as vertical dashed lines in each plot. Elution profiles of indicated synthases mixed with the respective wild-type glutaminase or mutated glutaminase are shown in black and orange, respectively. Glutaminase and synthase were mixed to a final concentration of 50 µM each and applied on a Superdex200 increase 10/300 GL column (GE Healthcare); elution was performed using 50 mM Tris/HCl pH 7.5, 50 mM KCl, 5 mM $MgCl_2$ and 2 mM DTT.

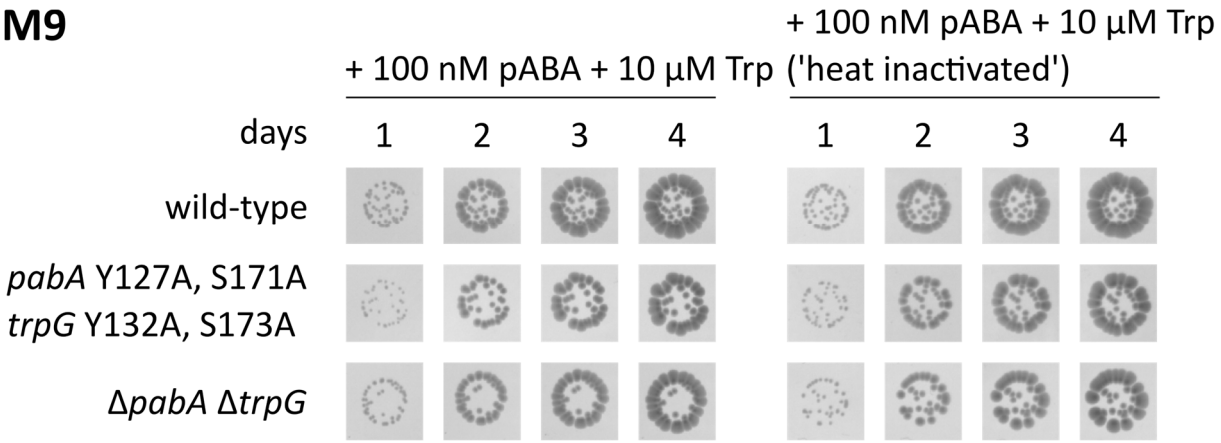

Figure S3.3: Growth of *E. coli* strains with genomic manipulations of ec*pabA* or/and ec*trpG* on solid M9 minimal medium supplemented with untreated or "heat inactivated" pABA and Trp. Colony formation velocity at 37 °C of an *E. coli* wild-type control strain (wild-type) is compared with a strain containing genomic manipulations of ec*pabA* and ec*trpG* (*pabA* Y127A, S171A, *trpG* Y132A, S171A) and the double deletion mutant *(*Δ*pabA* Δ*trpG*). Addition of para-amino-benzoate (pABA) and tryptophan (Trp) is indicated. Shown are growth plates after incubation for 1, 2, 3 and 4 days. Preincubation of pABA and Trp for 30 min at 56 °C had no effect on the growth of genomically modified strains, confirming the resilience of pABA and Trp against heat treatment.

4 Comprehensive discussion and outlook

In this work, two independent but related enzyme complexes were identified, that represent interesting polypharmacological targets in the fight against bacterial infections due to their inherent structural and sequential conservation. The two enzyme complexes, aminodeoxychorismate synthase (ADCS) and anthranilate synthase (AS), catalyze the committed steps in folate and tryptophan biosynthesis, respectively, and are essential for most bacteria. The successful validation of ADCS and AS as antibiotic targets for bispecific protein-protein interaction inhibitors presented in chapter 3 of this thesis lays the foundation for the subsequent inhibitor development.

As mentioned in section 3.5, the identification of lead compounds inhibiting subunit association could be achieved by (computationally driven) rational drug design, by high-throughput screenings of chemical or biological libraries or combinations thereof. Rational drug design approaches generally benefit from comprehensive data on the prospective target, including the enzymatic mechanism, structural properties and the determination of functional and structural roles of selected residues. The joint structural and functional analyses performed in chapter 2 of this work allow to draw the following conclusions about the processes underlying catalysis in ADCS:

(i) The glutaminase activity is strictly dependent on interactions with the synthase, which are required to complete and to seal the shared glutamine binding pocket and to induce a catalytically competent side chain conformation of the catalytic triad.
(ii) The ADCS complex adopts at least two states entailed by subunit rearrangements, enabling substrate access in the open complex state and the solvent-excluded glutaminase reaction in the closed complex state.
(iii) The observed rearrangements are triggered by the substrate glutamine, which induces a complex-stabilizing extension of the glutaminase-synthase interface.

These findings suggest two primary strategies for the development of PPI-inhibitors, namely the disruption of the glutamine-independent glutaminase-synthase association or the destabilization of the glutamine-induced closed complex state (**Figure 4.1**). The former target site includes the hotspot residues aY127 and aS171, and represents a highly conserved epitope suitable for a range of lead identification approaches. Extension of this site to the PabB-helix, which spans over a large part of the PabA-PabB interface and is involved in several additional

interactions with PabA, opens up further avenues such as helix-mimicry by macrocycles or peptide inhibitors (**Figure 4.1A**). The target site for the second strategy is less defined, however, since this approach is based on a shift in conformational equilibrium rather than competitive complex disruption, weaker binders would have higher propensities to exert an inhibiting effect (**Figure 4.1B**). It is unclear whether a direct extension of this approach to the AS enzyme complex would be feasible, since all AS structures, irrespective of bound ligands, correspond to a closed complex state as judged by structural superpositions with ADCS.[69, 83, 103] However, since the mode of glutamine access to the binding pocket of AS is not fully understood, a physiological second (open) state unfavored by crystallization conditions is conceivable, but requires clarifying orthogonal investigations on the AS complex.

After a successful identification of (lead) compounds, the presented crystallization conditions producing high-quality crystals of the target enzymes will facilitate the structural elucidation of target-inhibitor complexes to characterize the binding site and binding mode of inhibitors, and, moreover, will enable structure-based compound optimization.

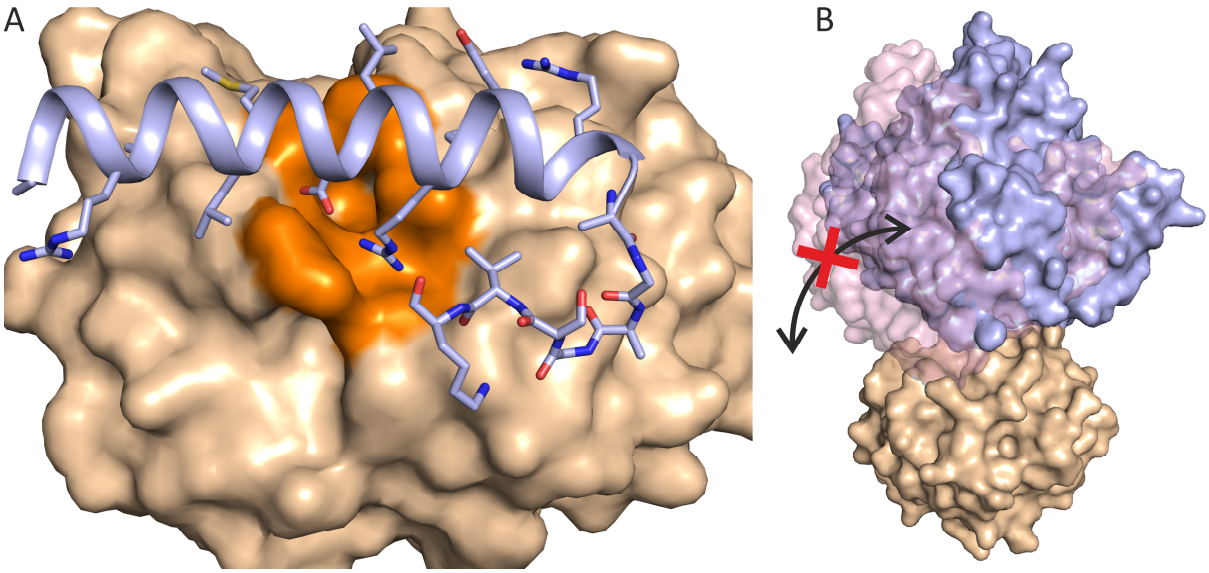

Figure 4.1: Strategies for inhibitors disrupting functional PPIs in ADCS and AS. (A) Competitive disruption of glutaminase-synthase complex formation at the glutaminase hot-spot region (orange) could for instance be achieved by mimicking the PabB helix located centrally in the PabA-PabB interface (light blue helix) or by small molecules binding specifically to the hot-spot residues (not shown). (B) Disruption of the equilibrium between the open (wheat-blue) and the closed (wheat-pink) complex state prospectively prevents efficient glutamine binding and thus catalytic activity of the complex.

The functional and structural characterization of *E. coli* ADCS presented in chapter 2 of this thesis provides comprehensive mechanistic insights. Nevertheless, further research on different aspects of the ADCS and AS enzymes will continue to unveil remaining enigmas. For instance, the evolutionary pathways leading to the development of extant ADCS, AS and the other MST

enzymes involved in primary and secondary metabolism have not been elucidated to date. Identifying the molecular determinants of similarities and differences between MST enzymes is expected to provide valuable insights. One such element is the conserved tryptophan-binding site in MST enzymes, which allows tryptophan-mediated feedback control in TrpE,[100-103] but is occupied by intrinsic aromatic side chains in other known MST enzymes.[105-107] An exception is PabB, which displays a seemingly erratic organism-dependent pattern of accessible and blocked tryptophan binding sites: While in ecPabB, the bound tryptophan cannot be removed without protein unfolding,[85] it displays a dissociation constant of about 12 µM in PabB from *Stenotrophomonas maltophilia*,[96] whereas in PabB from *Cytophaga hutchinsonii*, an intrinsic phenylalanine occupies the tryptophan binding site.[104] Generation of common ancestors by sequence reconstruction,[189] guided site-directed mutagenesis and investigation of tryptophan-binding in additional PabB enzymes are expected to shed light on the evolutionary origins of this observation.

Furthermore, while a unifying synthase reaction mechanism has been proposed for the MST enzymes,[86, 190, 191] the mechanisms differ in the identity of the nucleophile performing the initial nucleophilic attack (**Figure 1.4**). TrpE directly employs the ammonia provided by TrpG,[192, 193] in contrast, in PabB enzymes, the nucleophilic attack is performed by either a catalytic lysine or by ammonia. The different PabB classes can be distinguished by their active site motifs, displaying either a PI**K**GT or, like TrpE enzymes, a PI**A**GT motif.[96] Along the same lines, the observation that TrpE, but not PabB, has an additional lyase activity, is not fully understood to date. Pursuing an establishment of such activity in PabB and functional transformations between enzymes with PIKGT and PIAGT motifs is expected to add to the knowledge about the molecular prerequisites for these enzymatic reactions.

In the same context, the discovery of organisms expressing only one glutaminase subunit that functionally interacts with both PabB and TrpE raises questions about the regulatory mechanisms of glutaminase activation in these organisms. In light of the (seemingly) distinctly different glutaminase activation mechanism in *E. coli* ADCS and AS, investigations on organisms with a shared glutaminase will contribute to a deeper understanding of the underlying regulatory and evolutionary processes. In sum, these species containing an amphibolic PabA subunit represent valuable tools to investigate the evolutionary origins of MST enzymes based on combinatorial insights on tryptophan binding, enzymatic mechanisms as well as inter-subunit crosstalk.

5 References

1 Lukjancenko O, Wassenaar TM, Ussery DW (2010). Comparison of 61 sequenced *Escherichia coli* genomes. *Microb Ecol.* 60: 708-720

2 Hartwell LH, Hopfield JJ, Leibler S, Murray AW (1999). From molecular to modular cell biology. *Nature.* 402: 47-52

3 Youssef A, Bian F, Paniikov NS, Crovella M, Emili A (2023). Dynamic remodeling of *Escherichia coli* interactome in response to environmental perturbations. *Proteomics.* 23: 2200404

4 Wuchty S, Uetz P (2014). Protein-protein interaction networks of *E. coli* and *S. cerevisiae* are similar. *Sci Rep.* 4: 1-7

5 Arifuzzaman M, Maeda M, Itoh A, Nishikata K, Takita C, Saito R, Ara T, Nakahigashi K, Huang H-C, Hirai A (2006). Large-scale identification of protein-protein interaction of *Escherichia coli* K-12. *Genome Res.* 16: 686-691

6 Rajagopala SV, Sikorski P, Kumar A, Mosca R, Vlasblom J, Arnold R, Franca-Koh J, Pakala SB, Phanse S, Ceol A (2014). The binary protein-protein interaction landscape of *Escherichia coli*. *Nat Biotechnol.* 32: 285-290

7 Babu M, Bundalovic-Torma C, Calmettes C, Phanse S, Zhang Q, Jiang Y, Minic Z, Kim S, Mehla J, Gagarinova A (2018). Global landscape of cell envelope protein complexes in *Escherichia coli*. *Nat Biotechnol.* 36: 103-112

8 Gong W, Guerler A, Zhang C, Warner E, Li C, Zhang Y (2021). Integrating multimeric threading with high-throughput experiments for structural interactome of *Escherichia coli*. *J Mol Biol.* 433: 166944

9 Berggård T, Linse S, James P (2007). Methods for the detection and analysis of protein-protein interactions. *Proteomics.* 7: 2833-2842

10 Braselmann E, Chaney JL, Clark PL (2013). Folding the proteome. *Trends Biochem Sci.* 38: 337-344

11 Livesey BJ, Marsh JA (2022). The properties of human disease mutations at protein interfaces. *PLoS Comput Biol.* 18: e1009858

12 Schuster-Böckler B, Bateman A (2008). Protein interactions in human genetic diseases. *Genome Biol.* 9: 1-12

13 Jubb HC, Pandurangan AP, Turner MA, Ochoa-Montaño B, Blundell TL, Ascher DB (2017). Mutations at protein-protein interfaces: Small changes over big surfaces have large impacts on human health. *Prog Biophys Mol Biol.* 128: 3-13

14 Nooren IM, Thornton JM (2003). Structural characterisation and functional significance of transient protein-protein interactions. *J Mol Biol.* 325: 991-1018

15 Acuner Ozbabacan SE, Engin HB, Gursoy A, Keskin O (2011). Transient protein-protein interactions. *Protein Eng Des Sel.* 24: 635-648

16 Nooren IM, Thornton JM (2003). Diversity of protein-protein interactions. *EMBO J.* 22: 3486-3492

17 Willardson BM, Tracy CM (2012). Chaperone-mediated assembly of G protein complexes. *Subcell Biochem.* 131-153

18 Salier RT, Milla ME, Waldburger CD, Brown BM, Schildbach JF (1996). Sequence determinants of folding and stability for the P22 Arc repressor dimer. *FASEB J.* 10: 42-48

19 Krishna SS, Aravind L (2010). The bridge-region of the Ku superfamily is an atypical zinc ribbon domain. *J Struct Biol.* 172: 294-299

20 Lu LL, Suscovich TJ, Fortune SM, Alter G (2018). Beyond binding: antibody effector functions in infectious diseases. *Nat Rev Immunol.* 18: 46-61

21 Bendtsen KL, Brodersen DE (2017). Higher-order structure in bacterial VapBC toxin-antitoxin complexes. *Subcell Biochem.* 381-412

22 Tidow H, Nissen P (2013). Structural diversity of calmodulin binding to its target sites. *FEBS J.* 280: 5551-5565

23 Chin D, Means AR (2000). Calmodulin: a prototypical calcium sensor. *Trends Cell Biol.* 10: 322-328

24 Schreiber G, Keating AE (2011). Protein binding specificity versus promiscuity. *Curr Opin Struct Biol.* 21: 50-61

25 Patil A, Kinoshita K, Nakamura H (2010). Hub promiscuity in protein-protein interaction networks. *Int J Mol Sci.* 11: 1930-1943

26 Perutz M (1978). Hemoglobin structure and respiratory transport. *Sci Am.* 239: 68-86

27 Perutz MF, Wilkinson A, Paoli M, Dodson G (1998). The stereochemical mechanism of the cooperative effects in hemoglobin revisited. *Annu Rev Biophys Biomol Struct.* 27: 1-34

28 Wierenga R, Kapetaniou E, Venkatesan R (2010). Triosephosphate isomerase: a highly evolved biocatalyst. *Cell Mol Life Sci.* 67: 3961-3982

29 Momany C, Ernst S, Ghosh R, Chang N-L, Hackert ML (1995). Crystallographic structure of a PLP-dependent ornithine decarboxylase from *Lactobacillus* 30a to 3.0 Å resolution. *J Mol Biol.* 252: 643-655

30 Kern AD, Oliveira MA, Coffino P, Hackert ML (1999). Structure of mammalian ornithine decarboxylase at 1.6 Å resolution: stereochemical implications of PLP-dependent amino acid decarboxylases. *Structure.* 7: 567-581

31 Jacob F (1977). Evolution and tinkering. *Science.* 196: 1161-1166

32 Ohno S. Evolution by gene duplication (Springer Science & Business Media, 2013).

33 Khersonsky O, Tawfik DS (2010). Enzyme promiscuity: a mechanistic and evolutionary perspective. *Annu Rev Biochem.* 79: 471-505

34 Walden H, Bell GS, Russell RJ, Siebers B, Hensel R, Taylor GL (2001). Tiny TIM: a small, tetrameric, hyperthermostable triosephosphate isomerase. *J Mol Biol.* 306: 745-757

35 Dams T, Auerbach G, Bader G, Jacob U, Ploom T, Huber R, Jaenicke R (2000). The crystal structure of dihydrofolate reductase from *Thermotoga maritima*: molecular features of thermostability. *J Mol Biol.* 297: 659-672

36 Thoma R, Hennig M, Sterner R, Kirschner K (2000). Structure and function of mutationally generated monomers of dimeric phosphoribosylanthranilate isomerase from *Thermotoga maritima*. *Structure.* 8: 265-276

37 Ali MH, Imperiali B (2005). Protein oligomerization: how and why. *Bioorg Med Chem.* 13: 5013-5020

38 Lang D, Thoma R, Henn-Sax M, Sterner R, Wilmanns M (2000). Structural evidence for evolution of the β/α barrel scaffold by gene duplication and fusion. *Science.* 289: 1546-1550

39 Jenke-Kodama H, Sandmann A, Müller R, Dittmann E (2005). Evolutionary implications of bacterial polyketide synthases. *Mol Biol Evol.* 22: 2027-2039

40 Schulz L, Zarzycki J, Steinchen W, Hochberg GKA, Erb TJ (2024). Layered entrenchment maintains essentiality in protein-protein interactions. *bioRxiv.* 2024.2001. 2018.576253

41 Elcock AH, McCammon JA (2001). Identification of protein oligomerization states by analysis of interface conservation. *Proc Natl Acad Sci U S A.* 98: 2990-2994

42 Valdar WS, Thornton JM (2001). Protein-protein interfaces: analysis of amino acid conservation in homodimers. *Proteins.* 42: 108-124

43 Caffrey DR, Somaroo S, Hughes JD, Mintseris J, Huang ES (2004). Are protein-protein interfaces more conserved in sequence than the rest of the protein surface? *Protein Sci.* 13: 190-202

44 Grishin NV, Phillips MA (1994). The subunit interfaces of oligomeric enzymes are conserved to a similar extent to the overall protein sequences. *Protein Sci.* 3: 2455-2458

45 Mintseris J, Weng Z (2005). Structure, function, and evolution of transient and obligate protein-protein interactions. *Proc Natl Acad Sci U S A.* 102: 10930-10935

46 Teichmann SA (2002). The constraints protein-protein interactions place on sequence divergence. *J Mol Biol.* 324: 399-407

47 Andreani J, Guerois R (2014). Evolution of protein interactions: from interactomes to interfaces. *Arch Biochem Biophys.* 554: 65-75

48 Teppa E, Zea DJ, Marino-Buslje C (2017). Protein-protein interactions leave evolutionary footprints: High molecular coevolution at the core of interfaces. *Protein Sci.* 26: 2438-2444

49 Halperin I, Wolfson H, Nussinov R (2004). Protein-protein interactions: coupling of structurally conserved residues and of hot spots across interfaces. Implications for docking. *Structure.* 12: 1027-1038

50 Bogan AA, Thorn KS (1998). Anatomy of hot spots in protein interfaces. *J Mol Biol.* 280: 1-9

51 Clackson T, Wells JA (1995). A hot spot of binding energy in a hormone-receptor interface. *Science.* 267: 383-386

52 Hu Z, Ma B, Wolfson H, Nussinov R (2000). Conservation of polar residues as hot spots at protein interfaces. *Proteins.* 39: 331-342

53 Ma B, Elkayam T, Wolfson H, Nussinov R (2003). Protein-protein interactions: structurally conserved residues distinguish between binding sites and exposed protein surfaces. *Proc Natl Acad Sci U S A.* 100: 5772-5777

54 Conte LL, Chothia C, Janin J (1999). The atomic structure of protein-protein recognition sites. *J Mol Biol.* 285: 2177-2198

55 Jones S, Thornton JM (1996). Principles of protein-protein interactions. *Proc Natl Acad Sci U S A.* 93: 13-20

56 Petta I, Lievens S, Libert C, Tavernier J, De Bosscher K (2016). Modulation of protein-protein interactions for the development of novel therapeutics. *Mol Ther.* 24: 707-718

57 Arkin MR, Tang Y, Wells JA (2014). Small-molecule inhibitors of protein-protein interactions: progressing toward the reality. *Chem Biol.* 21: 1102-1114

58 Kramer VG, Schader SM, Oliveira M, Colby-Germinario SP, Donahue DA, Singhroy DN, Tressler R, Sloan RD, Wainberg MA (2012). Maraviroc and other HIV-1 entry inhibitors exhibit a class-specific redistribution effect that results in increased extracellular viral load. *Antimicrob Agents Chemother.* 56: 4154-4160

59 Kahan R, Worm DJ, de Castro GV, Ng S, Barnard A (2021). Modulators of protein–protein interactions as antimicrobial agents. *RSC Chem Biol.* 2: 387-409

60 Cossar PJ, Lewis PJ, McCluskey A (2020). Protein-protein interactions as antibiotic targets: A medicinal chemistry perspective. *Med Res Rev.* 40: 469-494

61 Helton LG, Kennedy EJ (2020). Targeting *Plasmodium* with constrained peptides and peptidomimetics. *IUBMB Life.* 72: 1103-1114

62 Modell AE, Blosser SL, Arora PS (2016). Systematic targeting of protein-protein interactions. *Trends Pharmacol Sci.* 37: 702-713

63 Robertson NS, Spring DR (2018). Using peptidomimetics and constrained peptides as valuable tools for inhibiting protein-protein interactions. *Molecules.* 23: 959

64 Kahan R, Worm DJ, de Castro GV, Ng S, Barnard A (2021). Modulators of protein-protein interactions as antimicrobial agents. *RSC Chem Biol.* 2: 387-409

65 Zalkin H (1993). The amidotransferases. *Adv Enzymol Relat Areas Mol Biol.* 66: 203-309

66 James TY, Boulianne RP, Bottoli AP, Granado JD, Aebi M, Kües U (2002). The *pab1* gene of *Coprinus cinereus* encodes a bifunctional protein for para-aminobenzoic acid (PABA) synthesis: implications for the evolution of fused PABA synthases. *J Basic Microbiol.* 42: 91-103

67 Camara D, Richefeu-Contesto C, Gambonnet B, Dumas R, Rébeillé F (2011). The synthesis of pABA: Coupling between the glutamine amidotransferase and aminodeoxychorismate synthase domains of the bifunctional aminodeoxychorismate synthase from *Arabidopsis thaliana*. *Arch Biochem Biophys.* 505: 83-90

68 Wurm JP, Sung S, Kneuttinger AC, Hupfeld E, Sterner R, Wilmanns M, Sprangers R (2021). Molecular basis for the allosteric activation mechanism of the heterodimeric imidazole glycerol phosphate synthase complex. *Nat Commun.* 12: 2748

69 Spraggon G, Kim C, Nguyen-Huu X, Yee M-C, Yanofsky C, Mills SE (2001). The structures of anthranilate synthase of *Serratia marcescens* crystallized in the presence

of (i) its substrates, chorismate and glutamine, and a product, glutamate, and (ii) its end-product inhibitor, L-tryptophan. *Proc Natl Acad Sci U S A.* 98: 6021-6026

70 Nakamichi Y, Kobayashi J, Toyoda K, Suda M, Hiraga K, Inui M, Watanabe M (2023). Structural basis for the allosteric pathway of 4-amino-4-deoxychorismate synthase. *Acta Crystallogr D Struct Biol.* 79

71 Strohmeier M, Raschle T, Mazurkiewicz J, Rippe K, Sinning I, Fitzpatrick TB, Tews I (2006). Structure of a bacterial pyridoxal 5′-phosphate synthase complex. *Proc Natl Acad Sci U S A.* 103: 19284-19289

72 Smith J (1995). Structures of glutamine amidotransferases from the purine biosynthetic pathway. *Biochem Soc Trans.* 23: 894-898

73 Massière F, Badet-Denisot M-A (1998). The mechanism of glutamine-dependent amidotransferases. *Cell Mol Life Sci.* 54: 205-222

74 Tesmer JJ, Klem TJ, Deras ML, Davisson VJ, Smith JL (1996). The crystal structure of GMP synthetase reveals a novel catalytic triad and is a structural paradigm for two enzyme families. *Nat Struct Biol.* 3: 74-86

75 Ollis DL, Cheah E, Cygler M, Dijkstra B, Frolow F, Franken SM, Harel M, Remington SJ, Silman I, Schrag J (1992). The α/β hydrolase fold. *Protein Eng Des Sel.* 5: 197-211

76 Brannigan JA, Dodson G, Duggleby HJ, Moody PC, Smith JL, Tomchick DR, Murzin AG (1995). A protein catalytic framework with an N-terminal nucleophile is capable of self-activation. *Nature.* 378: 416-419

77 Linhorst A, Lübke T (2022). The human Ntn-hydrolase superfamily: structure, functions and perspectives. *Cells.* 11: 1592

78 Raushel FM, Thoden JB, Holden HM (1999). The amidotransferase family of enzymes: molecular machines for the production and delivery of ammonia. *Biochemistry.* 38: 7891-7899

79 Semmelmann F, Straub K, Nazet J, Rajendran C, Merkl R, Sterner R (2019). Mapping the allosteric communication network of aminodeoxychorismate synthase. *J Mol Biol.* 431: 2718-2728

80 Mouilleron S, Golinelli-Pimpaneau B (2007). Conformational changes in ammonia-channeling glutamine amidotransferases. *Curr Opin Struct Biol.* 17: 653-664

81 Zalkin H, Smith J (1998). Enzymes utilizing glutamine as an amide donor. *Adv Enzymol Relat Areas Mol Biol.* 72: 87-144

82 Shelton CL, Lamb AL (2018). Unraveling the structure and mechanism of the MST (ery) enzymes. *Trends Biochem Sci.* 43: 342-357

83 Knöchel T, Ivens A, Hester G, Gonzalez A, Bauerle R, Wilmanns M, Kirschner K, Jansonius JN (1999). The crystal structure of anthranilate synthase from *Sulfolobus solfataricus*: functional implications. *Proc Natl Acad Sci U S A.* 96: 9479-9484

84 Zwahlen J, Kolappan S, Zhou R, Kisker C, Tonge PJ (2007). Structure and mechanism of MbtI, the salicylate synthase from *Mycobacterium tuberculosis*. *Biochemistry.* 46: 954-964

85 Parsons JF, Jensen PY, Pachikara AS, Howard AJ, Eisenstein E, Ladner JE (2002). Structure of *Escherichia coli* aminodeoxychorismate synthase: architectural

conservation and diversity in chorismate-utilizing enzymes. *Biochemistry.* 41: 2198-2208

86 Kolappan S, Zwahlen J, Zhou R, Truglio JJ, Tonge PJ, Kisker C (2007). Lysine 190 is the catalytic base in MenF, the menaquinone-specific isochorismate synthase from *Escherichia coli*: implications for an enzyme family. *Biochemistry.* 46: 946-953

87 Hubrich F, Müller M, Andexer JN (2021). Chorismate- and isochorismate converting enzymes: Versatile catalysts acting on an important metabolic node. *Chem Commun.* 57: 2441-2463

88 Bentley R, Haslam E (1990). The shikimate pathway - a metabolic tree with many branches. *Crit Rev Biochem Mol Biol.* 25: 307-384

89 Dahm C, Müller R, Schulte G, Schmidt K, Leistner E (1998). The role of isochorismate hydroxymutase genes *entC* and *menF* in enterobactin and menaquinone biosynthesis in *Escherichia coli*. *Biochim Biophys Acta.* 1425: 377-386

90 Quadri LE, Sello J, Keating TA, Weinreb PH, Walsh CT (1998). Identification of a *Mycobacterium tuberculosis* gene cluster encoding the biosynthetic enzymes for assembly of the virulence-conferring siderophore mycobactin. *Chem Biol.* 5: 631-645

91 Ye Q-Z, Liu J, Walsh CT (1990). p-Aminobenzoate synthesis in *Escherichia coli*: purification and characterization of PabB as aminodeoxychorismate synthase and enzyme X as aminodeoxychorismate lyase. *Proc Natl Acad Sci U S A.* 87: 9391-9395

92 Baker TI, Crawford I (1966). Anthranilate synthetase: partial purification and some kinetic studies on the enzyme from *Escherichia coli*. *J Biol Chem.* 241: 5577-5584

93 Culbertson JE, Toney MD (2013). Expression and characterization of PhzE from *P. aeruginosa* PAO1: aminodeoxyisochorismate synthase involved in pyocyanin and phenazine-1-carboxylate production. *Biochim Biophys Acta.* 1834: 240-246

94 Kerbarh O, Bulloch E, Payne R, Sahr T, Rébeillé F, Abell C (2005). Mechanistic and inhibition studies of chorismate-utilizing enzymes. *Biochem Soc Trans.* 33: 763-766

95 Schadt HS, Schadt S, Oldach F, Süssmuth RD (2009). 2-Amino-2-deoxyisochorismate is a key intermediate in *Bacillus subtilis* p-aminobenzoic acid biosynthesis. *J Am Chem Soc.* 131: 3481-3483

96 Bera AK, Atanasova V, Dhanda A, Ladner JE, Parsons JF (2012). Structure of aminodeoxychorismate synthase from *Stenotrophomonas maltophilia*. *Biochemistry.* 51: 10208-10217

97 Gorelova V, Bastien O, De Clerck O, Lespinats S, Rébeillé F, Van Der Straeten D (2019). Evolution of folate biosynthesis and metabolism across algae and land plant lineages. *Sci Rep.* 9: 5731

98 Goncharoff P, Nichols BP (1984). Nucleotide sequence of *Escherichia coli pabB* indicates a common evolutionary origin of p-aminobenzoate synthetase and anthranilate synthetase. *J Bacteriol.* 159: 57-62

99 Plach MG, Semmelmann F, Busch F, Busch M, Heizinger L, Wysocki VH, Merkl R, Sterner R (2017). Evolutionary diversification of protein-protein interactions by interface add-ons. *Proc Natl Acad Sci U S A.* 114: E8333-E8342

100 Crawford IP (1989). Evolution of a biosynthetic pathway: the tryptophan paradigm. *Annu Rev Microbiol.* 43: 567-600

101 Graf R, Mehmann B, Braus GH (1993). Analysis of feedback-resistant anthranilate synthases from *Saccharomyces cerevisiae*. *J Bacteriol.* 175: 1061-1068

102 Caligiuri M, Bauerle R (1991). Identification of amino acid residues involved in feedback regulation of the anthranilate synthase complex from *Salmonella typhimurium*. Evidence for an amino-terminal regulatory site. *J Biol Chem.* 266: 8328-8335

103 Morollo AA, Eck MJ (2001). Structure of the cooperative allosteric anthranilate synthase from *Salmonella typhimurium*. *Nat Struct Biol.* 8: 243-247

104 Sampathkumar P, Atwell S, Wasserman S, Do J, Bain K, Rutter M, Gheyi T, Sauder J, Burley S (2009). Crystal structure of para-aminobenzoate synthetase, component I from *Cytophaga hutchinsonii*. www.rcsb.org

105 Sridharan S, Howard N, Kerbarh O, Błaszczyk M, Abell C, Blundell TL (2010). Crystal structure of *Escherichia coli* enterobactin-specific isochorismate synthase (EntC) bound to its reaction product isochorismate: implications for the enzyme mechanism and differential activity of chorismate-utilizing enzymes. *J Mol Biol.* 397: 290-300

106 Kerbarh O, Chirgadze DY, Blundell TL, Abell C (2006). Crystal structures of *Yersinia enterocolitica* salicylate synthase and its complex with the reaction products salicylate and pyruvate. *J Mol Biol.* 357: 524-534

107 Li Q-A, Mavrodi DV, Thomashow LS, Roessle M, Blankenfeldt W (2011). Ligand binding induces an ammonia channel in 2-amino-2-desoxyisochorismate (ADIC) synthase PhzE. *J Biol Chem.* 286: 18213-18221

108 List F, Vega MC, Razeto A, Häger MC, Sterner R, Wilmanns M (2012). Catalysis uncoupling in a glutamine amidotransferase bienzyme by unblocking the glutaminase active site. *Chem Biol.* 19: 1589-1599

109 List F, Bocola M, Haeger MC, Sterner R (2012). Constitutively active glutaminase variants provide insights into the activation mechanism of anthranilate synthase. *Biochemistry.* 51: 2812-2818

110 Kneuttinger AC, Rajendran C, Simeth NA, Bruckmann A, König B, Sterner R (2020). Significance of the protein interface configuration for allostery in imidazole glycerol phosphate synthase. *Biochemistry.* 59: 2729-2742

111 Klem H, McCullagh M, Paton RS (2022). Modeling catalysis in allosteric enzymes: capturing conformational consequences. *Top Catal.* 65: 165-186

112 Roux B, Walsh CT (1993). p-Aminobenzoate synthesis in *Escherichia coli*: mutational analysis of three conserved amino acid residues of the amidotransferase PabA. *Biochemistry.* 32: 3763-3768

113 Lusty CJ, Liao M (1993). Substitution of Glu841 by lysine in the carbamate domain of carbamyl phosphate synthetase alters the catalytic properties of the glutaminase subunit. *Biochemistry.* 32: 1278-1284

114 Roux B, Walsh CT (1992). p-aminobenzoate synthesis in *Escherichia coli*: kinetic and mechanistic characterization of the amidotransferase PabA. *Biochemistry.* 31: 6904-6910

115 Semmelmann F, Hupfeld E, Heizinger L, Merkl R, Sterner R (2019). A fold-independent interface residue is crucial for complex formation and allosteric signaling in class I glutamine amidotransferases. *Biochemistry.* 58: 2584-2588

116 Bennett BD, Kimball EH, Gao M, Osterhout R, Van Dien SJ, Rabinowitz JD (2009). Absolute metabolite concentrations and implied enzyme active site occupancy in *Escherichia coli*. *Nat Chem Biol.* 5: 593-599

117 Rayl EA, Green JM, Nichols BP (1996). *Escherichia coli* aminodeoxychorismate synthase: analysis of *pabB* mutations affecting catalysis and subunit association. *Biochim Biophys Acta.* 1295: 81-88

118 Jurcik A, Bednar D, Byska J, Marques SM, Furmanova K, Daniel L, Kokkonen P, Brezovsky J, Strnad O, Stourac J (2018). CAVER Analyst 2.0: analysis and visualization of channels and tunnels in protein structures and molecular dynamics trajectories. *Bioinformatics.* 34: 3586-3588

119 Chovancova E, Pavelka A, Benes P, Strnad O, Brezovsky J, Kozlikova B, Gora A, Sustr V, Klvana M, Medek P (2012). CAVER 3.0: a tool for the analysis of transport pathways in dynamic protein structures. *PLoS Comput Biol.* 8: e1002708

120 Singh S, Anand R (2021). Tunnel architectures in enzyme systems that transport gaseous substrates. *ACS Omega.* 6: 33274-33283

121 Weeks A, Lund L, Raushel FM (2006). Tunneling of intermediates in enzyme-catalyzed reactions. *Curr Opin Struct Biol.* 10: 465-472

122 Gora A, Brezovsky J, Damborsky J (2013). Gates of enzymes. *Chem Rev.* 113: 5871-5923

123 Lee Y-m, Lim C (2008). Physical basis of structural and catalytic Zn-binding sites in proteins. *J Mol Biol.* 379: 545-553

124 Zheng H, Chordia MD, Cooper DR, Chruszcz M, Müller P, Sheldrick GM, Minor W (2014). Validation of metal-binding sites in macromolecular structures with the CheckMyMetal web server. *Nat Protoc.* 9: 156-170

125 Hou X, Jones BT. Inductively coupled plasma/optical emission spectrometry, Encyclopedia of Analytical Chemistry (John Wiley & Sons Chichester, UK, 2000), pp. 9468-9485.

126 Na H, Hinsen K, Song G (2021). The amounts of thermal vibrations and static disorder in protein X-ray crystallographic B-factors. *Proteins.* 89: 1442-1457

127 Sun Z, Liu Q, Qu G, Feng Y, Reetz MT (2019). Utility of B-factors in protein science: interpreting rigidity, flexibility, and internal motion and engineering thermostability. *Chem Rev.* 119: 1626-1665

128 Dosselaere F, Vanderleyden J (2001). A metabolic node in action: chorismate-utilizing enzymes in microorganisms. *Crit Rev Microbiol.* 27: 75-131

129 Chang Z, Sun Y, He J, Vining L (2001). p-Aminobenzoic acid and chloramphenicol biosynthesis in *Streptomyces venezuelae*: gene sets for a key enzyme, 4-amino-4-deoxychorismate synthase. *Microbiology.* 147: 2113-2126

130 Brown MP, Aidoo KA, Vining LC (1996). A role for *pabAB*, a p-aminobenzoate synthase gene of *Streptomyces venezuelae* ISP5230, in chloramphenicol biosynthesis. *Microbiology.* 142: 1345-1355

131 Rivalta I, Sultan MM, Lee N-S, Manley GA, Loria JP, Batista VS (2012). Allosteric pathways in imidazole glycerol phosphate synthase. *Proc Natl Acad Sci U S A.* 109: E1428-E1436

132 Calvó-Tusell C, Maria-Solano MA, Osuna S, Feixas F (2022). Time evolution of the millisecond allosteric activation of imidazole glycerol phosphate synthase. *J Am Chem Soc.* 144: 7146-7159

133 Beismann-Driemeyer S, Sterner R (2001). Imidazole glycerol phosphate synthase from *Thermotoga maritima*: Quaternary structure, steady-state kinetics, and reaction mechanism of the bienzyme complex. *J Biol Chem.* 276: 20387-20396

134 Raschle T, Amrhein N, Fitzpatrick TB (2005). On the two components of pyridoxal 5′-phosphate synthase from *Bacillus subtilis*. *J Biol Chem.* 280: 32291-32300

135 Smith AM, Brown WC, Harms E, Smith JL (2015). Crystal structures capture three states in the catalytic cycle of a pyridoxal phosphate (PLP) synthase. *J Biol Chem.* 290: 5226-5239

136 Merino E, Jensen RA, Yanofsky C (2008). Evolution of bacterial *trp* operons and their regulation. *Curr Opin Struct Biol.* 11: 78-86

137 Gunsalus RP, Yanofsky C (1980). Nucleotide sequence and expression of *Escherichia coli trpR*, the structural gene for the *trp* aporepressor. *Proc Natl Acad Sci U S A.* 77: 7117-7121

138 Squires CL, Lee FD, Yanofsky C (1975). Interaction of the *trp* repressor and RNA polymerase with the *trp* operon. *J Mol Biol.* 92: 93-111

139 Gollnick P, Babitzke P, Antson A, Yanofsky C (2005). Complexity in regulation of tryptophan biosynthesis in *Bacillus subtilis*. *Annu Rev Genet.* 39: 47-68

140 Hertle R, Nazet J, Semmelmann F, Schlee S, Funke F, Merkl R, Sterner R (2021). Reprogramming the specificity of a protein interface by computational and data-driven design. *Structure.* 29: 292-304

141 Antimicrobial Resistance Collaborators (2022). Global burden of bacterial antimicrobial resistance in 2019: a systematic analysis. *Lancet.* 399: 629-655

142 Jonas OB, Irwin A, Berthe FCJ, Le Gall FG, Marquez PV (2017). Drug-resistant infections: a threat to our economic future (Vol. 2): final report. *HNP/Agriculture Global Antimicrobial Resistance Initiative Washington, D.C. : World Bank Group.*

143 Tacconelli E, Carrara E, Savoldi A, Harbarth S, Mendelson M, Monnet DL, Pulcini C, Kahlmeter G, Kluytmans J, Carmeli Y, Ouellette M, Outterson K, Patel J, Cavaleri M, Cox EM, Houchens CR, Grayson ML, Hansen P, Singh N, Theuretzbacher U, Magrini N, WHO Pathogens Priority List Working Group (2018). Discovery, research, and development of new antibiotics: the WHO priority list of antibiotic-resistant bacteria and tuberculosis. *Lancet Infect Dis.* 18: 318-327

144 Liu Y-Y, Wang Y, Walsh TR, Yi L-X, Zhang R, Spencer J, Doi Y, Tian G, Dong B, Huang X (2016). Emergence of plasmid-mediated colistin resistance mechanism MCR-1 in animals and human beings in China: a microbiological and molecular biological study. *Lancet Infect Dis.* 16: 161-168

145 Butler MS, Paterson DL (2020). Antibiotics in the clinical pipeline in October 2019. *J Antibiot (Tokyo).* 73: 329-364

146 WHO (2022). 2021 antibacterial agents in clinical and preclinical development: an overview and analysis. *World Health Organization, Geneva.*

147 London N, Raveh B, Schueler-Furman O (2013). Druggable protein-protein interactions - from hot spots to hot segments. *Curr Opin Chem Biol.* 17: 952-959

148 Shin W-H, Kumazawa K, Imai K, Hirokawa T, Kihara D (2020). Current challenges and opportunities in designing protein-protein interaction targeted drugs. *Adv Appl Bioinform Chem.* 11-25

149 Kortemme T, Baker D (2002). A simple physical model for binding energy hot spots in protein-protein complexes. *Proc Natl Acad Sci U S A.* 99: 14116-14121

150 Kortemme T, Kim DE, Baker D (2004). Computational alanine scanning of protein-protein interfaces. *Sci STKE.* 2004: pl2-pl2

151 Lister PD, Wolter DJ, Hanson ND (2009). Antibacterial-resistant *Pseudomonas aeruginosa*: clinical impact and complex regulation of chromosomally encoded resistance mechanisms. *Clin Microbiol Rev.* 22: 582-610

152 Botelho J, Grosso F, Peixe L (2019). Antibiotic resistance in *Pseudomonas aeruginosa* - Mechanisms, epidemiology and evolution. *Drug Resist Updat.* 44: 100640

153 Proctor RA, Von Eiff C, Kahl BC, Becker K, McNamara P, Herrmann M, Peters G (2006). Small colony variants: a pathogenic form of bacteria that facilitates persistent and recurrent infections. *Nat Rev Microbiol.* 4: 295-305

154 Kriegeskorte A, Lorè NI, Bragonzi A, Riva C, Kelkenberg M, Becker K, Proctor RA, Peters G, Kahl BC (2015). Thymidine-dependent *Staphylococcus aureus* small-colony variants are induced by trimethoprim-sulfamethoxazole (SXT) and have increased fitness during SXT challenge. *Antimicrob Agents Chemother.* 59: 7265-7272

155 Pfefferkorn E (1984). Interferon gamma blocks the growth of *Toxoplasma gondii* in human fibroblasts by inducing the host cells to degrade tryptophan. *Proc Natl Acad Sci U S A.* 81: 908-912

156 Mehraj V, Routy J-P (2015). Tryptophan catabolism in chronic viral infections: handling uninvited guests. *Int J Tryptophan Res.* 8: IJTR. S26862

157 Schmidt SV, Schultze JL (2014). New insights into IDO biology in bacterial and viral infections. *Front Immunol.* 5: 384

158 Zhang Y, Anaya-Sanchez A, Portnoy DA (2022). para-Aminobenzoic acid biosynthesis is required for *Listeria monocytogenes* growth and pathogenesis. *Infect Immun.* 90: e00207-00222

159 Chimalapati S, Cohen J, Camberlein E, Durmort C, Baxendale H, de Vogel C, van Belkum A, Brown JS (2011). Infection with conditionally virulent *Streptococcus pneumoniae* Δ*pab* strains induces antibody to conserved protein antigens but does not protect against systemic infection with heterologous strains. *Infect Immun.* 79: 4965-4976

160 Brown JS, Aufauvre-Brown A, Brown J, Jennings JM, Arst Jr H, Holden DW (2000). Signature-tagged and directed mutagenesis identify PABA synthetase as essential for *Aspergillus fumigatus* pathogenicity. *Mol Microbiol.* 36: 1371-1380

161 Roland S, Ferone R, Harvey RJ, Styles V, Morrison RW (1979). The characteristics and significance of sulfonamides as substrates for *Escherichia coli* dihydropteroate synthase. *J Biol Chem.* 254: 10337-10345

162 Hitchings GH (1973). Mechanism of action of trimethoprim-sulfamethoxazole I. *J Infect Dis.* 128: S433-S436

163 Burchall JJ (1973). Mechanism of action of trimethoprim-sulfamethoxazole II. *J Infect Dis.* 128: S437-S441

164 Minato Y, Dawadi S, Kordus SL, Sivanandam A, Aldrich CC, Baughn AD (2018). Mutual potentiation drives synergy between trimethoprim and sulfamethoxazole. *Nat Commun.* 9: 1003

165 Burman LG (1986). The antimicrobial activities of trimethoprim and sulfonamides. *Scand J Infect Dis.* 18: 3-13

166 Cassir N, Rolain J-M, Brouqui P (2014). A new strategy to fight antimicrobial resistance: the revival of old antibiotics. *Front Microbiol.* 5: 551

167 Thiede JM, Kordus SL, Turman BJ, Buonomo JA, Aldrich CC, Minato Y, Baughn AD (2016). Targeting intracellular p-aminobenzoic acid production potentiates the anti-tubercular action of antifolates. *Sci Rep.* 6: 38083

168 Yang S-S, Hu Y-B, Wang X-D, Gao Y-R, Li K, Zhang X-E, Chen S-Y, Zhang T-Y, Gu J, Deng J-Y (2017). Deletion of *sigB* causes increased sensitivity to para-aminosalicylic acid and sulfamethoxazole in *Mycobacterium tuberculosis*. *Antimicrob Agents Chemother.* 61: 10.1128/aac. 00551-00517

169 Cook MA, Wright GD (2022). The past, present, and future of antibiotics. *Sci Transl Med.* 14: eabo7793

170 Maxson T, Mitchell DA (2016). Targeted treatment for bacterial infections: prospects for pathogen-specific antibiotics coupled with rapid diagnostics. *Tetrahedron.* 72: 3609-3624

171 Magee TV (2015). Progress in discovery of small-molecule modulators of protein-protein interactions via fragment screening. *Bioorg Med Chem Lett.* 25: 2461-2468

172 Jaroszewicz W, Morcinek-Orłowska J, Pierzynowska K, Gaffke L, Węgrzyn G (2022). Phage display and other peptide display technologies. *FEMS Microbiol Rev.* 46: fuab052

173 Momand J, Jung D, Wilczynski S, Niland J (1998). The MDM2 gene amplification database. *Nucleic Acids Res.* 26: 3453-3459

174 Kojima K, Konopleva M, Samudio IJ, Shikami M, Cabreira-Hansen M, McQueen T, Ruvolo V, Tsao T, Zeng Z, Vassilev LT (2005). MDM2 antagonists induce p53-dependent apoptosis in AML: implications for leukemia therapy. *Blood.* 106: 3150-3159

175 Seliger B, Papadileris S, Vogel D, Hess G, Brendel C, Störkel S, Ortel J, Kolbe K, Huber C, Huhn D (1996). Analysis of the p53 and MDM-2 gene in acute myeloid leukemia. *Eur J Haematol.* 57: 230-240

176 Wang S, Zhao Y, Bernard D, Aguilar A, Kumar S (2012). Targeting the MDM2-p53 protein-protein interaction for new cancer therapeutics. *Protein-protein interactions.* 57-79

177 Konopleva MY, Röllig C, Cavenagh J, Deeren D, Girshova L, Krauter J, Martinelli G, Montesinos P, Schäfer JA, Ottmann O (2022). Idasanutlin plus cytarabine in relapsed

or refractory acute myeloid leukemia: results of the MIRROS trial. *Blood Adv.* 6: 4147-4156

178 Scott DE, Bayly AR, Abell C, Skidmore J (2016). Small molecules, big targets: drug discovery faces the protein-protein interaction challenge. *Nat Rev Drug Discov.* 15: 533-550

179 Cwirla SE, Balasubramanian P, Duffin DJ, Wagstrom CR, Gates CM, Singer SC, Davis AM, Tansik RL, Mattheakis LC, Boytos CM (1997). Peptide agonist of the thrombopoietin receptor as potent as the natural cytokine. *Science.* 276: 1696-1699

180 Sarson-Lawrence KT, Hardy JM, Iaria J, Stockwell D, Behrens K, Saiyed T, Tan C, Jebeli L, Scott NE, Dite TA (2024). Cryo-EM structure of the extracellular domain of murine thrombopoietin receptor in complex with thrombopoietin. *Nat Commun.* 15: 1135

181 Kamaruzzaman NF, Kendall S, Good L (2017). Targeting the hard to reach: Challenges and novel strategies in the treatment of intracellular bacterial infections: Targeting intracellular bacteria. *Br J Pharmacol.* 174

182 Breijyeh Z, Jubeh B, Karaman R (2020). Resistance of gram-negative bacteria to current antibacterial agents and approaches to resolve it. *Molecules.* 25: 1340

183 Wesseling CM, Martin NI (2022). Synergy by perturbing the gram-negative outer membrane: opening the door for gram-positive specific antibiotics. *ACS Infect Dis.* 8: 1731-1757

184 Datsenko KA, Wanner BL (2000). One-step inactivation of chromosomal genes in *Escherichia coli* K-12 using PCR products. *Proc Natl Acad Sci U S A.* 97: 6640-6645

185 Yu D, Ellis HM, Lee E-C, Jenkins NA, Copeland NG, Court DL (2000). An efficient recombination system for chromosome engineering in *Escherichia coli*. *Proc Natl Acad Sci U S A.* 97: 5978-5983

186 Murphy KC (1998). Use of bacteriophage λ recombination functions to promote gene replacement in *Escherichia coli*. *J Bacteriol.* 180: 2063-2071

187 Cherepanov PP, Wackernagel W (1995). Gene disruption in *Escherichia coli*: TcR and KmR cassettes with the option of Flp-catalyzed excision of the antibiotic-resistance determinant. *Gene.* 158: 9-14

188 Buff W, Arnold C (1971). Untersuchungen an einer p-Aminobenzoesäure-Mangelmutante von *Chlamydomonas reinhardii*: Chloramphenicol als p-Aminobenzoesäure-Ersatz. *Arch Microbiol.* 75: 304-311

189 Merkl R, Sterner R (2016). Ancestral protein reconstruction: techniques and applications. *Biol Chem.* 397: 1-21

190 He Z, Stigers Lavoie KD, Bartlett PA, Toney MD (2004). Conservation of mechanism in three chorismate-utilizing enzymes. *J Am Chem Soc.* 126: 2378-2385

191 He Z, Toney MD (2006). Direct detection and kinetic analysis of covalent intermediate formation in the 4-amino-4-deoxychorismate synthase catalyzed reaction. *Biochemistry.* 45: 5019-5028

192 Morollo AA, Bauerle R (1993). Characterization of composite aminodeoxyisochorismate synthase and aminodeoxyisochorismate lyase activities of anthranilate synthase. *Proc Natl Acad Sci U S A.* 90: 9983-9987

193 Morollo AA, Finn M, Bauerle R (1993). Isolation and structure determination of 2-amino-2-deoxyisochorismate: an intermediate in the biosynthesis of anthranilate. *J Am Chem Soc.* 115: 816-817

6 Acknowledgement

First and foremost, I would like to thank Prof. Reinhard Sterner for his constant guidance, encouragement and support throughout my thesis, which was valuable for my personal and scientific development. I very much appreciate the friendly and productive atmosphere he created and his generosity in making time for (scientific) discussions.

Next, I want to thank the further members of the doctoral committee, Prof. Christine Ziegler, Prof. Markus Jeschek, Prof. Gernot Längst and PD Patrick Babinger.

I appreciate and thank all collaboration partners for contributing practically and/or with scientific advice to my work: Dr. Sihyun Sung and Prof. Matthias Wilmanns who solved the structures and for many enriching discussions; Vanessa Tomanek and Prof. Axel Dürkop for performing and discussing ICP-OES measurements; Prof. André Gessner for generously providing human plasma samples and sharing his medical knowledge; Dr. Maximilian Plach and 2bind for the joint work on the identification of inhibitors; and Bekas Alo and Jun.-Prof. Christina Lamers for the production and purification of inhibitor peptides.

I would like to express my gratitude to Jeannette Ueckert, Sonja Fuchs, Christiane Endres and Sabine Laberer, who are doing an outstanding job and whose tireless practical support has made this work much easier. I would also like to thank Klaus-Jürgen Tiefenbach and Claudia Pauer for their IT and administrative support.

I cordially thank Dr. Sandra Schlee, not only for generously sharing her vast scientific knowledge with me, but also for her personal support and the great time we spent together during my thesis.

I also would like to thank all former and current members of our group for the amazing time inside and outside of the lab and for the supportive environment. Many thanks to the Mensa crew, who made our lunch breaks cheerful and enriching, especially to Dr. Tommy Kinateder, Barbara Hufnagl and Miche Bartl.

Above all, I am deeply grateful to my friends, my family and Johannes for their unlimited and unconditional support all the way through and for making me who I am.